ABSTRACT

Brane Cosmology in String/M-Theory and Cosmological Parameters Estimation

Qiang Wu, Ph.D.

Chairperson: Anzhong Wang, Ph.D.

In this dissertation, I mainly focus on two subjects: (I) highly effective and efficient parameter estimation algorithms and their applications to cosmology; and (II) the late cosmic acceleration of the universe in string/M theory. In Part I, after developing two highly successful numerical codes, I apply them to study the holographical dark energy model and ΛCMD model with curvature. By fitting these models with the most recent observations, I find various tight constraints on the parameters involved in the models. In part II, I develop the general formulas to describe orbifold branes in both string and M theories, and then systematical study the two most important issues: (1) the radion stability and radion mass; and (2) the localization of gravity, the effective 4D Newtonian potential. I find that the radion is stable and its mass is in the order of GeV, which is well above the current observational constraints. The gravity is localized on the TeV brane, and the spectra of the gravitational Kluza-Klein towers are discrete and have a mass gap of TeV. The contributions of high order Yukawa corrections to the Newtonian potential are negligible. Using the large extra dimensions, I also show that the cosmological constant can be lowered to its current observational value. Applying the formulas to cosmology, I study several models in the two theories, and find that a late transient acceleration of the universe is a generic feature of our setups.

Brane Cosmology in String/M-Theory and Cosmological Parameters Estimation

by

Qiang Wu, M.Phys.

A Dissertation

Approved by the Department of Physics

Gregory A. Benesh, Ph.D., Chairperson

Submitted to the Graduate Faculty of
Baylor University in Partial Fulfillment of the
Requirements for the Degree
of
Doctor of Philosophy

Approved by the Dissertation Committee

Anzhong Wang, Ph.D., Chairperson

Gerald B. Cleaver, Ph.D.

Truell W. Hyde, Ph.D.

Dwight P. Russell, Ph.D.

Qin Sheng, Ph.D.

Accepted by the Graduate School
August 2009

J. Larry Lyon, Ph.D., Dean

Page bearing signatures is kept on file in the Graduate School.

TABLE OF CONTENTS

LIST OF FIGURES

LIST OF TABLES

ACKNOWLEDGMENTS

There are many people who have offered assistance to me during the five years of my graduate study.

I am deeply indebted to my advisor Dr. Wang, who provided me with the opportunity to pursue my graduate study at Baylor. I am grateful for his constant source of guidance, encouragement, valuable discussions. I value his friendship and thank him for being much more than just a supervisor.

I am particularly grateful to Dr. Yungui Gong. He instructed me to perform the numerical analysis in cosmology, which played such an important role in this dissertation.

I would like to express my appreciation to Dr. Qin Sheng for his valuable discussion in mathematics and his generous help.

I want to thank Dr. Gerald B. Cleaver, Dr. Truell W. Hyde, Dr. Dwight P. Russell and Dr. Qin Sheng for serving on my committee with their busy schedules. To all the faculty under which I studied, thank you for your encouragement and teaching.

Also, I want thank Andreas C Tziolas, Preet Sharma, Te Ha, Yongqing Huang, and Pamela Vo, for such a good experience working with you in our GCAP group.

I expend my thanks to Victor X. Guerrero, Sammy Joseph, Nan-Hsin Yu, Rui Wu, and my fellow graduate students for the good time we have shared at Baylor.

Finally I would like to acknowledge my parents for their loving support and encouragement.

DEDICATION

To My Parents

CHAPTER ONE

Introduction to Standard Cosmological Model

In this chapter, I will introduce the basic concepts of standard cosmological model that will be used later. I will discuss three assumptions and three pillars in building the standard cosmological model and give a brief review about dark energy in cosmology. In this chapter, my discussions are essentially based on several books [1, 2, 3]

1.1 Three Principles

The modern Cosmology is based on three assumptions, namely Cosmological principle, Weyl's postulate and Einstein's general relativity.

1.1.1 Cosmological Principle

Cosmological principle is, in essence, a generalization of the Copernican principle that the Earth does not occupy a privileged location in the Universe [1]. We state the principle as: on large spatial scales, the Universe is homogeneous and isotropic.

This kind of space-time can be described by the well-known Friedmann-Lemaître-Robertson-Walker (FRW) metric, defined by

$$ds^2 = dt^2 - a^2(t)\left(\frac{dr^2}{1-Kr^2} + r^2(d\theta^2 + \sin^2\theta d\varphi^2)\right) \tag{1.1}$$

where we have used spherical coordinates: r, θ and φ are the comoving coordinates; t is the proper time; $a(t)$ is a function of time, known as the "*scale factor*", and the constant K is the intrinsic curvature of the three-dimensional space. It parameterize the global geometry of the universe, which thus can be closed ($k > 0$), flat ($k = 0$) or open ($k < 0$).

1.1.2 Weyl's Postulate

A second assumption of the standard cosmological model is Weyl's postulate: the particles of the substratum lie in space-time on a congruence of timelike geodesics diverging from a point in finite or infinite past[1]. The postulate means that the substratum can be represented by a perfect fluid with energy-momentum tensor

$$T_\mu^\nu = (\rho + p)u_\mu u^\nu - p\delta_\mu^\nu \tag{1.2}$$

where, the energy density ρ and pressure p depend only on time, and related by the *equation of state*,

$$p = p(\rho). \tag{1.3}$$

In addition, the fluid is assumed to be at rest in the comoving frame in which the spacelike coordinates of each particle are constant along its geodesic. Thus in the synchronous gauge, $u^\mu = (1, 0, 0, 0, 0)$ and T_μ^ν becomes diagonal,

$$T_0^0 = \rho(t),\ T_i^j = -p(t)\delta_i^j. \tag{1.4}$$

1.1.3 Theory of Gravity

In the classical theory of general relativity, the gravitational interaction can be described by the four-dimensional action

$$S = -\frac{1}{16\pi G}\int d^4x\sqrt{-g}R + \int d^4x\sqrt{-g}L_m. \tag{1.5}$$

Here, R is the Ricci scalar, the contraction of the Ricci tensor; G is Newton's constant; and L_m is the Lagrangian density of the matter fields, acting as gravitational sources. The variation of the action Eq.(1.5) with respect to the metric $g_{\mu\nu}$ yields,

$$G_{\mu\nu} \equiv R_{\mu\nu} - \frac{1}{2}g_{\mu\nu}R = 8\pi G T_{\mu\nu} \tag{1.6}$$

where $G_{\mu\nu}$ is the Einstein tensor, and $T_{\mu\nu}$ is the energy-momentum tensor of all the sources, gravitationally coupled to the metric.

For the FRW metric (1.1), the non-zero independent components of the Einstein tensor are given by

$$G_{00} = \frac{3(\dot{a}^2 + K)}{a^2} \tag{1.7}$$
$$G_{11} = -\frac{2a\ddot{a} + \dot{a}^2 + K}{1 - Kr^2}. \tag{1.8}$$

Thus, the Einstein's field equation lead to two independent equations

$$H^2 + \frac{K}{a^2} = \frac{8\pi G}{3}\rho \tag{1.9}$$
$$\frac{\ddot{a}}{a} = -\frac{4\pi G}{3}(\rho + 3p) \tag{1.10}$$

Equation (1.9) is *Friedmann's equation* and the solution is called *Friedmann models* (or *FRW models*). Where $H = \dot{a}/a$ (the dot denotes the derivative with respect to the cosmic time) is the *Hubble parameter*, or *Hubble factor*.

Combining these two equations to eliminate $\ddot{a}$, we get

$$\dot{\rho} + 3H(\rho + p) = 0. \tag{1.11}$$

This equation can also be directly obtained from conservation equations

$$T^{\mu\nu}{}_{;\nu} = 0, \tag{1.12}$$

which is the result that the field equations (1.6) satisfy the contracted Bianchi identities

$$(G^{\mu\nu} - \Lambda g^{\mu\nu})_{;\nu} = 0. \tag{1.13}$$

Now we have three unknown functions $a(t)$, $\rho(t)$, $p(t)$, but only two independent equations. In order to solve this system, it is necessary to use the third equation, the *equation of state (EOS)* (Eq. (1.3)). In general, the energy density ρ counts all species: matter, radiation and other source, such as *dark energy* which we will discuss later. Since for each component, there is a different equation of state, the time evolution is different. For example, for matter and radiation the pressure p_m and p_γ are given by,

$$p_m = 0 \tag{1.14}$$

$$p_\gamma = \rho_\gamma/3 \tag{1.15}$$

where the pressureless matter component ρ_m represents the large-scale contribution of the macroscopic gravitational sources (galaxies, cluster, interstellar gas, ...), while the radiation component ρ_γ represents the contribution of all massless relativistic particles (photons, gravitons, neutrinos,...). Without energy transfer between the different fluid components, the Eq. (1.11) gives,

$$\rho_m \sim a^{-3} \tag{1.16}$$

$$\rho_\gamma \sim a^{-4} \tag{1.17}$$

More generally, if we specialize the equation of state (1.3) by

$$p = w\rho, \tag{1.18}$$

integrating equation (1.11), we get

$$\rho = \rho(a_0)(\frac{a_0}{a})^3 \exp\left(-3\int \frac{da'}{a'}w(a')\right) \tag{1.19}$$

which determines the evolution of the energy density of each species in terms of the functions $w(a)$. We summarized the equation of state of universe components in table 1.1.

1.2 Three Pillars

When Albert Einstein proposed his theory of gravitation , *Cosmological Considerations of the General Theory of Relativity* in 1917, he still believed that the universe was static and unchanging. In 1929, Edwin Hubble demonstrated that all galaxies and distant astronomical objects were moving away from us, and he also noticed the trend that the velocity increases with distance [9].

Table 1.1: Equation of state and universe species.

components	w_i	ρ_i
matter	0	$\rho_m \sim a^{-3}$
radiation	1/3	$\rho_\gamma \sim a^{-4}$
curvature	-1/3	$\rho_k \sim a^{-2}$
cosmological constant	-1/3	$\rho_c \sim$constant

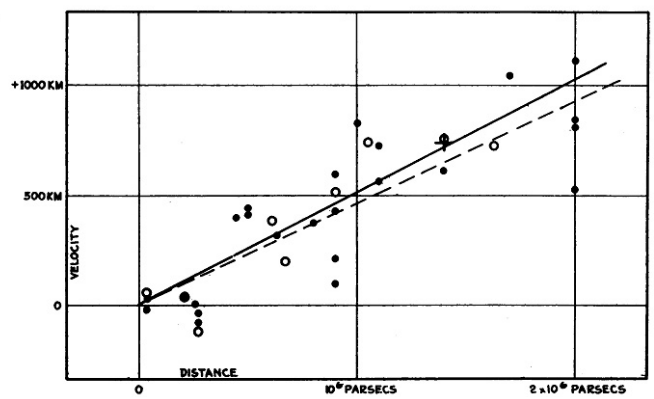

Figure 1.1: The original Hubble diagram [9]. Radial velocities are plotted against distances

Hubble's observation tells us that the universe has been expanding from a primordial hot and dense initial condition at some finite time in the past, and continues to expand to this day. There is a familiar name for this picture: *Big Bang* and the theory has been supported by the three observational pillars:

- Hubble diagram, which shows the expansion of the universe;
- Light element abundances, which are in accord with Big Bang nucleosynthesis (BBN);
- The cosmic microwave background (CMB).

1.2.1 Expanding Universe

As shown in Figure 1.1, the Hubble diagram is still the most direct evidence we have that the universe is expanding. The parameters that appear in Hubbles law: velocities and distances, are not directly measured. In reality we try to find

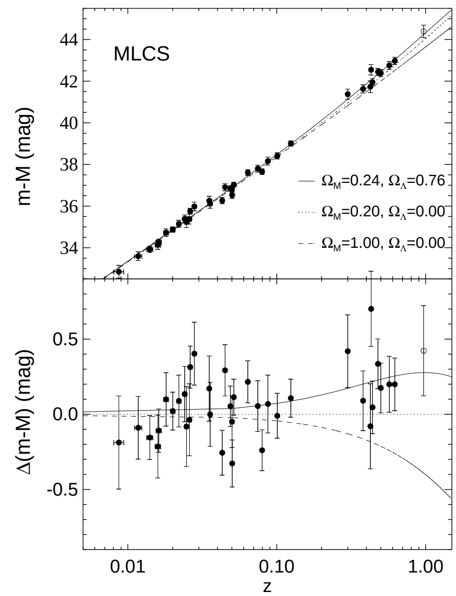

Figure 1.2: MLCS SNe Ia Hubble diagram [5]. The upper panel shows the Hubble diagram for the low-redshift and high-redshift SNe Ia samples with distances measured from the MLCS method. Bottom panel plots the residuals.

a *standard candle*, a class of objects which have the same intrinsic brightness. Any difference between the apparent brightness of two such objects then is a result of their different distances from us. Further more, the recent observations of Type Ia supernova give an ever stronger evidence that the universe is currently accelerating (Fig.1.2). In Fig.1.2, the light curve distances of the SNe Ia was inferred from *redshift* which can be defined by the observed and emitted wavelength of the light:

$$z + 1 = \frac{\lambda_{obs}}{\lambda_{emit}} = \frac{1}{a} \tag{1.20}$$

where, a is the scale factor in FRW metric Eq. (1.1).

1.2.2 Distances

In cosmology, there are several distances that are usually used in the literature. In this section, I shall first provide the definitions for each of them, and then give a brief comment.

The *comoving distance* of the light is the distance light could have traveled since $t = 0$. In a time dt, light travels a comving distance $dx = dt/a$ (set c=1), so the total comoving distance light could have traveled is

$$\eta \equiv \int_0^t \frac{dt'}{a(t')}. \tag{1.21}$$

Since the η is the distance traveled from the beginning of time by light, we can consider η as the *comoving horizon* and sometimes it is called *conformal time* as a time variable in cosmology.

Another important covmoving distance between a distant emitter and us can be expressed by

$$\chi(a) = \int_{t(a)}^{t_0} \frac{dt'}{a(t')} = \int_a^1 \frac{da'}{a'^2 H(a')} = \int_0^z \frac{dz'}{H(z')}. \tag{1.22}$$

Here we change the integration over time to one over the scale factor a or redshift ($z = 1/a - 1$). The comoving distance χ is useful in determining the distances in astronomy measurement.

Another way of inferring distances in astronomy is to measure the flux from an object of known luminosity. In static Euclidean space a object of luminosity L at distance d appears at apparent brightness, or observed energy flux

$$F = \frac{L}{4\pi d^2}, \tag{1.23}$$

Generalize to an expanding universe, the flux we observe is

$$F = \frac{La^2}{4\pi \chi^2(a)}. \tag{1.24}$$

To keep the Eq. (1.23) in an expanding universe , we define the *luminosity distance* as

$$d_L \equiv \frac{\chi}{a}. \tag{1.25}$$

It is a standard convention in astronomy to express L and F in logarithmic measures of absolute and apparent magnitudes. The apparent magnitude m of an object with received energy flux F is defined to be

$$m = -2.5 \log_{10} F + constant. \tag{1.26}$$

The absolute magnitude, M, of an object is related to its intrinsic luminosity, L, by the relation,

$$M = -2.5 \log_{10} L + constant. \tag{1.27}$$

Thus we find that the difference between the two magnitudes of an object at distance d_L is

$$\mu(z) = m - M = 5 \log_{10}(\frac{d_L}{\text{Mpc}}) + 25. \tag{1.28}$$

The distance is measured in units of megaparsecs (1 megaparses = 1Mpc = 3.0856×10^{24}cm), so that at $d_L = 10$pc this equation says $m - M = 0$, which is the definition of the absolute magnitude M. The magnitude difference $m - M$ is called the *distance modulus*.

1.2.3 Big Bang Nucleosynthesis

Big Bang nucleosynthesis (BBN) is the production of the light elements, ^2H (deuterium), ^3He (helium-3), ^4He (helium-4) and ^7Li (Lithium) during the first few minutes of the universe which we have a detailed understanding of physical processes. The BBN occurs at temperatures about 1 MeV since the nucleic binding energies are typically in the MeV range. The standard theory predicts the abundances of several light nuclei (H,D,^3He ^4He and ^7Li) as a function of a single cosmological parameter, the baryon to photon ratio, $\eta = n_b/n_\gamma$ [6]. The combined proton plus neutron density is called the *baryon* density, since both protons and neutrons have baryon number one and these are the only baryons around that. Thus, BBN gives us a way of measuring the baryon density in the universe [2]. With the evolution of the baryon density $\sim a^{-3}$, we can turn the measurements of light element abundances into measures of the baryon density today. The 5-years WMAP observations [12] gives that the parameterized baryon density is $\Omega_b = 0.0462 \pm 0.0015$.

1.2.4 Cosmic Microwave Background

The cosmic microwave background (CMB) is the electromagnetic radiation at wavelengths in the range of millimeters to centimeters. The CMB is isotropy and the spectrum is very close to a thermal Planck form at a temperature near $3K$. The CMB was discovered by Penzias and Wilson [14] in 1965. Its spectrum is well characterized by a $2.73K$ black body spectrum over more than three decades in frequency. Although many different processes might produce the general form of a black body spectrum, no model other than the Big Bang has yet explained the fluctuations. As a result, most cosmologists consider the Big Bang model of the universe to be the best explanation for the CMB.

The most important conclusion we obtained from the CMB over last 25 years surveying was that the early universe was very smooth. Penzias and Wilson reported that the CMB was isotropic and unpolarized at the 10% level. Current observations show that the CMB has an dipole anisotropy at $10 - 3$ level, indicating that the early universe was not completely smooth. The temperature anisotropies were detected. It is customary to express CMB anisotropies using two-point function of the temperature distribution on the sky in a spherical harmonic expansion,

$$\frac{\Delta T}{T}(\theta, \phi) = \sum_{lm} a_{lm} Y_{lm}(\theta, \phi). \tag{1.29}$$

Figure. 1.3 show a measurement of temperature (TT) power spectrum from WMAP5. There is a theoretical curve fitting from ΛCDM model in this figure which appears to agree well with the data. Indeed, understanding the development of the large-scale structure in the universe has become a major goal of most cosmologists today.

1.3 Dark Energy

One of the major challenges in cosmology today is to explain the observational result that our universe has currently been expanding with an increasing expansion

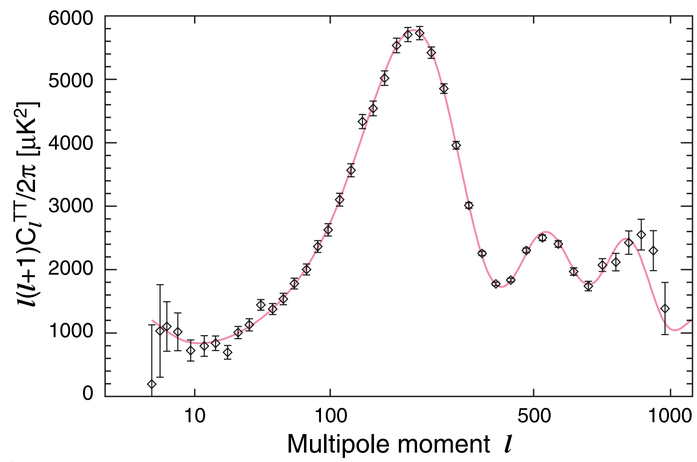

Figure 1.3: The WMAP 5-year temperature (TT) power spectrum. The red curve is the best-fit theory spectrum from the CDM/WMAP chain based on WMAP alone (Dunkley et al. 2008) [8]. The uncertainties include both cosmic variance and instrumental noise.

velocity (acceleration). Einstein tried to find a static solution of the field equation, so he was forced to modify the field equations by introducing an extra term, the cosmological term $\Lambda g_{\mu\nu}$, where Λ is a constant called the cosmological constant, so that the equations become

$$G_{\mu\nu} - \Lambda g_{\mu\nu} = 8\pi G T_{\mu\nu} \tag{1.30}$$

This is Einstein's field equation with cosmological constant.

Under the standard cosmology, there is significant observational evidence of the detection of Einstein's cosmological constant, Λ, or a dynamic component of the material, called *Dark Energy* which tends to increase the rate of expansion of the universe [4]. In 1998, observations of Type Ia supernovae by the High-Redshift Supernova Search Team followed in 1999 by the Supernova Cosmology Project [7] suggested that the expansion of the universe is accelerating. Since then, several independent sources confirmed this conclusion. Measurements of the cosmic microwave background (CMB), gravitational lensing, and the large scale structure of the cosmos as well as improved measurements of supernovae have been all consistent with the dark energy model [8].

The simplest way to explain the accelerating expansion is to use the cosmological constant, which is often referred to as the ΛCDM model with dark energy density $\rho_\Lambda = \Lambda/8\pi G$, and negative pressure p_Λ, given by

$$p_\Lambda = -\rho_\Lambda \tag{1.31}$$

The cosmological constant is not only theory describing dark energy which drives an accelerated phase in present universe. There are many dynamical models of dark energy. For example, we can introduce some new components with negative pressure, thus the equation of state (1.3) is,

$$p_{DE} = w\rho_{DE}, \quad w < -\frac{1}{3} \tag{1.32}$$

where w is a negative constant. Then the deceleration parameter derived from Eq. (1.10) can be written as,

$$q = -\frac{\ddot{a}}{aH^2} = \frac{4\pi G}{3H^2}[\rho_m + \rho_{DE}(1+3w)]. \tag{1.33}$$

We can choose the value of w to have a negative deceleration parameter, or an accelerating expansion. I will give a detail discussion about this kind of model in chapter 2.

1.4 Cosmological Constant Problem

In fact, the cosmological constant is well consistent with all observations carried out so far [90]. However, a serious problem occurs when we consider the source of this term, the so-called *cosmological constant problem*.

From the point of view of particle physics, vacuum has contributions to the cosmological constant [13]. Within the framework of Newtonian gravity, the vacuum energy does not cause serious problem since the gravitational interactions do not depend on the absolute value of the potential energy. The situation changes in general relativity, because the gravitational force couples to all forms of energy including vacuum. The connection is Einstein's field equations. Further more, the vacuum state had to have a Lorentz-invariant form which is satisfied by the equation of state $p_{vac} = -\rho_{vac}$, since the vacuum energy-momentum tensor

$$T_{\mu\nu} = -\rho_{vac} g_{\mu\nu} \tag{1.34}$$

is manifestly Lorentz-invariant [10].

The cosmological constant problem comes from the inconsistency of the vacuum energy value between cosmological observation and quantum field theory prediction. In a simple view, the energy of vacuum state is given by $E = \sum_k 1/2\hbar\omega(k)$, or in integral form

$$\rho_{vac} \sim \int_0^{k_{max}} \sqrt{k^2 + m^2} k^2 dk. \tag{1.35}$$

We have several estimations of this value based on different particle physics [11]. In the electroweak model, the value is

$$k_{EW} \sim 200GeV, \quad \rho_{vac}^{EW} \sim (200GeV)^4 \sim 3 \times 10^{47} erg/cm^3. \tag{1.36}$$

In the QCD scale, we have

$$k_{QCD} \sim 0.3GeV, \quad \rho_{vac}^{QCD} \sim (0.3GeV)^4 \sim 1.6 \times 10^{36} erg/cm^3. \tag{1.37}$$

In the Planck scale, we have

$$k_{PL} \sim 10^{18}GeV, \quad \rho_{vac}^{PL} \sim (10^{18}GeV)^4 \sim 2 \times 10^{110} erg/cm^3. \tag{1.38}$$

However, the cosmological observations show

$$\rho_{\Lambda}^{obs} \leq (10^{-12}GeV)^4 \sim 2 \times 10^{-10} erg/cm^3, \tag{1.39}$$

which is much smaller then any of the values listed above. The ratio of ρ_{vac} to ρ_{Λ} is 47 even 120 orders of magnitude between the theoretical and observational values of the cosmological constant.

The cosmological constant problem still remains unresolved. We will carry out further discussion in following chapters about this problem.

Table 1.2: Parameters values from 5-years WMAP observations for ΛCDM model.

Parameters	Symbol	Values
Hubble constant	H_0	$70.5 \pm 1.3\ \ km\ \ s^{-1}\ \ Mpc^{-1}$
Baryon density	Ω_b	0.0462 ± 0.0015
Cold dark matter density	Ω_c	0.233 ± 0.013
Matter density	Ω_m	0.279 ± 0.013
Dark energy	Ω_Λ	0.726 ± 0.0015
Radiation density	Ω_γ	$(5.0 \pm 0.2) \times 10^{-5}$
Neutrino density	Ω_ν	$< 0.013(95\% CL)$

1.5 Parameterizations of Cosmological Models

To solve the cosmological model numerically, we prefer to use the parameters with dimensionless quantities, which can be defined by

$$E = \frac{H}{H_0}, \quad \Omega_m = \frac{\rho_m}{\rho_{cr}}, \quad \Omega_k = -\frac{K}{a^2 H_0^2}, \quad \Omega_\gamma = \frac{\rho_\gamma}{\rho_{cr}}, \quad \Omega_\Lambda = \frac{\rho_\Lambda}{\rho_{cr}}, \tag{1.40}$$

where H_0 is the present value of the Hubble parameter, named *Hubble constant*, and $\rho_{cr} = {}^{3H_0^2}/{}_{8\pi G}$ is called *critical density.* Ω_m, Ω_k, Ω_γ, and Ω_Λ are the parameterized density of matter, curvature, radiation and dark energy. With these parameters, Eq. (1.9) can be rewritten as

$$E^2 = \Omega_m + \Omega_\gamma + \Omega_k + \Omega_\Lambda, \tag{1.41}$$

This is Friedmann's equation, and the newest cosmological observations give the present values of each parameter in table 1.2 [12].

CHAPTER TWO

Cosmological Parameters Estimation

The analysis of cosmological observational data to estimate the cosmological parameters is a complicated, computationally difficult problem. The supernova, CMB, and large scale structure of the universe provide tight constraints on these cosmological parameters. In this chapter, I shall give an overview of parameters estimation and discuss the applications of Markov Chain Monte Carlo sampling techniques and function optimization methods.

In numerical analysis of the cosmological models we are interested in using the given observational data to determine the values of the parameters involved in the models. In statistics, this is a statistical inference problem. There are two main approaches to statistical inference, which we call *frequentist* and *Bayesian* [15].

- In frequentist statistics, probability is interpreted as the frequency of the outcome of a repeatable experiment, but one does not define a probability for a hypothesis or for a parameter. We will discuss the parameter estimation in this framework in section 2.1.
- In Bayesian statistics, the interpartation of the probability is more general and includes degree of belief. One can speak of a probability density function for a parameter. Bayesian statistics allow one to use the subjective information, such as the prior probability of the parameters in the model. We will discuss the Monte-Carlo Markov Chain method based on Bayes' theorem in section 2.2.

2.1 Function Optimization

To check a theoretical model using various observations, the problem we are facing is the optimization, searching a set parameters to minimize χ^2 function or maximize the Likelihood function. Here I introduce the point estimation method in which an estimator of the parameters θ are denoted by $\hat{\theta}$, where $\theta = (\theta_1, ..., \theta_n)$ is the set of n parameters.

2.1.1 Maximum Likelihood and Least Squares

The maximum likelihood method finds the estimator $\hat{\theta}$ that maximizes the *likelihood function*,

$$L(\theta) = \prod_{i=1}^{N} f(x_i; \theta), \tag{2.1}$$

where x_i are a set of N independent measured quantities from a probability density function (p.d.f) $f(x_i; \theta)$. The likelihood function $L(\theta)$ is the joint p.d.f for the data, evaluated with the data obtained in the experiment. Here $L(\theta)$ is the function of parameters θ, but it is not a p.d.f for the parameters that is not defined in the frequentist statistics framework.

The maximum likelihood method coincides with the *least squares* method when a set of N independent quantities y_i are measured at known points x_i with a Gaussian distribution,

$$L(\theta) \sim \exp\left[-\frac{1}{2}\sum_{i=1}^{N}\frac{(y_i - \bar{y}(x_i;\theta))^2}{\sigma_i^2}\right], \tag{2.2}$$

where $\bar{y}(x_i, \theta)$ are the predicted values of y_i and σ_i^2 is the known variance. Then the χ^2 function can be defined by,

$$\chi^2(\theta) = -2\ln L(\theta) + constant = \sum_{i=1}^{N}\frac{(y_i - \bar{y}(x_i;\theta))^2}{\sigma_i^2} \tag{2.3}$$

The set of parameters θ which maximize L is the same as those which minimize χ^2. For the more general case, if y_i are not Gaussian distributed as long as they are dependent with a covariance matrix $V_{ij} = cov[y_i, y_j]$, then the least squares estimators are determined by the minimum of

$$\chi^2(\theta) = (\mathbf{y} - \bar{\mathbf{y}}(\theta))^{\mathbf{T}}\mathbf{V}^{-1}(\mathbf{y} - \bar{\mathbf{y}}(\theta)), \tag{2.4}$$

where $y = (y_1, ..., y_N)$ is the vector of measurements, $\bar{y}$ is the predicted values.

As the minimum value of the χ^2 represents the level of agreement between the measurements and the fitted function, it can be used to assess the goodness of the fit. The errors of estimators or bias can be obtained from covariant matrix or its inverse called *Hessian matrix* defined by

$$(\hat{V}^{-1})_{ij} = -\frac{\partial^2 \ln L}{\partial\theta_i \partial\theta_j}\Big|_{\hat{\theta}} = \frac{1}{2}\frac{\partial^2\chi^2}{\partial\theta_i\partial\theta_j}\Big|_{\hat{\theta}}, \tag{2.5}$$

where, $\hat{\theta}$ is the best estimator. The diagonal elements of the error (covariant) matrix are the squares of the individual parameter errors, including the effects of correlations with the other parameters. For joint parameter estimate, the error estimate is,

$$\sigma_i^2 = \sqrt{\Delta\chi^2 V_{ii}}. \tag{2.6}$$

For a function $y(\theta)$, the error is

$$\sigma_y^2 = \sum_{ij} \frac{\partial y}{\partial \theta_i}\frac{\partial y}{\partial \theta_j} V_{ij}. \tag{2.7}$$

2.1.2 Optimization Method

In general, the function for which we try to minimize are referred to as $f(\mathbf{x})$, where $\mathbf{x}$ are the unknown variables. We can start to seek the minimum of f from an initial value $\mathbf{x_0}$. Then the searching direction and step length have to be chosen to walk to the next step. This can be represented in the iterative picture

$$\mathbf{x_{k+1}} = \mathbf{x_k} + \lambda_{\mathbf{k}}\mathbf{d_k}, \quad \mathbf{k} = \mathbf{0}, \mathbf{1}, ..., \tag{2.8}$$

where, $\mathbf{d_i}$ is the direction and $|\lambda_i \mathbf{d_i}|$ is the step size. The different optimization methods presented differ in the choice of $\mathbf{d_i}$ and λ_i. In the following sections, I will give a review of several optimization methods.

Table 2.1: Algorithm for steepest descent method

1. Set starting point: $\mathbf{x_k}$, and $f(\mathbf{x_k})$,
2. Calculate the gradient: $\mathbf{g_k} = \nabla \mathbf{f}(\mathbf{x_k})$, set $\mathbf{d_k} = -\mathbf{g_k}$,
3. Determine the step length λ_k,
4. Calculate the new point: $\mathbf{x_{k+1}} = \mathbf{x_k} + \lambda_\mathbf{k} \mathbf{d_k}$.

2.1.2.1 *Steepest decent method* The method of steepest descent is the simplest of the gradient methods. We can choose the new direction in the direction opposite to the gradient of $f(\mathbf{x})$ since in this direction the function slides down fastest. Then the iterative equation becomes

$$\mathbf{x_{k+1}} = \mathbf{x_k} - \lambda_\mathbf{k} \mathbf{g}(\mathbf{x_k}), \tag{2.9}$$

where $\mathbf{g}(\mathbf{x_k}) = \nabla \mathbf{f}(\mathbf{x})$ is the gradient at point $\mathbf{x_k}$. The next step is to choose the step size λ_k to minimize the function f at point $\mathbf{x_{k+1}}$, which referred to as a *line search* scheme. This is a repeating process until the convergence is satisfied. The algorithm of this method is given in table 2.1 [16].

The steepest descent method is simple, fast in each iteration and very stable. If the minimum points exist, the method is guaranteed to find them in an infinite number of iterations, but there is shortcoming. The algorithm can take many iterations to converge towards a local minimum, if the curvature in different directions is very different. Note that the searching direction (negative gradient) at a point is orthogonal to the direction of the next point, so that it has to consequently search in the same direction as earlier steps.

2.1.2.2 *Newton method* The steepest descent method is based on the gradient or the first derivative of the function. The Newton method converges much faster towards a local maximum or minimum than gradient descent, since the second

Table 2.2: Algorithm for Newton method

1. Set starting point: $\mathbf{x_k}$, and $f(\mathbf{x_k})$,
2. Calculate the gradient: $\mathbf{g_k} = \nabla \mathbf{f}(\mathbf{x_k})$,
3. Calculate the Hessian: $\mathbf{H_k} = \nabla^2 \mathbf{f}(\mathbf{x_k})$, set $\mathbf{d_k} = -\mathbf{H_k^{-1}} \cdot \mathbf{g_k}$,
4. Calculate the new point: $\mathbf{x_{k+1}} = \mathbf{x_k} + \mathbf{d_k}$.

derivative is used here. The idea comes from the Taylor expansion of function $f(x)$

$$f(x + \Delta x) \approx f(x) + f'(x)\Delta x + \frac{1}{2} f''(x)\Delta x^2, \tag{2.10}$$

where $f'(x)$ and $f''(x)$ are the first and second derivatives. When $f''(x) > 0$, the right side of Eq. (2.10) is the quadratic function of Δx, and it has the minimum at

$$\frac{\partial}{\Delta x}[f(x) + f'(x)\Delta x + \frac{1}{2} f''(x)\Delta x^2] = f'(x) + f''(x)\Delta x = 0. \tag{2.11}$$

Thus, the sequence x_n defined by

$$x_{k+1} = x_k - \frac{f'(x_k)}{f''(x_k)}, \quad k \geq 0 \tag{2.12}$$

will converge towards the minimum point.

This scheme can be generalized to multiple dimensions by replacing the derivative with gradient $\mathbf{g}(\mathbf{x}) = \nabla \mathbf{f}(\mathbf{x})$, and the second derivative with the inverse of the Hessian matrix, $\mathbf{H}(\mathbf{x}) = \nabla^2 \mathbf{f}(\mathbf{x})$. Then the iterative formula is

$$\mathbf{x}_{k+1} = \mathbf{x}_k - \mathbf{H_k^{-1}} \cdot \mathbf{g_k}, \quad k = 0, 1, ... \tag{2.13}$$

The algorithm for the Newton method is given in table 2.2.

2.1.2.3 *Conjugate gradients method* In Newton's method, finding the inverse of the Hessian will be very time-consuming if the function $f(\mathbf{x})$ has a large number of variables. The conjugate gradients method is introduced to improve the convergence speed without calculating the second derivative.

We say that two non-zero vectors $\mathbf{d_i}$ and $\mathbf{d_j}$ are conjugate if they are orthogonal with respect to any symmetric positive definite matrix $\mathbf{A}$,

$$\mathbf{d_i^T} \cdot \mathbf{A} \cdot \mathbf{d_j} = \mathbf{0} \tag{2.14}$$

The idea is to let each search direction $\mathbf{d_i}$ be dependent on all other directions search to locate the minimum of $f(\mathbf{x})$ through equation 2.14. We call this the *Conjugate Directions* method. The *Conjugate Gradients* method is a special case of the conjugate Direction method, where the conjugate vectors generated by the gradients of the function $f(\mathbf{x})$, so that the iteration is

$$\mathbf{d_{k+1}} = -\mathbf{g_{k+1}} + \beta_{\mathbf{k}}\mathbf{d_k}, \quad k = 0, 1, ..., \tag{2.15}$$

where we have several choices for the coefficient β_k. For example [17], the so-called Fletcher-Reeves formula gives,

$$\beta_k = \frac{\|\mathbf{g_{k+1}} - \mathbf{g_k}\|^{\mathbf{2}}}{\|\mathbf{g_k}\|^{\mathbf{2}}} \tag{2.16}$$

or Polyak-Polak-Ribiere,

$$\beta_k = \frac{\mathbf{g'_{k+1}} \cdot (\mathbf{g_{k+1}} - \mathbf{g_k})}{\mathbf{g'_k} \cdot \mathbf{g_k}}. \tag{2.17}$$

The algorithm is shown in table 2.3.

2.1.2.4 *Variable metric method* In order to avoid the Hessian matrix $\mathbf{H}$ in Newton method, one can select a matrix $\mathbf{G}$ with "quasi-Newton" requirement,

$$\lim_{k\to\infty} \mathbf{G_k} = \mathbf{H_k^{-1}}. \tag{2.18}$$

or

$$\mathbf{G_{k+1}}\mathbf{\Delta g_k} = \mathbf{\Delta x_k}, \tag{2.19}$$

with $\Delta\mathbf{g_k} = \mathbf{g_{k+1}} - \mathbf{g_k}$, and $\Delta\mathbf{x}_k = \mathbf{x}_{k+1} - \mathbf{x}_k$. Then, the iterative formula is

$$\mathbf{x}_{k+1} = \mathbf{x}_k - \lambda_k\mathbf{G_k} \cdot \mathbf{g_k}, \quad k = 0, 1, ... \tag{2.20}$$

Table 2.3: Algorithm for conjugate gradients method

1. Set start point: $\mathbf{x_k}$, and $f(\mathbf{x_k})$,
2. Calculate the gradient: $\mathbf{g_k} = \nabla\mathbf{f}(\mathbf{x_k})$ set $\mathbf{d_k} = -\mathbf{g_k}$,
3. Determine the step length λ_k: $\min f(\mathbf{x_k} + \lambda_\mathbf{k}\mathbf{d_k})$,
4. Calculate the new point: $\mathbf{x_{k+1}} = \mathbf{x_k} + \lambda_\mathbf{k}\mathbf{d_k}$, $\mathbf{g_{k+1}} = \nabla\mathbf{f}(\mathbf{x_{k+1}})$,
5. Determine the new direction of search: $\mathbf{d_{k+1}} = -\mathbf{g_{k+1}} + \beta_\mathbf{k}\mathbf{d_k}$,
$\beta_k = \frac{\mathbf{g'_{k+1}}\cdot(\mathbf{g_{k+1}}-\mathbf{g_k})}{\mathbf{g'_k}\cdot\mathbf{g_k}}$ (PPR); $\beta_k = \frac{\Vert\mathbf{g_{k+1}}\Vert^2}{\Vert\mathbf{g_k}\Vert^2}$ (FR).

There are many methods to update $\mathbf{G_k}$ to satisfy quasi-Newton condition Eq. (2.19), for example the Davidon-Fletcher-Powell (DFP) scheme. In DFP algorithm, at a point $\mathbf{x}_k$, the approximated inverse Hessian at the subsequent point is given by [17]

$$\mathbf{G_{k+1}} = \mathbf{G_k} + \frac{\mathbf{\Delta x_k \Delta x'_k}}{\mathbf{\Delta x_k \Delta g'_k}} - \frac{\mathbf{G_k \Delta g_k \Delta g'_k G_k}}{\mathbf{\Delta g'_k G_k \Delta g_k}}, \tag{2.21}$$

where the prime denotes the transpose. This is the DFP algorithm in variable metric method listed in table 2.4. Other algorithms were introduced to improve the DFP formula, for example, SR1 formula and the widespread BFGS method, that was suggested independently by Broyden, Fletcher, Goldfarb, and Shanno, in 1970. I will not discuss them here in details.

The variable metric method has become very popular for optimization: it converges fast, it is stable, and spends relatively modest computing time at each iteration [16]. The CERN package MINUIT [18] is an application of the variable metric method.

2.2 Monte-Carlo Method

In this section, I will give an introduction of another way for estimation method, Markov Chain Monte Carlo (MCMC) techniques based on the Bayesian

Table 2.4: Algorithm for variable metric method

1. Set starting point: $\mathbf{x_k}$, and $f(\mathbf{x_k})$, $\mathbf{G_k} = \mathbf{I}$
2. Calculate the gradient: $\mathbf{g_k} = \nabla \mathbf{f}(\mathbf{x_k})$ set $\mathbf{d_k} = -\mathbf{g_k}$,
3. Determine the step length λ_k: $\min f(\mathbf{x_k} + \lambda_\mathbf{k} \mathbf{d_k})$,
4. Calculate the new point: $\mathbf{x_{k+1}} = \mathbf{x_k} + \lambda_\mathbf{k} \mathbf{d_k}$, $\mathbf{g_{k+1}} = \nabla \mathbf{f}(\mathbf{x_{k+1}})$,
5. Calculate the update to the inverse Hessian: $\mathbf{G_{k+1}} = \mathbf{G_k} + \frac{\mathbf{\Delta x_k \Delta x'_k}}{\mathbf{\Delta x_k \Delta g'_k}} - \frac{\mathbf{G_k \Delta g_k \Delta g'_k G_k}}{\mathbf{\Delta g'_k G_k \Delta g_k}}$ (DFP), ,
6. Determine the direction of search: $\mathbf{d_{k+1}} = -\mathbf{G_{k+1} g_{k+1}}$.

statistics theory.

Since the likelihood function can be described by the probability of the parameters, which allows us to estimate unknown parameters based on known outcomes, the Monte-Carlo method is an appropriate tool to simulate a system and carries out some statistical inferences.

2.2.1 Probability

Let's start from several basic concepts. The *probability* $P(A)$ can be defined by the events that occur in countable sample spaces (discrete probability).

The probability of an even B occurring when it is known that some event A has occurred is called a *conditional probability*, denoted by $P(B|A)$ (read P of B given A). It can be defined by

$$P(B|A) = \frac{P(A \cap B)}{P(A)}. \tag{2.22}$$

Multiplying the formula of definition Eq. (2.22) by $P(A)$, we obtain the multiplicative rule: If two events A and B both occur, then

$$P(A \cap B) = P(A)P(B|A). \tag{2.23}$$

Since $A \cap B$ and $B \cap A$ are the same, one obtains Bayes's theorem,

$$P(B|A) = \frac{P(A|B)P(B)}{P(A)} \tag{2.24}$$

If the events $B_1,\ B_2,\ \ldots\ ,\ B_k$ constitute a partition of the sample space such that $P(B_i) \neq 0$ for $i = 1, 2, ..., k$, then for any event A, the total probability is given by,

$$P(A) = \sum_i P(B_i \cap A) = \sum_i P(B_i)P(A|B_i). \tag{2.25}$$

This can be combined with Bayes's theorem to give

$$P(B|A) = \frac{P(A|B)P(B)}{\sum_i P(B_i)P(A|B_i)}. \tag{2.26}$$

In the probability distribution theory, for two random variables, X and Y, we define the *joint probability distribution*

$$f(x, y) = P(X = x, Y = y), \tag{2.27}$$

that is, the values $f(x, y)$ give the probability that outcomes x and y occur at the same time.

The *marginal distribution* of X and Y alone are defined by

$$g(x) = \sum_y f(x, y), \quad h(y) = \sum_x f(x, y). \tag{2.28}$$

The *conditional distribution* of the random variable Y given that $X = x$ is

$$f(y|x) = \frac{f(x, y)}{g(x)}, \quad g(x) > 0. \tag{2.29}$$

Similarly the conditional distribution of the random variable X given that $Y = y$ is

$$f(x|y) = \frac{f(x, y)}{h(y)}, \quad h(y) > 0. \tag{2.30}$$

Then, the Bayes's rule can be written as

$$f(y|x) = \frac{f(x|y)h(y)}{g(x)}. \tag{2.31}$$

2.2.2 Bayesian Statistics

Because the observed data are the only experimental results to the practitioner, statistical inference is based on the actual observed data from a given experiment. Furthermore, in Bayesian concepts, since the parameter is treated as random, a probability distribution can be specified, by using the *subjective probability* for the parameter. Such a distribution is called a *prior distribution* and it usually reflects the experimenter's prior belief about the parameter. In Bayesian perspective, once an experiment is conducted and data are observed, all knowledge about a parameter is contained in the actual observed data as well as in the prior information.

In Bayesian data analysis the model consists of a joint probability distribution (PDF) over all unobserved (parameters) and observed (data) quantities, denoted by $\theta = (\theta_{\mathbf{1}}, ..., \theta_{\mathbf{d}})$ and $\mathbf{x} = x_1, ..., x_n$. Using the definition of conditional probability distribution, the joint PDF, $f(\mathbf{x}, \theta)$ can be decomposed into the product of the PDF of parameter, $\pi(\theta)$, referred to as the prior PDF of θ, and the conditional PDF of the observables given the unovservables, $f(\mathbf{x}|\theta)$, referred to as the sampling distribution or *likelihood*, i.e. [19]

$$f(\mathbf{x}, \theta) = \pi(\theta) f(\mathbf{x}|\theta). \tag{2.32}$$

From Eq. (2.31), the distribution of θ, given data $\mathbf{x}$, which is called the *posterior distribution*, is given by

$$\pi(\theta|\mathbf{x}) = \frac{f(\mathbf{x}|\theta)\pi(\theta)}{g(\mathbf{x})}, \tag{2.33}$$

where

$$g(\mathbf{x}) = \int f(\mathbf{x}|\theta)\pi(\theta) d\theta, \tag{2.34}$$

is the marginal PDF of $\mathbf{x}$ which can be regarded as a normalizing constant as it is independent of θ.

Once the posterior distribution is derived, we can easily use it to make inference on the parameters. For example, the mean of a single parameter θ_i can be obtained by

$$E[\theta_i|\mathbf{x}] = \int \theta_i \pi(\theta_i|\mathbf{x}) d\theta_i, \tag{2.35}$$

where

$$\pi(\theta_i|\mathbf{x}) = \int ... \int \pi(\theta|\mathbf{x}) d\theta_i ... d\theta_{i-1} d\theta_{i+1} ... d\theta_d, \tag{2.36}$$

is called *marginalization distribution function* of the parameter θ_i.

In addition, we can calculate a $100(1-\alpha)\%$ Bayesian interval in $a < \theta_i < b$ for θ_i

$$\int_{-\infty}^{a} \pi(\theta_i|\mathbf{x}) d\theta_i = \int_{b}^{\infty} \pi(\theta_i|\mathbf{x}) d\theta_i = \frac{\alpha}{2}. \tag{2.37}$$

2.2.3 Markov Chain Monte Carlo

Since the multiple dimensional integration is involved in the calculations, a direct sampling method is very time consuming. The complexity of the grid-based method exponentially increases with increasing number of parameters. The Markov Chain Monte Carlo (MCMC) method can markedly improve the calculational speed since in MCMC the sample chain is constructed with correlation whose equilibrium distribution is just the joint posterior.

Many algorithms can be implemented to generate the MCMC samples. Here, we introduce one of them, Metropolis-Hastings algorithm (MH) which generates multidimensional points θ distributed according to a target PDF that is proportional to a given function $p(\theta)$. To generate points that follow $p(\theta)$, one first need a *proposal density distribution* $q(\theta_n, \theta_{n+1})$ to propose a new point θ_{n+1} given the chain is currently at θ_n. The proposed new point is then accepted with probability

$$\alpha(\theta_n, \theta_{n+1}) = min\left[1, \frac{p(\theta_{n+1})q(\theta_{n+1}, \theta_n)}{p(\theta_n)q(\theta_n, \theta_{n+1})}\right]. \tag{2.38}$$

Then, the MH algorithm can be shown in table 2.5.

If one takes the proposal density to be symmetric in θ and θ_n, then the test ratio becomes

$$\alpha = min[1, p(\theta)/p(\theta_n)]. \tag{2.39}$$

Table 2.5: Algorithm for Metropolis-Hastings in MCMC

1. Start with an arbitrary value θ_n,
2. Generate a value θ using the proposal density $q(\theta, \theta_n)$,
3. Form the Hastings test ratio, $\alpha = min\{1, \frac{p(\theta)q(\theta,\theta_n)}{p(\theta_n)q(\theta_n,\theta)}\}$,
4. Generate a value u uniformly distributed in $[0, 1]$,
5. If $u < \alpha$ set $\theta_n = \theta$ (acceptance)
If $u > \alpha$ set $\theta_n = \theta_n$ (rejection),
6. Repeat.

,

That is, if the proposed θ is at a value of probability higher than θ_n, the step will be taken.

The code package COSMOMC developed by Antony Lewis [67] implanted the MCMC method including Metropolis-Hastings algorithm.

2.3 Cosmological Parameter Estimation on Holographic Dark Energy Model

The current idea of a *negative-pressure* dominated universe seems to be inevitable in light of the impressive convergence of the recent observational results (see, e.g., [21, 22, 23, 24, 25]). This has in turn led cosmologists to hypothesize on the possible existence of an exotic dark component that not only could explain these experimental data but also could reconcile them with the inflationary flatness prediction ($\Omega_{\text{Total}} = 1$). This extra component, or rather, its gravitational effects is thought of as the first observational piece of evidence for new physics beyond the domain of the standard model of particle physics and constitutes a link between cosmological observations and a fundamental theory of nature (for some dark energy models, see [26]. For recent reviews, see also [27]). On the other hand, based on the effective local quantum field theories, the authors of Ref. [28] proposed a relationship between the ultraviolet (UV) and the infrared (IR) cutoffs due to the limit set by the formation of a black hole (BH). The UV-IR relationship in turn gives an upper bound on the zero point energy density $\rho_\Lambda \leq M_p^2 L^{-2}$, which means that the maximum entropy is of the order of $S_{BH}^{3/4}$. This zero point energy density has the same order of magnitude as the dark energy density [29], and is widely referred to as the holographic dark energy (HDE) [30] (see also [31]). However, the HDE model based on the Hubble scale as the IR cutoff seems not to lead to an accelerating universe [29]. A solution to this matter was subsequently given in Ref. [30] that discussed the possibilities of the particle and the event horizons as the IR cutoff, and found that only the event horizon identified as the IR cutoff gave a viable HDE model [30]. The HDE model based on the event horizon as the IR cutoff was found to be consistent with the observational data [32].

A subsequent development concerning the idea of a holographic dark energy is the possibility of considering interaction between this latter component and the dark matter in the context of a holographic dark energy model with the event horizon as the IR cutoff. As an interesting result, it was shown that the interacting HDE model realized the phantom crossing behavior [33], which is also obtained in the context of non-minimally coupled scalar fields (see, e.g, [34] and references therein). Other recent discussions on interacting HDE models can be found in [35, 36, 37].

In this section, we [20] test the viability of the interacting HDE model discussed in Ref. [33] by using the new 182 *gold* supernovae Ia (SNe Ia) data [22], the 192 ESSENCE SNe Ia data [23], the baryon acoustic oscillation (BAO) measurement from the Sloan Digital Sky Survey (SDSS) [24], and the shift parameter determined from the three-year Wilkinson Microwave Anisotropy Probe (WMAP3) data [25].

2.3.1 Interacting HDE *Model*

We consider a spatially flat Friedmann-Robertson-Walker universe with dark matter, HDE and radiation. Due to the interaction between the two dark components, the balance equations between them can be written as

$$\dot{\rho}_m + 3H\rho_m = \Gamma \ , \tag{2.40}$$

$$\dot{\rho}_D + 3H(1+\omega_D)\rho_D = -\Gamma \tag{2.41}$$

where the HDE density is

$$\rho_D = 3c^2 M_p^2 L^{-2} \ . \tag{2.42}$$

In the above equations, L is the IR cutoff, $M_p = 1/\sqrt{8\pi G}$ is the reduced Planck mass, ω_D is the equation of state of the HDE, $\Gamma = 9b^2 M_p^2 H^3$ is a particular interacting term with the coupling constant b^2, and the subscript 0 means the current value of the variable. The HDE, dark matter and radiation density parameters are defined, respectively, as $\Omega_D = \rho_D/(3H^2M_p^2)$, $\Omega_m = \rho_m/(3H^2M_p^2)$, and $\Omega_\gamma = \rho_\gamma/(3H^2M_p^2)$. Note that, if we choose the Hubble scale as the IR cutoff, i.e., $L = 1/H$, then we find that $\Omega_m/\Omega_D = (1-c^2)/c^2$, which means that the HDE always follows the dark matter. Even though the HDE equation of state w_D can be less than $-1/3$ with the help of the interaction [36], this model cannot explain the transition from deceleration to acceleration.

As suggested by Li [30], one can choose the future event horizon or particle horizon as the IR cutoff. For the future event horizon,

$$L(t) = a(t)\int_t^\infty \frac{dt'}{a(t')} = a\int_a^\infty \frac{da'}{H'a'^2} \ , \tag{2.43}$$

whereas for the particle horizon,

$$L(t) = a(t)\int_0^t \frac{dt'}{a(t')} = a\int_0^a \frac{da'}{H'a'^2}. \tag{2.44}$$

Substituting Eqs. (2.43) and (2.44) into Eq. (2.42) and taking the derivative with respect to $x = \ln a$, we obtain

$$\rho_D' \equiv \frac{d\rho_D}{dx} = -6M_p^2 H^2 \Omega_D \pm \frac{6M_p^2}{c} H^2 \Omega_D^{3/2}, \tag{2.45}$$

where the upper (lower) sign is for the event (particle) horizon. Since $\dot{\rho}_D \equiv d\rho_D/dt = \rho_D' H$, Eq. (2.41) can be written as

$$\rho_D' + 3(1+\omega_D)\rho_D = -9M_p^2 b^2 H^2. \tag{2.46}$$

Combining Eqs. (2.45) and (2.46), we obtain the equation of state of this interacting holographic dark energy, i.e.,

$$\omega_D = -\frac{1}{3} \mp \frac{2}{3}\frac{\sqrt{\Omega_D}}{c} - \frac{b^2}{\Omega_D}. \tag{2.47}$$

When the interaction is absent, $b^2 = 0$, it is clear from the above expression that we cannot choose the particle horizon as the IR cutoff. In [37], it was argued that the effective equation of state of the HDE in the interacting case should be

$$\omega_D^{\text{eff}} = \omega_D + \frac{b^2}{\Omega_D} = -\frac{1}{3} \mp \frac{2}{3}\frac{\sqrt{\Omega_D}}{c}. \tag{2.48}$$

Based on this effective equation of state, it was concluded that there was no phantom crossover even for an interacting HDE model. In fact, by combining the Friedmann equation with Eqs. (2.40) and (2.41), we obtain the acceleration equation

$$\dot{H} = -4\pi G(\rho + p). \tag{2.49}$$

For a flat universe, the physical consequence of the phantom dark energy is a super-acceleration when the dark energy dominates. Note that it is ω_D, not ω_D^{eff}, that appears in the acceleration equation (2.49). Therefore, the effective equation of state seems not to show the true physical meaning of the equation of state of the HDE, and ω_D should be used instead.

Substituting Eq. (2.47) into Eq. (2.46) and applying the definition of Ω_D, we have

$$\frac{H'}{H} = -\frac{\Omega_D'}{2\Omega_D} - 1 \pm \frac{\sqrt{\Omega_D}}{c}. \tag{2.50}$$

On the other hand, substituting $\dot{H} = H'H$ and $p_D = \omega_D \rho_D$ into Eq. (2.49), we obtain

$$\frac{H'}{H} = \frac{1}{2}\Omega_D \pm \frac{\Omega_D^{3/2}}{c} + \frac{3}{2}b^2 - \frac{3}{2} - \frac{1}{2}\Omega_\gamma. \tag{2.51}$$

Now, combining Eqs. (2.50) and (2.51), we find the differential equation for Ω_D, i.e.,

$$\frac{\Omega_D'}{\Omega_D} = 1 - \Omega_D \pm \frac{2\sqrt{\Omega_D}}{c}(1-\Omega_D) - 3b^2 + \Omega_\gamma\ , \tag{2.52}$$

a result that is consistent with Eq. (5) of Ref. [38] when the radiation term Ω_γ is neglected.

If we choose the particle horizon as the IR cutoff, the current acceleration requires that $\omega_{D0} < -1/3 - (\Omega_{m0} + 2\Omega_{\gamma 0})/3\Omega_{D0}$. From Eq. (2.47), we also obtain a lower bound on b^2,

$$b^2 > \frac{\Omega_{m0}}{3} + \frac{2}{3}\frac{\Omega_{D0}^{3/2}}{c} + \frac{2}{3}\Omega_{\gamma 0}. \tag{2.53}$$

The past deceleration and the transition from deceleration to acceleration requires that $\Omega_{D0}' \geq 0$, so Eq. (2.52) gives the upper bound on b^2,

$$b^2 \leq \frac{\Omega_{m0}}{3}\left(1 - 2\frac{\sqrt{\Omega_{D0}}}{c}\right) + \frac{1}{3}\Omega_{\gamma 0}. \tag{2.54}$$

By comparing Eqs. (2.53) and (2.54), we see that the upper bound is lower than the lower bound, so that the inequalities are not satisfied. The model based on the particle horizon as the IR cutoff is not, therefore, a viable dark energy model. In what follows, we consider only the HDE based on the event horizon. As discussed in [38], the interaction Γ cannot be too strong and the parameters b^2 and c are not totally free; they need to satisfy some constraints. Following [38], we take $0 \leq b^2 \leq 0.2$ and $\sqrt{\Omega_D} < c < 1.255$.

2.3.2 Observational Constraints

There are three parameters Ω_{m0}, c and b^2 in the interacting HDE model since $\Omega_{D0} = 1 - \Omega_{m0} - \Omega_{\gamma 0}$ and $\Omega_{\gamma 0} \sim 10^{-5}$. In order to place limits on them and test the viability of the model, we apply both the 182 gold SNe Ia [22] and the 192 ESSENCE SNe Ia data [23] to fit these parameters by minimizing

$$\chi^2 = \sum_i \frac{[\mu_{obs}(z_i) - \mu(z_i)]^2}{\sigma_i^2}, \tag{2.55}$$

where the extinction-corrected distance modulus $\mu(z) = 5\log_{10}(d_L(z)/\mathrm{Mpc}) + 25$, σ_i is the total uncertainty in the μ_{obs} observations, and the luminosity distance is given by

$$\begin{aligned} d_L &= (1+z)\int_0^z \frac{\mathrm{d}z'}{H(z')} \\ &= [\frac{c(1+z)^2}{H(z)\sqrt{\Omega_D(z)}} - (1+z)\frac{c}{\sqrt{\Omega_{D0}}H_0}], \end{aligned} \tag{2.56}$$

where $z = a_0/a - 1$. In all the subsequent analyses, we have marginalized the Hubble parameter H_0.

In addition to the SNe Ia data, we also use the BAO measurement from the SDSS data [24, 25]

$$A = \frac{\sqrt{\Omega_{m0}}}{E(0.35)^{1/3}}\left[\frac{1}{0.35}\int_0^{0.35}\frac{dz}{E(z)}\right]^{2/3} \tag{2.57}$$

$$= 0.469\left(\frac{0.95}{0.98}\right)^{-0.35} \pm 0.017, \tag{2.58}$$

and the CMB shift parameter measured from WMAP3 data [40, 25]

$$\mathcal{R} = \sqrt{\Omega_{m0}}\int_0^{z_{ls}}\frac{dz}{E(z)} = 1.70 \pm 0.03, \tag{2.59}$$

where the dimensionless function $E(z) = H(z)/H_0$ and $z_{ls} = 1089 \pm 1$. In order to obtain the distance, we need to find out the evolution of $\Omega_D(z)$ and $H(z)$, so we need to solve Eqs. (2.51) and (2.52) numerically. Since the derivatives in Eqs. (2.51) and

Table 2.6: The best-fit results for the HDE parameters

Model	Results	Gold	Gold+A+$\mathcal{R}$	ESSENCE	ESSENCE+A+$\mathcal{R}$
With Interaction	χ^2	158.27	158.66	195.34	196.16
	Ω_{m0}	$0.32^{+0.29}_{-0.13}$	0.29 ± 0.04	$0.27^{+0.23}_{-0.15}$	$0.27^{+0.04}_{-0.03}$
	b^2	$0^{+0.2}_{-0.0}$	$0^{+0.01}_{-0.00}$	$0.02^{+0.09}_{-0.02}$	$0.002^{+0.01}_{-0.002}$
	c	$0.82^{+0.48}_{-0.18}$	$0.88^{+0.40}_{-0.07}$	$0.85^{+0.45}_{-0.18}$	$0.85^{+0.18}_{-0.02}$
$b^2 = 0$	χ^2	158.27	158.66	195.75	196.29
	Ω_{m0}	$0.31^{+0.07}_{-0.1}$	0.29 ± 0.03	$0.27^{+0.03}_{-0.14}$	$0.27^{+0.03}_{-0.02}$
	c	$0.82^{+0.48}_{-0.04}$	$0.88^{+0.24}_{-0.06}$	$0.85^{+0.45}_{-0.02}$	$0.85^{+0.1}_{-0.02}$
ΛCDM	χ^2	158.49	161.87	195.34	196.12
	Ω_{m0}	0.34 ± 0.04	0.29 ± 0.02	0.27 ± 0.03	0.27 ± 0.02

(2.52) are with respect to $x = \ln a$, we need to rewrite them with respect to z. We find

$$\frac{dH}{dz} = -\frac{H}{1+z}\left(\frac{1}{2}\Omega_D + \frac{\Omega_D^{3/2}}{c} + \frac{3}{2}b^2 - \frac{3}{2} - \frac{1}{2}\Omega_\gamma\right), \tag{2.60}$$

and

$$\frac{d\Omega_D}{dz} = -\frac{\Omega_D}{1+z}\left[(1-\Omega_D)(1+\frac{2\sqrt{\Omega_D}}{c}) - 3b^2 + \Omega_\gamma\right]. \tag{2.61}$$

By solving numerically the above equations, we then obtain the evolutions of Ω_D and H as a function of the redshift.

In Figs. 2.1 to 2.4 we show the results of our statistical analyses. Figure 2.1 shows the $c - b^2$ plane for the joinf analysis involving the 192 ESSENCE SNe Ia data [23] and the other cosmological observables discussed above. For this analysis the best fit values are $\Omega_{m0} = 0.27^{+0.04}_{-0.03}$, $c = 0.85^{+0.18}_{-0.02}$, and $b^2 = 0.002^{+0.01}_{-0.002}$ (at 68.3% c.l.) with $\chi^2_{min} = 196.16$. If we fix $c = 1$, we find $\Omega_{m0} = 0.26^{+0.04}_{-0.03}$ and $b^2 = 0.005^{+0.008}_{-0.005}$ (at 68.3% c.l.) with $\chi^2 = 198.96$. The plane $\Omega_{m0} - c$ is shown in Fig. 2.2. Figures 2.3 and 2.4 show the same parametric space $c - b^2$ when the 192 ESSENCE data is replaced by the new 182 *gold* sample [22]. In this case, we find $\Omega_{m0} = 0.29 \pm 0.04$, $b^2 = 0^{+0.01}_{-0}$, $c = 0.88^{+0.40}_{-0.07}$ (at 68.3% c.l.) with $\chi^2 = 158.66$. We note that from both combinations the value of b^2 is very close to 0, which suggests a very weak coupling

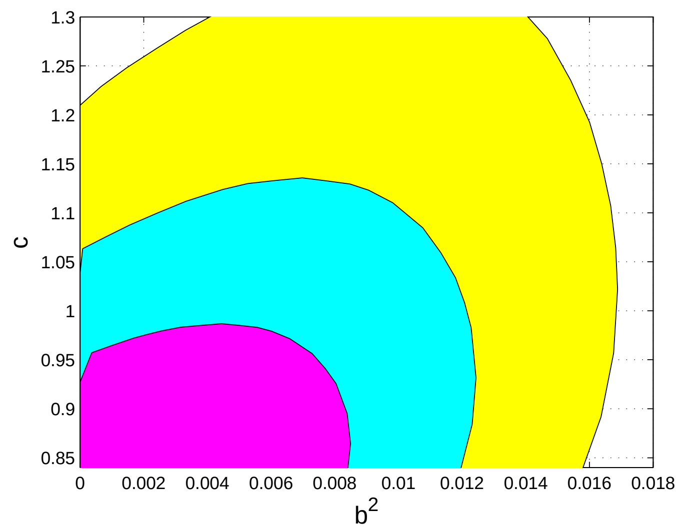

Figure 2.1: The results of our joint analysis involving the ESSENCE (192 SNe Ia) plus BAO plus CMB shift parameter. Confidence contours (1σ, 2σ and 3σ) in the $b^2 - c$ parametric space. As discussed in the text (see also Table 2.6), at 68.3% c.l. we find $c = 0.85^{+0.18}_{-0.02}$, and $b^2 = 0.002^{+0.01}_{-0.002}$.

or a noninteracting HDE. Such a result is also in agreement with the limits found in Ref. [33]. By fixing $b^2 = 0$, we also fit the HDE model without interaction to the observational data discussed above. These results are summarized in Table 2.6. For the sake of comparison, we also list the best-fit results for a flat ΛCDM model.

Finally, by fixing the value of the matter density parameter at $\Omega_{m0} = 0.27$ we show, in Fig. 2.5, the evolutions of Ω_D and ω_D with the scale factor a. The behavior of $\dot{H}/H$ is also shown in Fig. 2.6. The curves displayed in these figures are complementary in the sense that from them, we see that while ω_D crosses the cosmological constant barrier to the phantom region, $\dot{H}$ increases from negative to positive values. The distinctive future super-acceleration, which is an evidence of a phantom behavior, is apparent from Fig. 2.6.

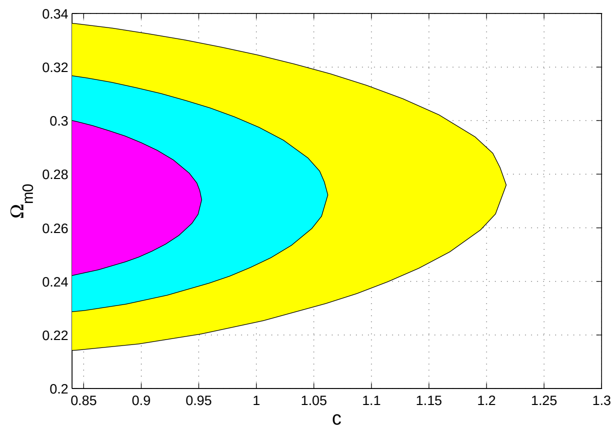

Figure 2.2: The same as in the figure 2.1 for the $c - \Omega_{m0}$ parametric plane.

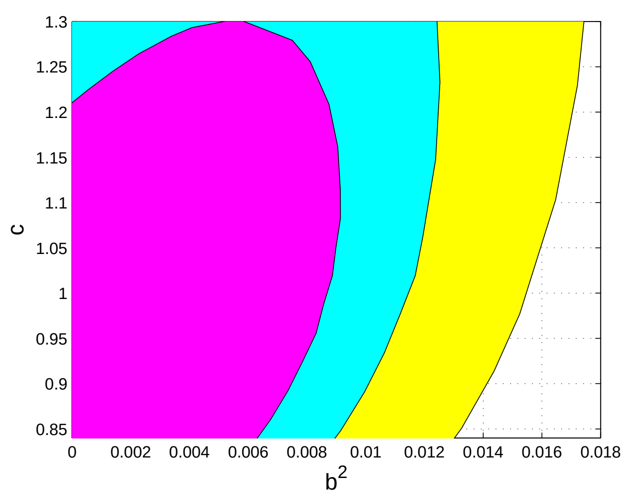

Figure 2.3: The results of our joint analysis involving the ESSENCE (192 SNe Ia) plus BAO plus CMB shift parameter. Confidence contours (1σ, 2σ and 3σ) in the $b^2 - c$ parametric space. As discussed in the text (see also Table I), at 68.3% c.l. we find $c = 0.85^{+0.18}_{-0.02}$, and $b^2 = 0.002^{+0.01}_{-0.002}$.

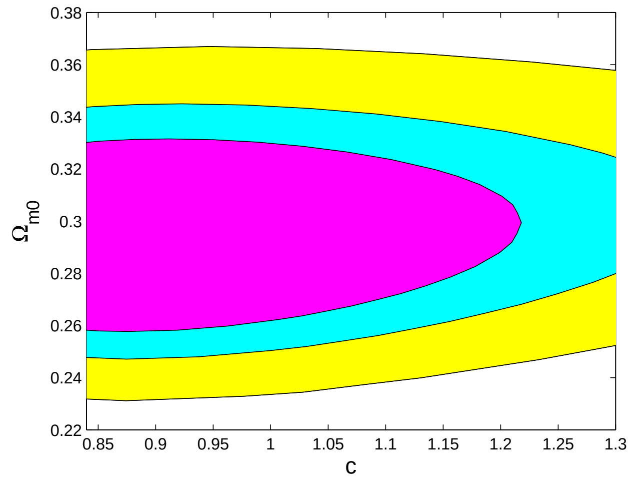

Figure 2.4: When the ESSENCE (192 SNe Ia) data are replaced by the new 182 *Gold* sample. The contours in the $c - \Omega_{m0}$ plane also correspond to 1σ, 2σ and 3σ.

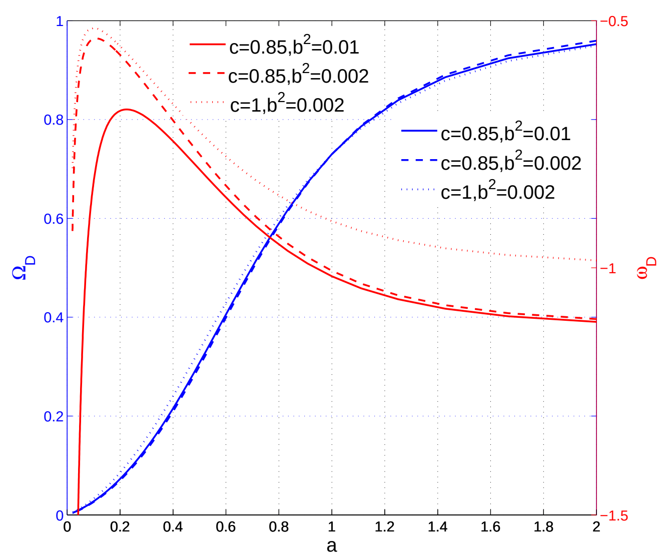

Figure 2.5: **a)** Evolution of Ω_D and ω_D with the scale factor a. To plot these curves we have fixed the best-fit value of $\Omega_{m0} = 0.27$. The solid, dashed and dotted lines stand, respectively, for the pairs ($b^2 = 0.01$, $c = 0.85$), ($b^2 = 0.002$, $c = 0.85$), and ($b^2 = 0.002$, $c = 1$).

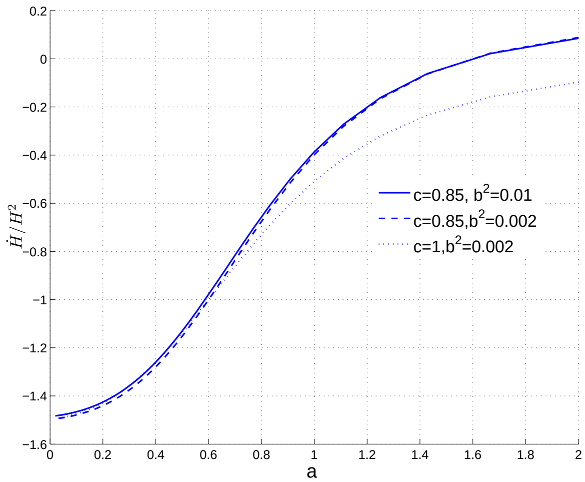

Figure 2.6: Evolution of $\dot{H}/H^2$ with the scale factor a. Note that, as ω_D is becoming more and more negative and crosses the phantom divide line (fig. 2.5), the function $\dot{H}$ increases from negative to positive values. As in the previous figure, the value of the matter density parameter has been fixed at $\Omega_{m0} = 0.27$ and the solid, dashed and dotted lines correspond to the above combinations of the parameters b^2 and c.

2.4 Monte Carlo Markov Chain Approach in Dark Energy Model

The supernova (SN) Ia observations indicate the accelerated expansion of the Universe [72, 71]. The direct and model independent evidence of the acceleration of the Universe was shown by using the energy conditions in Gong & Wang [59] and Gong et al. [60]. The driving force of the late time acceleration of the Universe, dubbed "dark energy (DE)", imposes a big challenge to theoretical physics. Although the cosmological constant is the simplest candidate of DE and consistent with current observations, other possibilities are also explored due to many orders of magnitude discrepancy between the theoretical estimation and astronomical observations for the cosmological constant. For a review of DE models, see for example, Sahni & Starobinsky [74], Padmanabhan [69], Peebles & Ratra [70], Sahni [75], Copeland et al. [47].

There are model independent studies on the nature of dark energy by using the observational data. In particular, one usually parameterizes DE density or the equation of state parameter $w(z)$ of DE [41, 42, 43, 44, 45, 46, 48, 49, 53, 54, 55, 56, 57, 58, 61, 62, 63, 64, 65, 66, 68, 76, 77, 80, 81, 82, 83, 84]. Due to the degeneracies among the parameters in the model, complementary cosmological observations are needed to break the degeneracies. The Wilkinson Microwave Anisotropic Probe (WMAP) measurement on the Cosmic Microwave Background (CMB) anisotropy, together with the SN Ia observations provide complementary data. In this paper, we use the three-year WMAP (WMAP3) data [25], the SN Ia data [73, 23] and the Baryon Acoustic Oscillation (BAO) measurement from the Sloan Digital Sky Survey [50] to study the property of DE and the cosmic curvature. Two DE models $w(z) = w_0 + w_a z/(1+z)$ [45, 68] and $w(z) = w_0 + w_a z/(1+z)^2$ [64] are considered. In Elgarøy & Multamäki [51], the authors showed that combining the shift parameters R and the angular scale l_a of the sound horizon at recombination appears to be a good approximation of the full WMAP3 data. Wang and Mukherjee gave model independent constraints on R and l_a by using the WMAP3 data, they also provided the covariance matrix of the parameters R, l_a and $\Omega_b h^2$ [79]. So we use the shift parameter R, the angular scale l_a of the sound horizon at recombination and their covariance matrix given in Wang & Mukherjee [79] instead to avoid using several inflationary model parameters and calculating the power spectrum. When the covariance matrix is used, we have six parameters. We use the Monte-Carlo Markov Chain (MCMC) method to explore the parameter space. Our MCMC code is based on the publicly available package COSMOMC [67].

2.4.1 Method

For the SN Ia data, we calculate

$$\chi^2 = \sum_i \frac{[\mu_{obs}(z_i) - \mu(z_i)]^2}{\sigma_i^2}, \tag{2.62}$$

where the extinction-corrected distance modulus $\mu(z) = 5\log_{10}[d_L(z)/\text{Mpc}] + 25$, σ_i is the total uncertainty in the SN Ia data, and the luminosity distance is

$$d_{\rm L}(z) = \frac{1+z}{H_0\sqrt{|\Omega_k|}}\text{sinn}\left[\sqrt{|\Omega_k|}\int_0^z \frac{dz'}{E(z')}\right], \tag{2.63}$$

where

$$\frac{\text{sinn}(\sqrt{|\Omega_k|}x)}{\sqrt{|\Omega_k|}} = \begin{cases} \sin(\sqrt{|\Omega_k|}x)/\sqrt{|\Omega_k|}, & \Omega_k < 0; \\ x, & \Omega_k = 0; \\ \sinh(\sqrt{|\Omega_k|}x)/\sqrt{|\Omega_k|}, & \Omega_k > 0, \end{cases} \tag{2.64}$$

the nuisance parameter H_0 is marginalized over with flat prior (the analytical marginalization method is discussed in section 2.5), and the dimensionless Hubble parameter is

$$E(z) = H(z)/H_0 = \Omega_m(1+z)^3 + \Omega_r(1+z)^4 + \Omega_k(1+z)^2 + \Omega_{DE}, \tag{2.65}$$

where $\Omega = 8\pi G\rho/(3H_0^2)$, $\rho_r = \sigma_b T_{cmb}^4$, σ_b is the Stefan-Boltzmann constant, the CMB temperature $T_{cmb} = 2.726$K, and Ω_{DE} is the DE density. For the DE model [45, 68]

$$w(z) = w_0 + \frac{w_a z}{1+z}, \tag{2.66}$$

the dimensionless DE density is

$$\Omega_{DE}(z) = (1 - \Omega_m - \Omega_k - \Omega_r)(1+z)^{3(1+w_0+w_a)}\exp[-3w_a z/(1+z)]. \tag{2.67}$$

For the DE model [64]

$$w(z) = w_0 + \frac{w_a z}{(1+z)^2}, \tag{2.68}$$

the dimensionless DE density is

$$\Omega_{DE}(z) = (1 - \Omega_m - \Omega_k - \Omega_r)(1+z)^{3(1+w_0)}\exp\left[3w_a z^2/2(1+z)^2\right]. \tag{2.69}$$

For the SDSS data, we add the BAO parameter [50, 25]

$$A = \frac{\sqrt{\Omega_m}}{0.35}\left[\frac{0.35}{E(0.35)}\frac{1}{|\Omega_k|}\text{sinn}^2\left(\sqrt{|\Omega_k|}\int_0^{0.35}\frac{dz}{E(z)}\right)\right]^{1/3} = 0.469(0.95/0.98)^{-0.35}\pm 0.017, \tag{2.70}$$

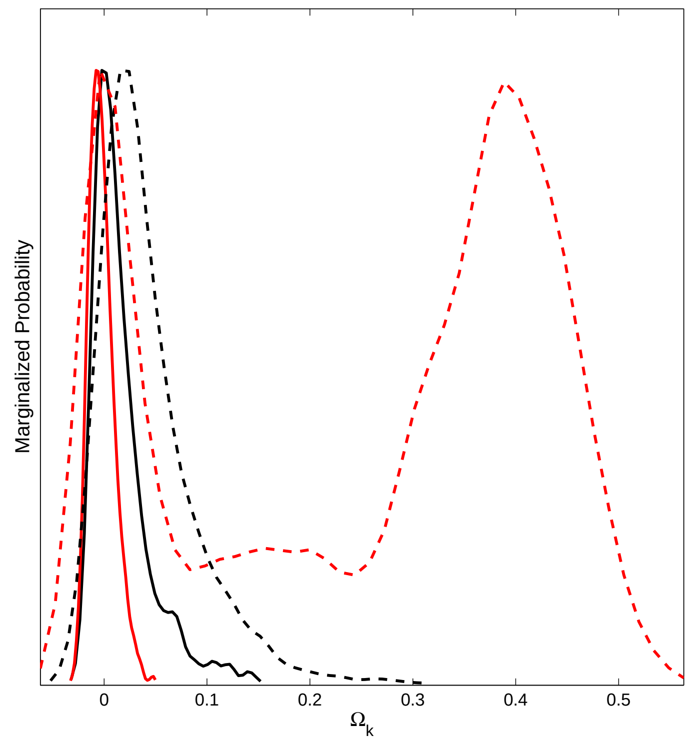

Figure 2.7: The marginalized probabilities of Ω_k. The solid lines denote the results using the shift parameter R, the angular scale l_a, and the full covariance matrix. The dashed lines denote the results using the shift parameter only. The black lines are for the dark energy model $w_0 + w_a z/(1+z)^2$ and the red lines are for the model $w_0 + w_a z/(1+z)$.

and for WMAP3 data, we first add the shift parameter [79]

$$R = \frac{\sqrt{\Omega_m}}{\sqrt{|\Omega_k|}} \mathrm{sinn}\left(\sqrt{|\Omega_k|}\int_0^{z_{ls}} \frac{dz}{E(z)}\right) = 1.71 \pm 0.03, \tag{2.71}$$

to χ^2, where $z_{ls} = 1089 \pm 1$.

When we fit the DE models (2.66) and (2.68) to the observational data, we have four parameters Ω_m, Ω_k, w_0 and w_a. The MCMC method is used to explore the parameter space. The marginalized probability of Ω_k is shown in Fig. 2.7. It is obvious that the cosmic curvature cannot be constrained for the DE model (2.66). As discussed in Elgarøy & Multamäki [51] and Wang & Mukherjee [79], the combination of the shift parameter and the angular scale of the sound horizon at recombination gives much better constraints on cosmological parameters. So we add

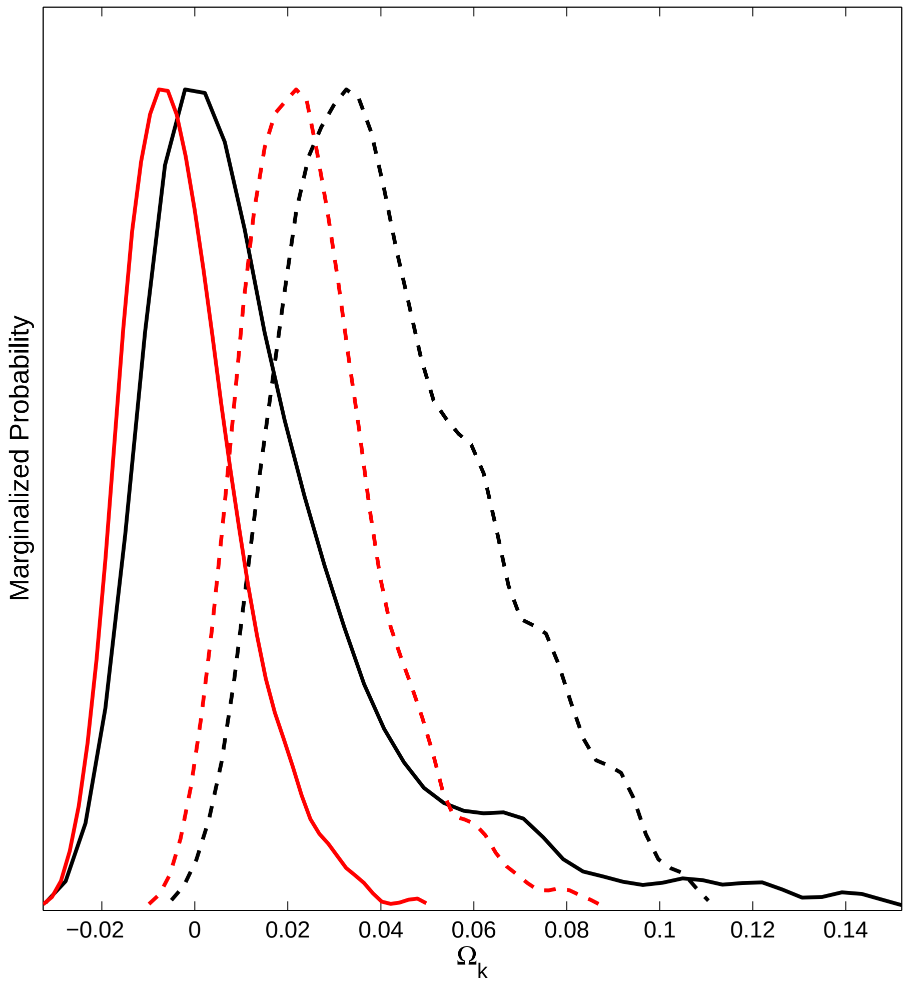

Figure 2.8: The marginalized probabilities of Ω_k. The solid lines denote the results with $H_0 = 65$. The dashed lines denote the results with $H_0 = 72$. The black lines are for the dark energy model $w_0 + w_a z/(1+z)^2$ and the red lines are for the model $w_0 + w_a z/(1+z)$.

the angular scale of the sound horizon at recombination [79]

$$l_a = \frac{\pi R/\sqrt{\Omega_m}}{\int_{z_{ls}}^{\infty} dz c_s/E(z)} = 302.5 \pm 1.2, \tag{2.72}$$

where the sound speed $c_s = 1/\sqrt{3(1+\bar{R}_b a)}$, $\bar{R}_b = 315000\Omega_b h^2 (T_{cmb}/2.7\mathrm{K})^{-4}$, a is the scale factor, and $\Omega_b h^2 = 0.02173 \pm 0.00082$ [79]. Now we have one more fitting parameter $\Omega_b h^2$. Follow Wang and Mukherjee, we also use the covariance matrix for $(R,\ l_a,\ \Omega_b h^2)$ derived in Wang & Mukherjee [79]. The marginalized probability of Ω_k is shown in Fig. 2.7. We see that the cosmic curvature is constrained better with the addition of the angular scale l_a of the sound horizon at recombination.

Since Ω_r depends on H_0, the results may depend on the value of H_0. The marginalized probabilities of Ω_k for $H_0 = 65$ km/s/Mpc and $H_0 = 72$ km/s/Mpc are shown in Fig. 2.8. We see that the results indeed depend on H_0. During the matter dominated era, the radiation term in (2.65) is negligible, so the distance modulus $\mu(z)$ and the shift parameter R do not depend on H_0 much, but the angular scale of the sound horizon at recombination l_a depends on Ω_r. As discussed in [51], the combination of R and l_a approximates the WMAP3 data and the WMAP3 data depends on H_0. So, as expected, l_a also depends on H_0. From now on we also take H_0 as a fitting parameter, and impose a prior of $H_0 = 72 \pm 8$ km/s/Mpc [52]. In summary, we have six fitting parameters for the DE models (2.66) and (2.68).

2.4.2 Results

In this section, we present our results. We first use the 182 gold SN Ia data [73], then we use the ESSENCE data [73, 23]. For the SN Ia data, we consider both the SN Ia flux averaging with marginalization over H_0 [76, 77, 80] and the analytical marginalization without the flux averaging. The results with the analytical marginalization are shown in solid lines and the results with flux averaging are shown in dashed lines. We also put the ΛCDM model with the symbol + in the contour plot.

2.4.2.1 *Gold SN Ia data* Fig. 2.9 shows the marginalized probabilities for Ω_m, Ω_k, w_0 and w_a for the DE model $w_0 + w_a z/(1+z)$. Fig. 2.10 shows the marginalized Ω_m-Ω_k and w_0-w_a contours. The w_0-w_a contour with the flux averaging is consistent with the result in Wang & Mukherjee [79]. From Figs. 2.9 and 2.10, we see that the difference in the results between the analytical marginalization and the flux averaging is small. The ΛCDM model is consistent with the observation at the 1σ level. The value of w_a is better constrained with the analytical marginalization.

Fig. 2.11 shows the marginalized probabilities for Ω_m, Ω_k, w_0 and w_a for the DE model $w_0 + w_a z/(1+z)^2$. Fig. 2.12 shows the marginalized Ω_m-Ω_k and w_0-w_a contours. From Figs. 2.11 and 2.12, we see that the parameters are a little better constrained with the flux averaging. For the analytical marginalization, the ΛCDM model is consistent with the observation at the 2σ level. For the flux averaging, the ΛCDM model is consistent with the observation at the 1σ level.

2.4.2.2 *ESSENCE data* Fig. 2.13 shows the marginalized probabilities for Ω_m, Ω_k, w_0 and w_a for the DE model $w_0 + w_a z/(1+z)$. Fig. 2.14 shows the marginalized Ω_m-Ω_k and w_0-w_a contours. From Figs. 2.13 and 2.14, we see that the difference in the results between the analytical marginalization and the flux averaging is small. The ΛCDM model is consistent with the observation at the 1σ level.

Fig. 2.15 shows the marginalized probabilities for Ω_m, Ω_k, w_0 and w_a for the DE model $w_0 + w_a z/(1+z)^2$. Fig. 2.16 shows the marginalized Ω_m-Ω_k and w_0-w_a contours. From Figs. 2.15 and 2.16, we see that the parameters are a little better constrained with the analytical marginalization. The ΛCDM model is consistent with the observation at the 1σ level.

We summarize the results in Tables 2.7 and 2.8. We do not see much improvement on the constraints on the DE parameters and the cosmic curvature by using the flux averaging method. For the DE model $w_0 + w_a z/(1+z)$, the gold data gives better constraints than the ESSENCE data on the DE parameters w_0 and w_a, but both data give good constraints on the cosmic curvature. For the DE model $w_0 + w_a z/(1+z)^2$, the ESSENCE data gives much better constraint on the cosmic curvature than the gold data, although the constraints on the DE parameters w_0 and w_a are almost the same for both data. For the 182 gold data, the DE model $w_0 + w_a z/(1+z)$ gives much better constraints on the cosmic curvature Ω_k. For the ESSENCE data, the two DE models give almost the same constraint on Ω_m and Ω_k. For the DE model $w_0 + w_a z/(1+z)$, the mean value of w_0 determined from the observation tends to be $w_0 \geq -1$, while the mean value of w_0 is less than -1 for the DE model $w_0 + w_a z/(1+z)^2$.

In conclusion, we first confirm previous results that the shift parameter R alone does not give good constraint on Ω_k, we must combine R and l_a to constrain Ω_k. By using R, l_a and their covariance matrix, we get almost the same results as those obtained by using the original WMAP3 data. Without calculating the power spectrum, the fitting process is much faster and efficient. The cosmic curvature is found to be $|\Omega_k| \leq 0.03$.

2.5 Analytical Marginalization on H_0

By assuming a flat prior $P(H_0) = 1$ for H_0, the marginalization over H_0 means

$$L = e^{-\chi_m^2/2} = \int e^{-\chi^2/2} P(H_0) dH_0 = \int e^{-\chi^2/2} dH_0. \tag{2.73}$$

Let $x = 5\log_{10} H_0$ and

$$\alpha_i = \mu_{obs}(z_i) - 25 - 5\log_{10}[(1+z_i)\mathrm{sinn}(\sqrt{|\Omega_k|}\int_0^{z_i} dz'/E(z'))/\sqrt{|\Omega_k|}], \tag{2.74}$$

and substitute Eq. (2.55) into the above Eq. (2.73), we get

$$L = \frac{\ln 10}{5} \int dx \exp\left[-\frac{1}{2}\sum_i \frac{(\alpha_i + x)^2}{\sigma_i^2} + \frac{\ln 10}{5} x\right] \tag{2.75}$$

Table 2.7: The marginalized results with 1σ errors for the model $w_0 + w_a z/(1+z)$

	Gold Data		Essence Data	
	Analytical	Flux	Analytical	Flux
Ω_m	$0.29^{+0.03}_{-0.02}$	0.29 ± 0.02	$0.28^{+0.03}_{-0.02}$	0.28 ± 0.02
Ω_k	$0.007^{+0.023}_{-0.019}$	0.002 ± 0.018	-0.007 ± 0.016	$-0.004^{+0.015}_{-0.016}$
w_0	$-0.99^{+0.18}_{-0.16}$	-0.95 ± 0.22	-0.94 ± 0.25	$-1.0^{+0.24}_{-0.26}$
w_a	0.34 ± 0.77	$-0.05^{+1.04}_{-1.09}$	$-0.70^{+1.54}_{-1.52}$	$-0.26^{+1.29}_{-1.31}$

Table 2.8: The marginalized results with 1σ errors for the model $w_0 + w_a z/(1+z)^2$

	Gold Data		Essence Data	
	Analytical	Flux	Analytical	Flux
Ω_m	$0.27^{+0.03}_{-0.02}$	$0.27^{+0.03}_{-0.02}$	$0.28^{+0.02}_{-0.03}$	0.29 ± 0.02
Ω_k	0.05 ± 0.04	$0.02^{+0.03}_{-0.02}$	$-0.002^{+0.015}_{-0.016}$	-0.013 ± 0.011
w_0	$-1.8^{+0.6}_{-0.5}$	$-1.6^{+0.6}_{-0.5}$	-1.1 ± 0.4	$-1.1^{+0.4}_{-0.5}$
w_a	6.4 ± 3.6	4.5 ± 3.6	0.5 ± 3.1	0.6 ± 3.3

$$= \frac{\ln 10}{5} \int dx \exp\left[-\frac{1}{2} \left(\sum_i \frac{1}{\sigma_i^2} \right) \left(x + \frac{\sum_i \alpha_i/\sigma_i^2 - \ln 10/5}{\sum_i 1/\sigma_i^2} \right)^2 \right. \tag{2.76}$$

$$\left. -\frac{1}{2} \sum_i \frac{\alpha_i^2}{\sigma_i^2} + \frac{1}{2} \frac{(\sum_i \alpha_i/\sigma_i^2 - \ln 10/5)^2}{\sum_i 1/\sigma_i^2} \right] \tag{2.77}$$

$$= \frac{\ln 10}{5} \left(\frac{2\pi}{\sum_i 1/\sigma_i^2} \right)^{1/2} \exp\left[-\frac{1}{2} \sum_i \frac{\alpha_i^2}{\sigma_i^2} + \frac{1}{2} \frac{(\sum_i \alpha_i/\sigma_i^2 - \ln 10/5)^2}{\sum_i 1/\sigma_i^2} \right]. \tag{2.78}$$

So the minimum χ^2 is

$$\chi_m^2 = \sum_i \frac{\alpha_i^2}{\sigma_i^2} - \frac{(\sum_i \alpha_i/\sigma_i^2 - \ln 10/5)^2}{\sum_i 1/\sigma_i^2} - 2 \ln \left(\frac{\ln 10}{5} \sqrt{\frac{2\pi}{\sum_i 1/\sigma_i^2}} \right). \tag{2.79}$$

In analysis of 2.3.2, and we marginalized the Hubble parameter H_0 with flat prior. In analysis of 2.4.1, we marginalized the H_0 for distance modulus and shift parameter which do not depends on H_0 much, however take H_0 as a fitting parameter for angular scale of the sound horizon at recombination l_a which depend on H_0.

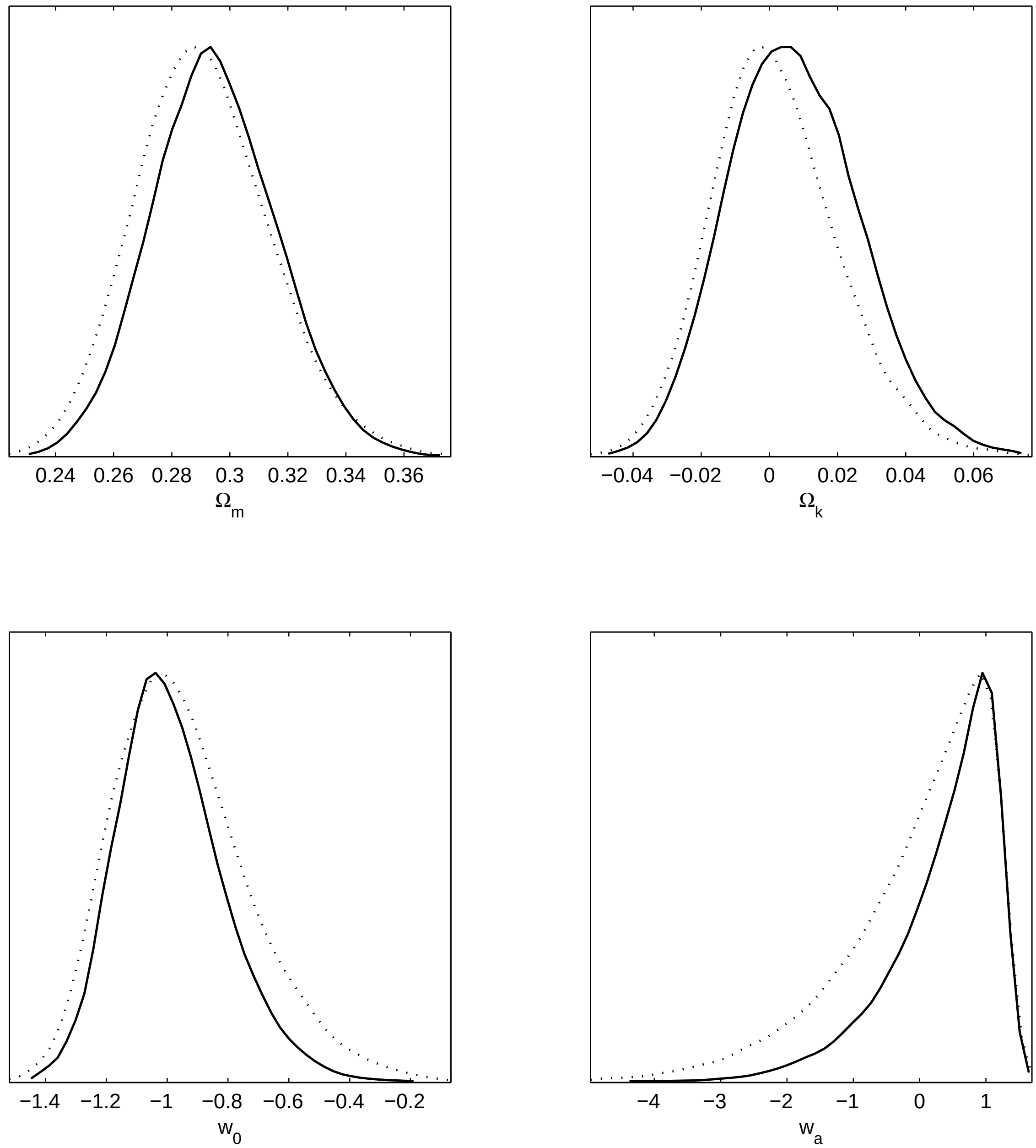

Figure 2.9: The marginalized probabilities for the DE model $w_0 + w_a z/(1+z)$ by using the gold SN Ia data. The solid lines denote the results with analytical marginalization and the dashed lines denote the results with flux averaging.

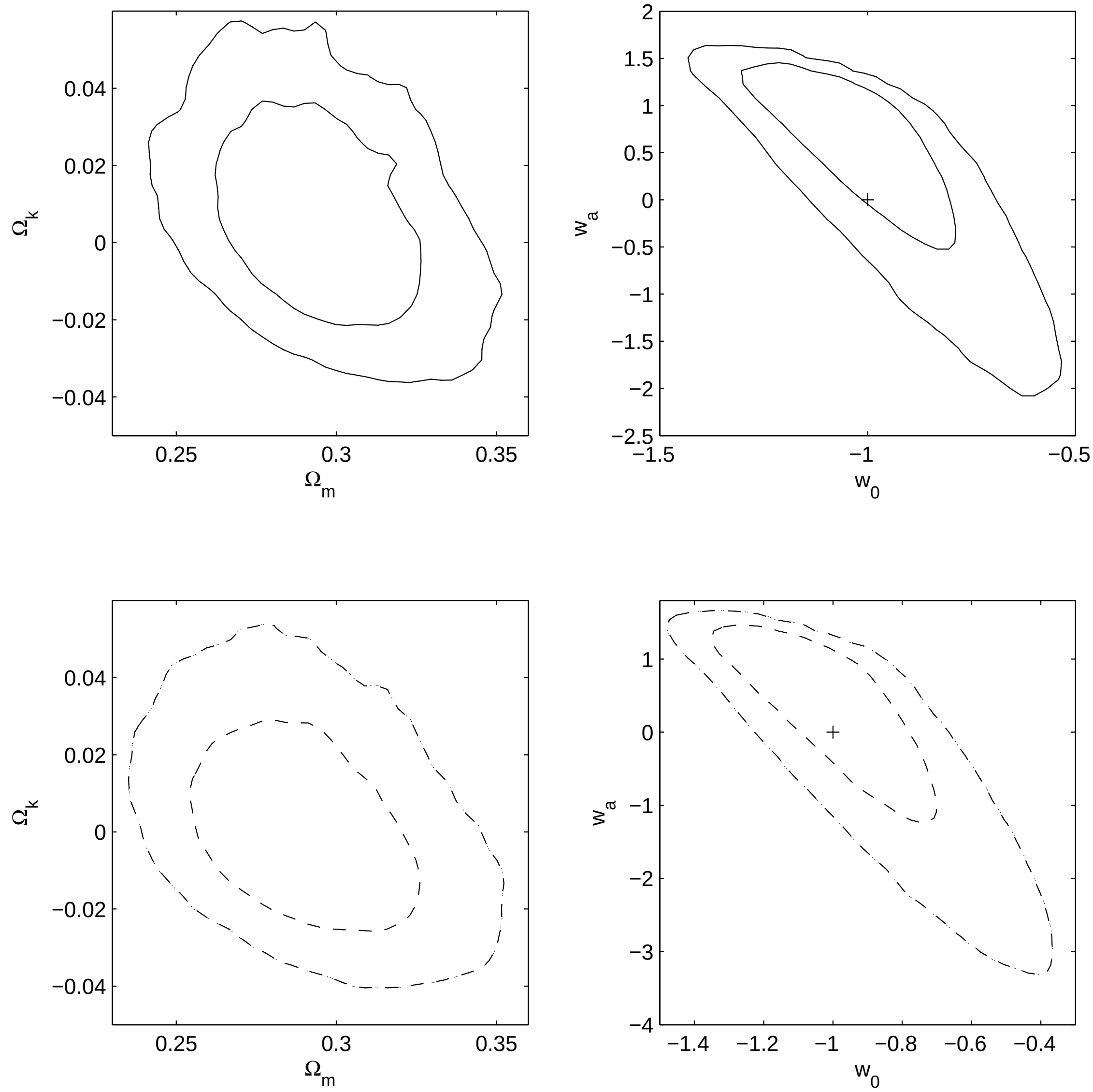

Figure 2.10: The marginalized 1σ and 2σ Ω_m-Ω_k and w_0-w_a contours for the DE model $w_0 + w_a z/(1+z)$ by using the gold SN Ia data. The upper panels denote the results with analytical marginalization and the lower panels denote the results with flux averaging.

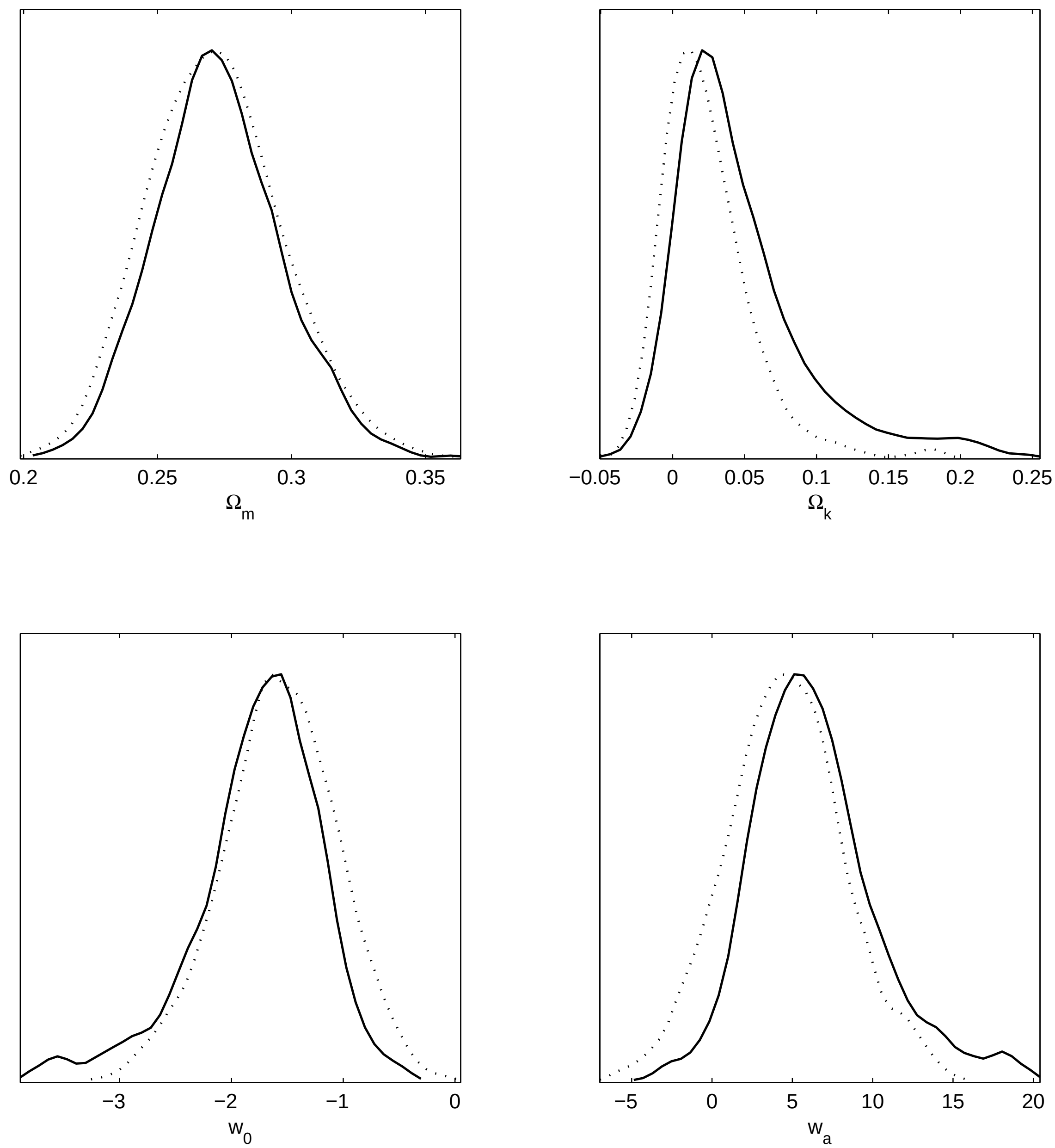

Figure 2.11: The marginalized probabilities for the DE model $w_0 + w_a z/(1+z)^2$ by using the gold SN Ia data. The solid lines denote the results with analytical marginalization and the dashed lines denote the results with flux averaging.

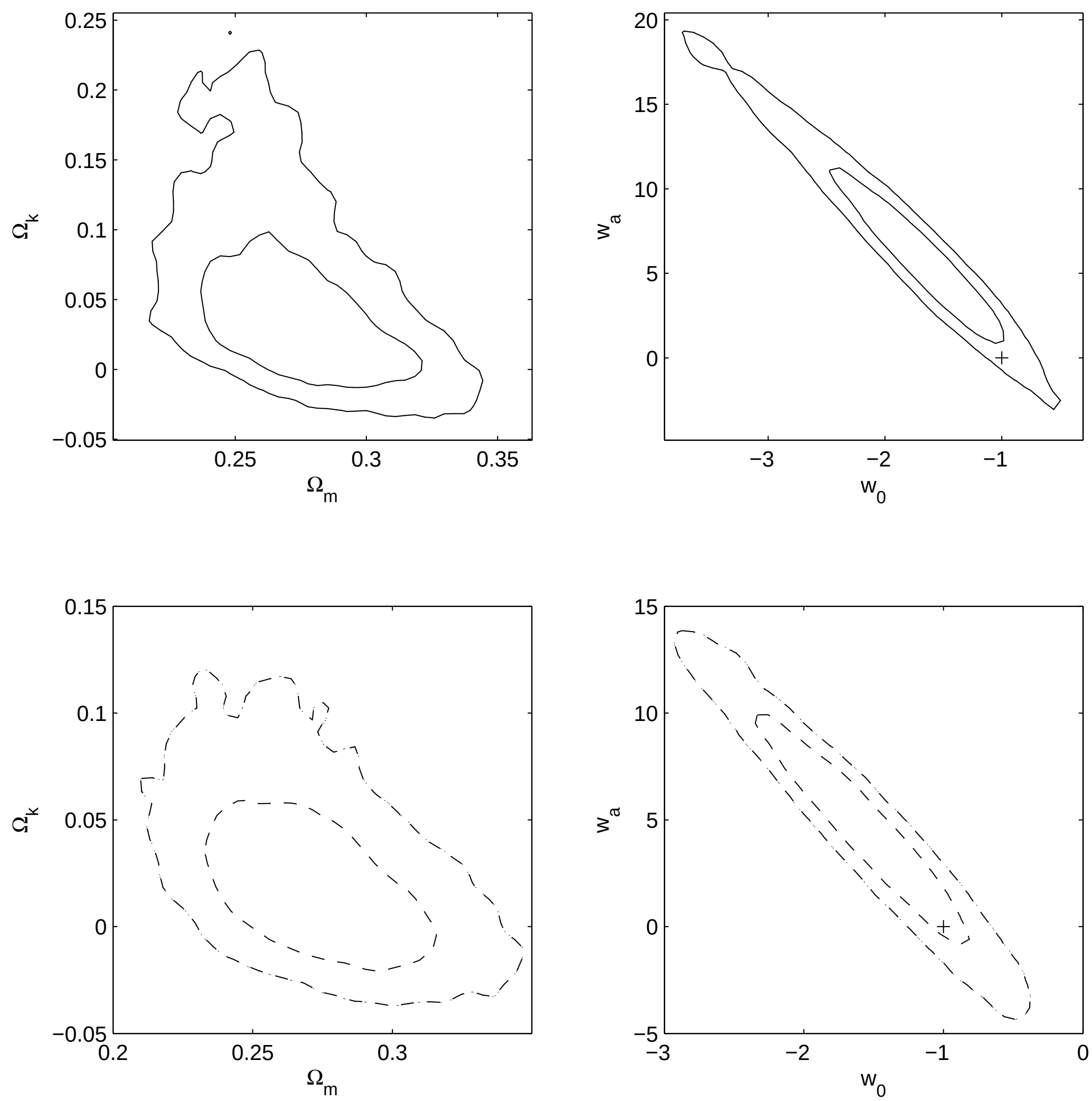

Figure 2.12: The marginalized 1σ and 2σ Ω_m-Ω_k and w_0-w_a contours for the DE model $w_0 + w_a z/(1+z)^2$ by using the gold SN Ia data. The upper panels denote the results with analytical marginalization and the lower panels denote the results with flux averaging.

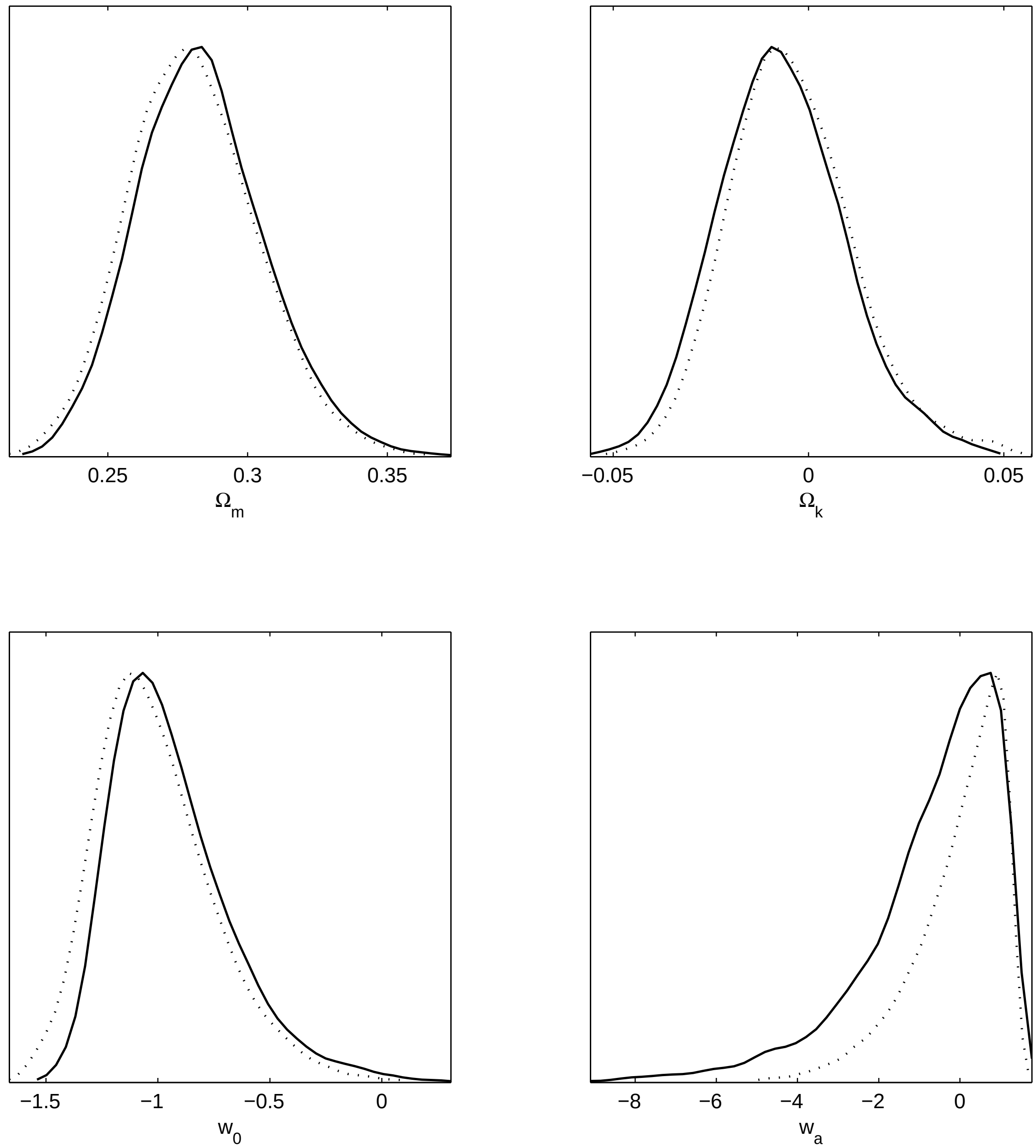

Figure 2.13: The marginalized probability distributions for the dark energy model $w_0 + w_a z/(1+z)$ by using the ESSENCE data. The solid lines denote the results without flux average and the dashed lines denote the results with flux average.

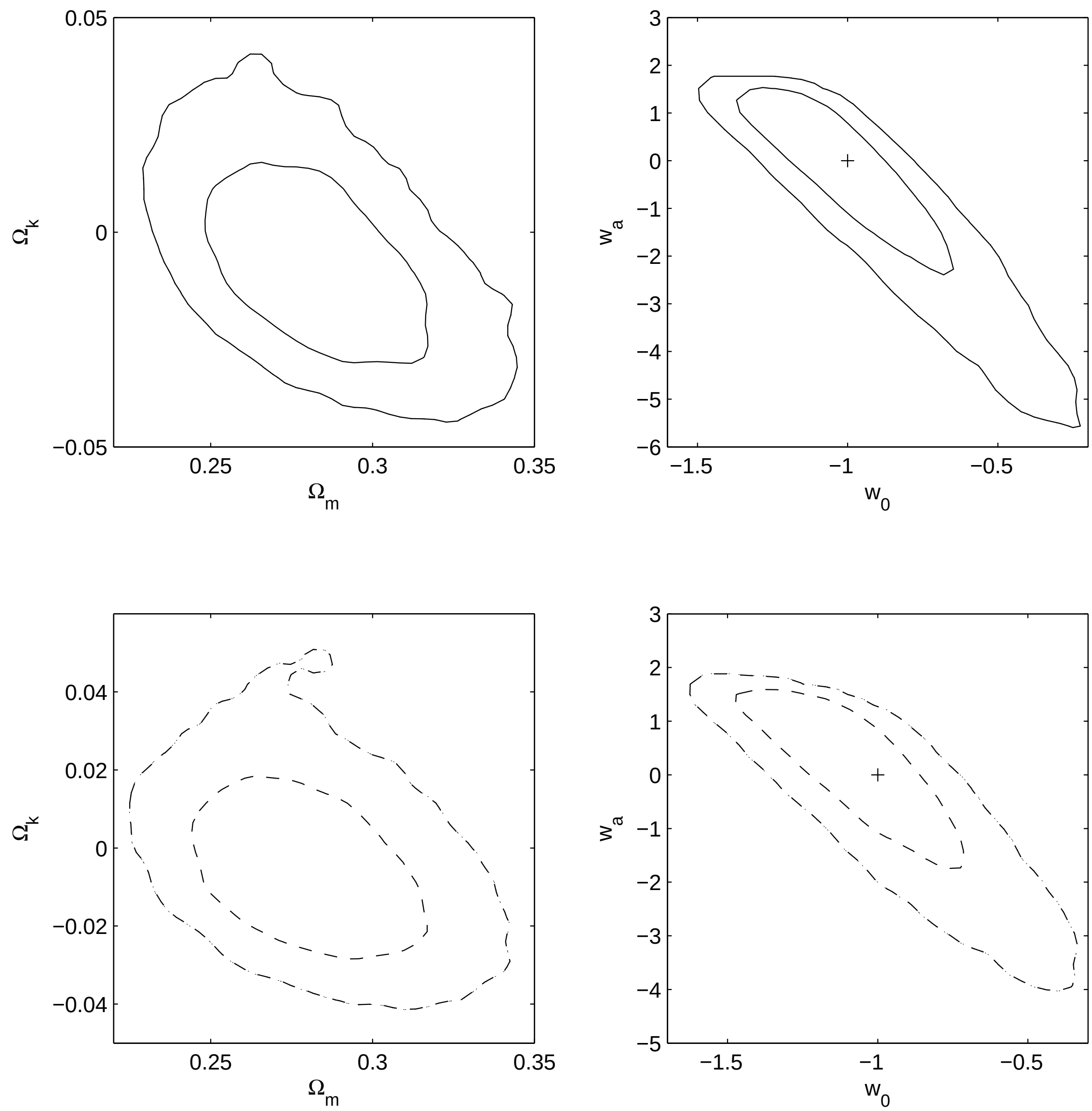

Figure 2.14: The marginalized Ω_m-Ω_k and w_0-w_a contours for the dark energy model $w_0 + w_a z/(1+z)$ by using the ESSENCE data. The upper panels denote the results without flux average and the lower panels denote the results with flux average.

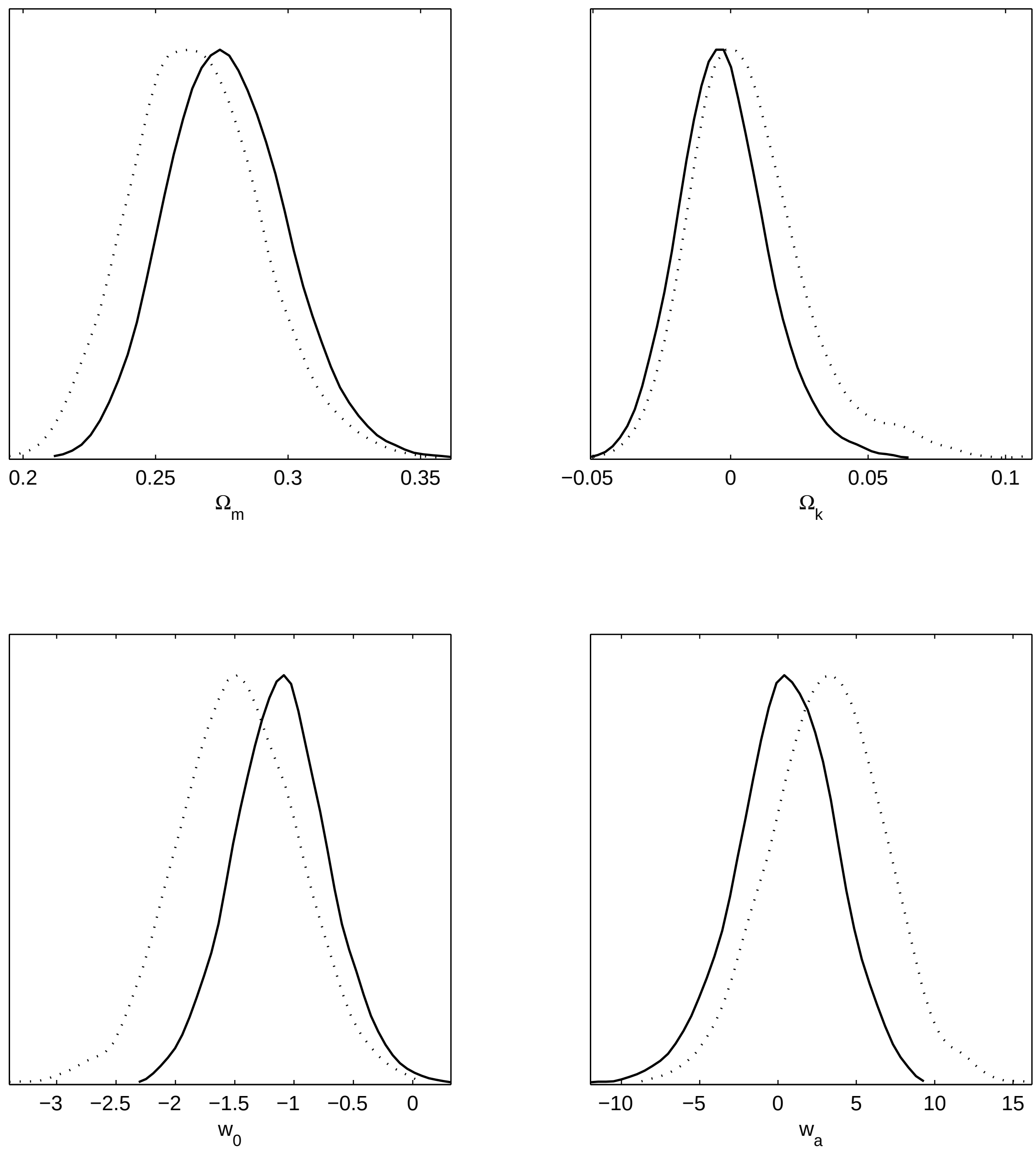

Figure 2.15: The marginalized probability distributions for the dark energy model $w_0 + w_a z/(1+z)^2$ by using the ESSENCE data. The solid lines denote the results without flux average and the dashed lines denote the results with flux average.

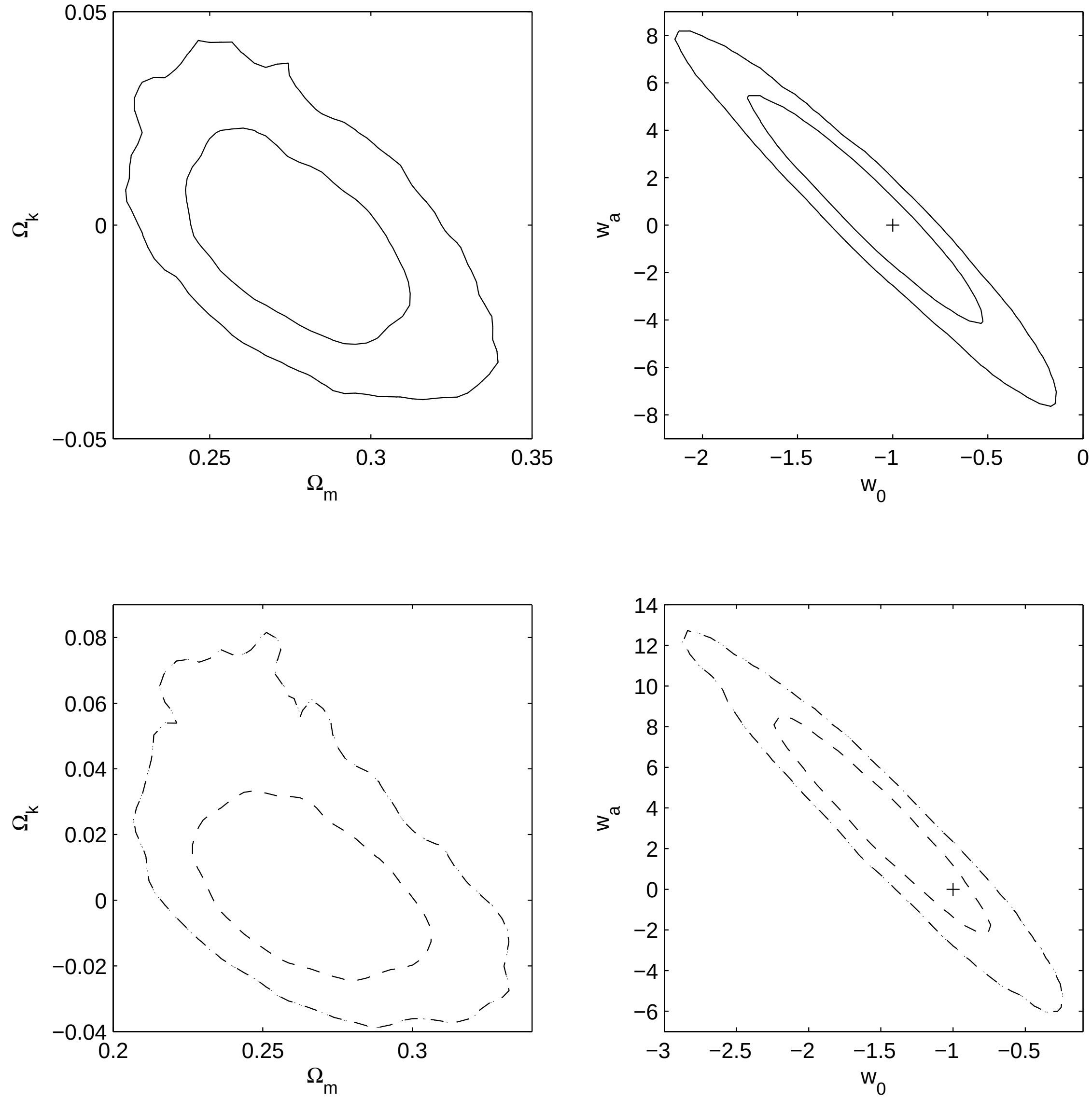

Figure 2.16: The marginalized Ω_m-Ω_k and w_0-w_a contours for the dark energy model $w_0 + w_a z/(1+z)^2$ by using the ESSENCE data. The upper panels denote the results without flux average and the lower panels denote the results with flux average.

CHAPTER THREE

Brane Cosmology in the Hořava-Witten Heterotic M-Theory on S^1/Z_2

Since the cosmological constant problem is intimately related to quantum gravity, its solution is expected to come from quantum gravity, too. At the present, string/M-Theory is our best bet for a consistent quantum theory of gravity, so it is reasonable to ask what string/M-Theory has to say about the cosmological constant. In the string landscape [96], it is expected there are many different vacua with different local cosmological constants [97]. Using the anthropic principle, one may select the low energy vacuum in which we can exist. However, many theorists still hope to explain the problem without invoking the existence of ourselves. In addition, to have a late time accelerating universe from string/M-Theory, Townsend and Wohlfarth [98] invoked a time-dependent compactification of pure gravity in higher dimensions with hyperbolic internal space to circumvent Gibbons' non-go theorem [99]. Their exact solution exhibits a short period of acceleration. The solution is the zero-flux limit of spacelike branes [100]. If non-zero flux or forms are turned on, a transient acceleration exists for both compact internal hyperbolic and flat spaces [101]. Other accelerating solutions by compactifying more complicated time-dependent internal spaces can be found in [102].

In this chapter, I will give a very brief introduce to sting/M-theory and then provide a systematical study of brane worlds in the framework of both the Hořava-Witten (HW) heterotic M-Theory and string theory on S^1/Z_2 [104, 110]. We first address two important issues, which are fundamental in order for the model to be viable: (i) the radion stability and its mass; and (ii) the localization of gravity, the 4D effective Newtonian potential and its corrections from the high order gravitational KK modes. Then, we apply the model to cosmology, and write down explicitly the general gravitational and matter field equations both in the bulk and on the two branes.

In particular, this chapter is organized as follows: In Sec. 3.1 I shall give a brief introduction to string and M-theory. In Sec. 3.2, we consider the HW heterotic M-Theory on S^1/Z_2 along the line set up by Lukas *et al.* in [110]. To consider its cosmological applications, we add a potential term and matter fields on each of the two branes. In Sec. 3.3, we consider the radion stability and radion mass, using the Goldberger-Wise mechanism [109]. In Sec. 3.4, we study the localization of gravity and calculate the 4-dimensional effective Newtonian potential. The spectrum of gravitational Kaluza-Klein (KK) modes is worked out explicitly, and found to be discrete and can have a mass gap of TeV. In Sec. 3.5, applying the model to cosmology, we separate the gravitational and matter field equations into two group, one holds outside of the two branes, and one holds on each of the two branes. In particular, we find the most general generalized Friedmann-like equations on each of the two orbifold branes. The chapter is ended with Sec. 3.6, in which we apply the formulas developed in previous sections to a particular case.

It should be noted that brane worlds have been studied intensively in the past decade [114]. However, to our best knowledge, such studies in the HW setup have not been carried out in details [111].

It is also interesting to note that in 4-dimensional spacetimes there exists Weinberg's no-go theorem for the adjustment of the cosmological constant [144]. However, in higher dimensional spacetimes, the 4-dimensional vacuum energy on the brane does not necessarily give rise to an effective 4-dimensional cosmological constant. Instead, it may only curve the bulk, while leaving the brane still flat [112], whereby Weinberg's no-go theorem is evaded. It was exactly in this vein, the cosmological constant problem was studied in the framework of brane worlds in 5-dimensional spacetimes [113] and 6-dimensional supergravity [115]. However, it was soon found that in the 5-dimensional case hidden fine-tunings are required [116]. In the 6-dimensional case such fine-tunings may not be needed, but it is still not clear whether loop corrections can be as small as expected [117, 118].

3.1 Introduction to String/M-Theory

The standard model of particle physics was designed within a framework known as *quantum field theory* (QFT), which gives us the tools to build theories consistent both with quantum mechanics and the special theory of relativity. This theory includes three of the four known interactions in the nature: electromagnetic interactions, strong and weak interactions. Furthermore a combined electorweak theory was achieved, and promising ideas put forward to try to include the strong interactions. But unfortunately, the standard model does not include the effects of the fourth interaction, gravity, which has been described by Einstein's general relativity successfully.

The bosonic string theory, which the myriad of particle types is represented by a single fundamental building block, a *'string'*, is the first candidate for the theory of everything. This theory described all the known natural forces including gravitational interactions and matter (bosons) in a mathematically complete system. By introducing supersymmetry to bosonic string theory, we can obtain a new theory that describes both the forces and the matter which make up the universe. This is the *superstring theory*. Prior to 1995 there were five known consistent superstring theories, which were give the names *Type I string theory*, *Type IIA string theory*, *Type IIB string theory*, *heterotic SO(32) theory (the HO theory)*, and *heterotic E8× E8 theory (the HE theory)*. In 1995 an underlying 11-dimensional theory called M-theory appear [86]. This theory encompasses all five, anomaly free, 10-dimensional superstring theories, so that in this sense, no particular string theory is necessarily more fundamental than any of the others.

Hořava and Witten identified the strongly coupled $E_8 \times E_8$ heterotic string as the 11-dimensional limit of M-theory compactified on an S^1/Z_2 orbifold with a set of E_8 gauge fields at each 10-dimensional orbifold fixed plane. The orbifold S^1/Z_2 may be viewed as a segment of the real line that is bounded by two fixed points on the circle. The Z_2 reverses the orientation of the circle, $y \to -y$, where y is the 11th dimension coordinate [87]. Motivated by Hořava Witten theory, Lukas et al. derived an effective 5-dimensional theory by a direct compactification of the HW theory on a Calabi-Yau space [110].

3.2 General Formula Devolvement

Let us consider the 11-dimensional spacetime of the Horava-Witten heterotic M-Theory, described by the metric [110],

$$ds_{11}^2 = V^{-2/3} g_{ab} dx^a dx^b - V^{1/3} \Omega_{ij} dz^i dz^j, \tag{3.1}$$

where $ds_{CY,6}^2 \equiv \Omega_{ij} dz^i dz^j$ denotes the Calabi-Yau 3-fold, and V is the Calabi-Yau volume modulus that measures the deformation of the Calabi-Yau space, and depends only on x^a, where $a = 0, 1, ..., 4$.

3.2.1 5-Dimensional Effective Actions

By integrating the corresponding 11-dimensional action over Calabi-Yau 3-fold, the 5-dimensional effective action of the Horava-Witten theory is given by [110]

$$\begin{aligned} S_5 &= -\frac{1}{2\kappa_5^2} \int_{M_5} \sqrt{g} \left(R[g] - \frac{1}{2} (\nabla \phi)^2 + 6\alpha^2 e^{-2\phi} \right) \\ &\quad - \sum_{I=1}^{2} \epsilon_I \frac{6\alpha}{\kappa_5^2} \int_{M_4^{(I)}} \sqrt{-g^{(I)}} e^{-\phi}, \end{aligned} \tag{3.2}$$

where $I = 1,\ 2,\ \epsilon_1 = -\epsilon_2 = 1$, ∇ denotes the covariant derivative with respect to g_{ab}, and

$$\phi \equiv \ln(V), \quad \kappa_5^2 \equiv \frac{\kappa_{11}^2}{v_{CY,6}}, \tag{3.3}$$

with $v_{CY,6}$ being the volume of the Calabi-Yau space,

$$v_{CY,6} \equiv \int_X \sqrt{\Omega}. \tag{3.4}$$

The constant α is related to the internal four-form that has to be included in the dimensional reduction [110]. This four-form results from the source terms in the 11-dimensional Bianchi identity, which are usually non-zero. $g^{(I)}$'s are the reduced metrics on the two boundaries $M_4^{(I)}$.

It should be noted that in general the dimensional reduction of the graviton and the four-form flux generates a large number of fields [110]. However, it is consistent to set all the fields zero except for the 5-dimensional graviton and the volume modulus. This setup implies that all components of the four-form now point in the Calabi-Yau directions [111]. In addition, it can be shown that the above action is indeed the bosonic sector of a minimal $\mathcal{N} = 1$ gauged supergravity theory in 5-dimensional spacetimes coupled to chiral boundary theories [119].

To study cosmology in the above setup, we add matter fields on each of the two branes [88, 103],

$$\begin{aligned} S_{4,\,m}^{(I)} \;=\; & \int_{M_4^{(I)}} \sqrt{-g^{(I)}} \left[\mathcal{L}_{4,m}^{(I)} \left(\phi, \chi\right) \right. \\ & \left. - \left(g_k^{(I)} + V_4^{(I)}(\phi)\right)\right], \end{aligned} \tag{3.5}$$

where χ collectively denotes the SM fields localized on the branes, $V_4^{(I)}(\phi)$ and $g_k^{(I)}$ are, respectively, the potential of the scalar field and the tension of the I-th brane. As to be shown below, $g_k^{(I)}$ is directly related to the four-dimensional Newtonian constant G_4 [120]. Clearly, these actions in general make the two branes no longer supersymmetric, although the bulk still is.

It should be noted that in general one also needs to include the Gibbons-Hawking boundary term [121] in the action (3.5) [122]. However, here we work with the so-called upstars picture of the S^1/Z_2 orbifold [123], where all total derivatives integrate to zero, while the boundary conditions are obtained by imposing the Lanczos equations [156], as was done earlier by Israel [124].

Variation of the action,

$$S_5^{total} = S_5 + \sum_{I=1}^{2} S_{4,\, m}^{(I)}, \tag{3.6}$$

with respect to g_{ab} yields the field equations,

$$G_{ab}^{(5)} = \kappa_5^2 T_{ab}^{(5,\, \phi)} + \kappa_5^2 \sum_{I=1}^{2} \mathcal{T}_{\mu\nu}^{(I)} e_a^{(\mu)} e_b^{(\nu)} \sqrt{\left|\frac{g^{(I)}}{g}\right|}\, \delta\left(\Phi_I\right), \tag{3.7}$$

where $T_{ab}^{(5,\, \phi)}$ and $\mathcal{T}_{\mu\nu}^{(I)}$'s are the energy-momentum tensors of the bulk and branes, respectively, and are given by

$$\begin{aligned}
\kappa_5^2 T_{ab}^{(5,\, \phi)} &\equiv \frac{1}{2}\left(\nabla_a \phi\right)\left(\nabla_b \phi\right) \\
&\quad -\frac{1}{4} g_{ab}\left[\left(\nabla\phi\right)^2 - 12\alpha^2 e^{-2\phi}\right], && (3.8)\\
\mathcal{T}_{\mu\nu}^{(I)} &\equiv \left(\tau_\phi^{(I)} + g_k^{(I)}\right) g_{\mu\nu}^{(I)} + \tau_{\mu\nu}^{(I)}, && (3.9)\\
\tau_{\mu\nu}^{(I)} &\equiv 2\frac{\delta \mathcal{L}_{4,\, m}^{(I)}}{\delta g^{(I)\, \mu\nu}} - g_{\mu\nu}^{(I)} \mathcal{L}_{4,\, m}^{(I)}, && (3.10)\\
\tau_\phi^{(I)} &\equiv 6\epsilon_I \alpha \kappa_5^{-2} e^{-\phi} + V_4^{(I)}(\phi), && (3.11)\\
e_{(\mu)}^{(I)a} &\equiv \frac{\partial x^a}{\partial \xi_{(I)}^{\mu}}, && (3.12)\\
g_{\mu\nu}^{(I)} &\equiv e_{(\mu)}^{(I)\, a} e_{(\nu)}^{(I)\, b} g_{ab}\Big|_{M_4^{(I)}}, && (3.13)
\end{aligned}$$

where $\xi_{(I)}^{\mu}$ $(\mu = 0, 1, 2, 3)$ are the intrinsic coordinates on the orbifold branes. $\delta\left(\Phi_I\right)$ denotes the Dirac delta function, normalized in the sense of [125]. The two orbifold branes are located on the hypersurfaces,

$$\Phi_I\left(x^a\right) = 0,\ (I = 1, 2), \tag{3.14}$$

from which we find that the normal vector to the I-th brane is given by

$$n_a^{(I)} = \frac{1}{N^{(I)}} \frac{\partial \Phi_I(x)}{\partial x^a}, \tag{3.15}$$

where

$$N^{(I)} \equiv \sqrt{|\Phi_{I,c}\Phi_I^{;c}|}. \tag{3.16}$$

It is interesting to note that the contribution of the modulus field to the branes acts as a varying cosmological constant, as can be seen clearly from Eqs. (3.9) and (3.11).

Variation of the total action (3.6) with respect to ϕ, on the other hand, yields the generalized Klein-Gordon equation,

$$\Box\phi = 12\alpha^2 e^{-2\phi} + \sum_{I=1}^{2}\left(12\alpha\epsilon_I e^{-\phi} - 2\kappa_5^2\frac{\partial V_4^{(I)}}{\partial\phi} - \sigma_\phi^{(I)}\right)\sqrt{\left|\frac{g^{(I)}}{g}\right|}\,\delta\left(\Phi_I\right), \tag{3.17}$$

where $\Box \equiv g^{ab}\nabla_a\nabla_b$, and

$$\sigma_\phi^{(I)} \equiv -2\kappa_5^2\,\frac{\delta\mathcal{L}_{4,\,m}^{(I)}}{\delta\phi}. \tag{3.18}$$

Note the difference signs of $\sigma_\phi^{(I)}$ defined here and the one used in [103].

To solve Eqs. (3.7) and (3.17), it is found convenient to separate them into two groups: one is defined outside the two orbifold branes, and the other is defined on the two branes.

3.2.2 Field Equations Outside the Two Branes

To obtain the equations outside the two orbifold branes is straightforward, and they are simply the 5-dimensional Einstein field equations (3.7), and the matter field equation Eq. (3.17) without the delta function parts,

$$\begin{aligned} G_{ab}^{(5)} &= \frac{1}{2}\left(\nabla_a\phi\right)\left(\nabla_b\phi\right) \\ &\quad -\frac{1}{4}g_{ab}\left[\left(\nabla\phi\right)^2 - 12\alpha^2 e^{-2\phi}\right], \end{aligned} \tag{3.19}$$

$$\Box\phi = 12\alpha^2 e^{-2\phi}. \tag{3.20}$$

Therefore, in the rest of this section, we shall concentrate ourselves on the derivation of the field equations on the branes.

3.2.3 Field Equations on the Two Orbifold Branes

To obtain the field equations on the two orbifold branes, one can follow two different approaches: (1) First express the delta function parts in the left-hand sides of Eqs. (3.7) and (3.17) in terms of the discontinuities of the first derivatives of the metric coefficients and matter fields, and then equal the corresponding delta function parts in the right-hand sides of these equations, as shown systematically in [126]. (2) The second approach is to use the Gauss-Codacci and Lanczos equations to write down the 4-dimensional gravitational field equations on the branes [127, 128]. It should be noted that these two approaches are equivalent and complementary one to the other. In this paper, we follow the second approach to obtain the gravitational field equations, and the first approach to obtain the matter field equations on the two branes.

3.2.3.1 *Gravitational field equations on the two branes* For a timelike brane, the 4-dimensional Einstein tensor $G^{(4)}_{\mu\nu}$ can be written as [127, 128, 108],

$$G^{(4)}_{\mu\nu} = \mathcal{G}^{(5)}_{\mu\nu} + E^{(5)}_{\mu\nu} + \mathcal{F}^{(4)}_{\mu\nu}, \tag{3.21}$$

with

$$\begin{aligned}
\mathcal{G}^{(5)}_{\mu\nu} &\equiv \frac{2}{3}\Big\{G^{(5)}_{ab}e^{a}_{(\mu)}e^{b}_{(\nu)} \\
&\quad - \left[G_{ab}n^a n^b + \frac{1}{4}G^{(5)}\right]g_{\mu\nu}\Big\}, \\
E^{(5)}_{\mu\nu} &\equiv C^{(5)}_{abcd}n^a e^{b}_{(\mu)}n^c e^{d}_{(\nu)}, \\
\mathcal{F}^{(4)}_{\mu\nu} &\equiv K_{\mu\lambda}K^{\lambda}_{\nu} - KK_{\mu\nu} \\
&\quad -\frac{1}{2}g_{\mu\nu}\left(K_{\alpha\beta}K^{\alpha\beta} - K^2\right),
\end{aligned} \tag{3.22}$$

where $G^{(5)} \equiv g^{ab}G^{(5)}_{ab}$, and $C^{(5)}_{abcd}$ the Weyl tensor. The extrinsic curvature $K_{\mu\nu}$ is defined as

$$K_{\mu\nu} \equiv e^{a}_{(\mu)}e^{b}_{(\nu)}\nabla_a n_b. \tag{3.23}$$

A crucial step of this approach is the Lanczos equations [156],

$$\left[K^{(I)}_{\mu\nu}\right]^{-} - g^{(I)}_{\mu\nu}\left[K^{(I)}\right]^{-} = -\kappa_5^2\mathcal{T}^{(I)}_{\mu\nu}, \tag{3.24}$$

where

$$\begin{aligned} \left[K^{(I)}_{\mu\nu}\right]^{-} &\equiv \lim_{\Phi_I\to 0^+}K^{(I)\,+}_{\mu\nu} - \lim_{\Phi_I\to 0^-}K^{(I)\,-}_{\mu\nu}, \\ \left[K^{(I)}\right]^{-} &\equiv g^{(I)\,\mu\nu}\left[K^{(I)}_{\mu\nu}\right]^{-}. \end{aligned} \tag{3.25}$$

On the other hand, from the Codacci equation, one finds [128, 108]

$$G^{(5)}_{ab}n^{(I)a}e^{(I)b}_{(\mu)} = \left(K^{(I)\,\mu}_{\nu} - \delta^{\mu}_{\nu}K^{(I)}\right)_{;\mu}, \tag{3.26}$$

where a semicolon ";" denotes the covariant derivative with respect to the reduced metric $g^{(I)}_{\mu\nu}$. The combination of Eqs. (3.24) and (3.26) yields the conservation law,

$$\left[G^{(5)}_{ab}n^{(I)a}e^{(I)b}_{(\mu)}\right]^{-} = -\kappa_5^2\mathcal{T}^{(I)\lambda}{}_{\mu;\lambda}. \tag{3.27}$$

Since $n^{(I)a}e^{(I)\,b}_{(\mu)}g_{ab} = 0$, from Eqs. (3.7), (3.8), and (3.27), we find

$$\mathcal{T}^{(I)\lambda}{}_{\mu;\lambda} = -\frac{1}{2\kappa_5^2}\left[\phi_{,n}\phi_{,\mu}\right]^{-}, \tag{3.28}$$

where $\phi_{,n} \equiv n^a\phi_{,a}$ and $\phi_{,\mu} \equiv e^a_{(\mu)}\phi_{,a}$.

Assuming that the branes have Z_2 symmetry, we have

$$K^{(I)\,+}_{\mu\nu} = -K^{(I)\,-}_{\mu\nu}. \tag{3.29}$$

Then, we can express the intrinsic curvatures $K^{(I)}_{\mu\nu}$ appearing in the expression of $\mathcal{F}^{(4)}_{\mu\nu}$ in terms of the effective energy-momentum tensor $\mathcal{T}^{(I)}_{\mu\nu}$ through the Lanczos equations (3.24). Hence, $G^{(4)}_{\mu\nu}$ given by Eq. (3.21) can be cast in the form [106],

$$\begin{aligned} G^{(4)}_{\mu\nu} &= \mathcal{G}^{(5)}_{\mu\nu} + E^{(5)}_{\mu\nu} + \mathcal{E}^{(4)}_{\mu\nu} + \kappa_5^4\pi_{\mu\nu} \\ &\quad +\kappa_4^2\tau_{\mu\nu} + \Lambda_4 g_{\mu\nu}, \end{aligned} \tag{3.30}$$

where

$$\begin{aligned}
\pi_{\mu\nu} &\equiv \frac{1}{4}\left\{\tau_{\mu\lambda}\tau_{\nu}^{\lambda} - \frac{1}{3}\tau\tau_{\mu\nu} - \frac{1}{2}g_{\mu\nu}\left(\tau^{\alpha\beta}\tau_{\alpha\beta} - \frac{1}{3}\tau^2\right)\right\}, \\
\mathcal{E}^{(4)}_{\mu\nu} &\equiv \frac{\kappa_5^4}{6}\tau_{\phi}\left[\tau_{\mu\nu} + \left(g_k + \frac{1}{2}\tau_{\phi}\right)g_{\mu\nu}\right],
\end{aligned} \tag{3.31}$$

and

$$\kappa_4^2 = \frac{1}{6}g_k\kappa_5^4, \quad \Lambda_4 = \frac{1}{12}g_k^2\kappa_5^4. \tag{3.32}$$

For a perfect fluid,

$$\tau_{\mu\nu} = (\rho + p)\,u_{\mu}u_{\nu} - pg_{\mu\nu}, \tag{3.33}$$

where u_μ is the four-velocity of the fluid on the brane, we find that

$$\pi_{\mu\nu} = \frac{1}{6}\rho\left[(\rho + p)\,u_{\mu}u_{\nu} - \left(p + \frac{1}{2}\rho\right)g_{\mu\nu}\right]. \tag{3.34}$$

Note that in writing Eqs. (3.30)-(3.34), without causing any confusion, we had dropped the super indices (I).

It should also be noted that the definitions of κ_4 and Λ_4 in Eq. (3.32) are unique, because in Eqs. (3.30) their corresponding terms are the only ones that linearly proportional to the matter field $\tau_{\mu\nu}$ and the spacetime geometry $g_{\mu\nu}$. In addition, they are exactly the ones widely used in brane-worlds [114].

3.2.3.2 *Matter field equations on the two branes* On the other hand, the I-th brane, localized on the surface $\Phi_I(x) = 0$, divides the spacetime into two regions, one with $\Phi_I(x) > 0$ and the other with $\Phi_I(x) < 0$ [Cf. Fig. 3.1]. Since the field equations are the second-order differential equations, the matter fields have to be at least continuous across this surface, although in general their first-order derivatives are not. Introducing the Heaviside function, defined as

$$H(x) = \begin{cases} 1, & x > 0, \\ 0, & x < 0, \end{cases} \tag{3.35}$$

for any given C^0 function $F(x)$, in the neighborhood of $\Phi_I(x) = 0$ we can always write it in the form,

$$F(x) = F^+(x)H(\Phi_I) + F^-(x)\left[1 - H(\Phi_I)\right], \tag{3.36}$$

where F^+ (F^-) is defined in the region $\Phi_I > 0$ ($\Phi_I < 0$), and

$$F^+(x)\Big|_{\Phi_I=0^+} = F^-(x)\Big|_{\Phi_I=0^-}. \tag{3.37}$$

Then, we find that

$$\begin{aligned} F_{,a}(x) &= F^+_{,a}(x)H(\Phi_I) + F^-_{,a}(x)\left[1 - H(\Phi_I)\right], \\ F_{,ab}(x) &= F^+_{,ab}(x)H(\Phi_I) + F^-_{,ab}(x)\left[1 - H(\Phi_I)\right] \\ &\quad + \left[F_{,a}\right]^- \frac{\partial \Phi_I(x)}{\partial x^b}\,\delta(\Phi_I), \end{aligned} \tag{3.38}$$

where $[F_{,a}]^-$ is defined as that in Eq. (3.25). Projecting $F_{,a}$ onto n^a and $e^a_{(\mu)}$ directions, we find

$$F_{,a} = F_{,\mu}e^{(\mu)}_a - F_{,n}n_a, \tag{3.39}$$

where

$$F_{,n} \equiv n^a F_{,a}, \quad F_{,\mu} \equiv e^a_{(\mu)}F_{,a}. \tag{3.40}$$

Then, it can be shown that

$$\begin{aligned} \left[F_{,n}\right]^- &= \left[F_{,a}\right]^- n^a \neq 0, \\ \left[F_{,\mu}\right]^- &= \left[F_{,a}\right]^- e^a_{(\mu)} = 0. \end{aligned} \tag{3.41}$$

Inserting Eqs. (3.39)-(3.41) into Eq. (3.38), we find

$$\begin{aligned} F_{,ab}(x) &= F^+_{,ab}(x)H(\Phi_I) + F^-_{,ab}(x)\left[1 - H(\Phi_I)\right] \\ &\quad - \left[F_{,n}\right]^- n^{(I)}_a n^{(I)}_b N^{(I)}\,\delta(\Phi_I). \end{aligned} \tag{3.42}$$

Due to the Z_2 symmetry, we can further write $\left[F^{(I)}_{,n}\right]^-$ as

$$\left[F^{(I)}_{,n}\right]^- = -2\epsilon_I F^{(I)}_{,n}, \tag{3.43}$$

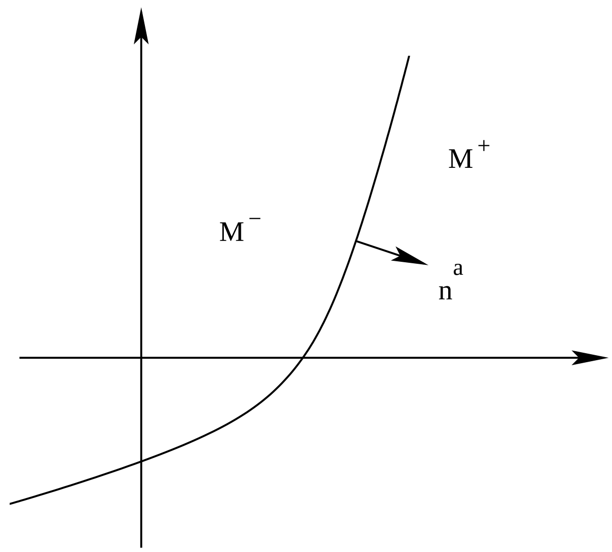

Figure 3.1: The surface $\Phi_I(x) = 0$ divides the spacetimes into two regions, $\Phi_I(x) > 0$ and $\Phi_I(x) < 0$. The normal vector defined by Eq.(3.15) points from M^- to M^+, where $M^+ \equiv \{x : \Phi_I(x) > 0\}$ and $M^- \equiv \{x : \Phi_I(x) < 0\}$.

where

$$
\begin{aligned}
F_{,n}^{(1)} &\equiv \lim_{\Phi_1 \to 0^-} (n^a F_{,a}) \\
F_{,n}^{(2)} &\equiv \lim_{\Phi_2 \to 0^+} (n^a F_{,a}).
\end{aligned} \tag{3.44}
$$

Substituting Eq. (3.42) into Eq. (3.17), we find that the matter field equation on the branes reads,

$$
\phi_{,n}^{(I)} = \frac{\epsilon_I}{2N^{(I)}} \left(2\kappa_5^2 \frac{\partial V_4^{(I)}}{\partial \phi} - 12\alpha\epsilon_I e^{-\phi} + \sigma_\phi^{(I)} \right) \sqrt{\left| \frac{g^{(I)}}{g} \right|}, \tag{3.45}
$$

where $\phi_{,n}^{(I)}$ is defined as that given by Eq. (3.44). Similarly, Eq. (3.28) can be written as

$$
\mathcal{T}^{(I)\lambda}{}_{\mu;\lambda} = \frac{\epsilon_I}{\kappa_5^2} \phi_{,n}^{(I)} \phi_{,\mu}^{(I)}. \tag{3.46}
$$

Eqs. (3.19), (3.20), (3.30), (3.45), and (3.46) consist of the complete set of both the gravitational and the matter field equations in the framework of the Horava-Witten heterotic M-Theory on S^1/Z_2.

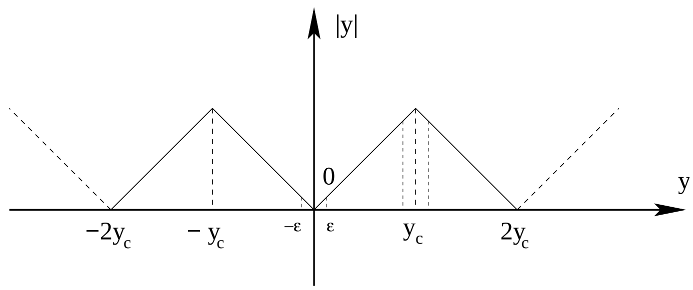

Figure 3.2: The function $|y|$ appearing in Eq. (3.48).

3.3 Radion stability and radion mass

In the studies of orbifold branes, an important issue is the radion stability [114]. In this section, we shall address this problem.

3.3.1 Static Solution with 4D Poincaré Symmetry

To begin with, let us first consider the 5-dimensional static metric with a 4-dimensional Poincaré symmetry [110],

$$ds_5^2 = e^{2\sigma(y)}\left(\eta_{\mu\nu}dx^\mu dx^\nu - dy^2\right), \tag{3.47}$$

where

$$\begin{aligned}\sigma(y) &= \frac{1}{5}\ln\left(\frac{|y|+y_0}{L}\right), &(3.48)\\ \phi(y) &= \frac{6}{5}\ln\left(\frac{|y|+y_0}{L}\right)+\phi_0, &(3.49)\\ \phi_0 &= \ln(5L\alpha)\end{aligned}$$

where $|y|$ is defined as that given in Fig.3.2, L and y_0 are positive constants.

Then, it can be shown that the above solution satisfies the gravitational and matter field equations outside the branes, Eqs. (3.19) and (3.20). On the two branes, assuming that the spacetime is vacuum, i.e., $\tau_{\mu\nu}^{(I)} = 0 = \sigma_\phi^{(I)}$, Eqs. (3.30) and (3.45) require

$$V_4^{(I)}(\phi_I) + g_k^{(I)} = 0, \tag{3.50}$$

$$\frac{\partial V_4^{(I)}(\phi_I)}{\partial \phi} = 0, \tag{3.51}$$

while Eq. (3.46) is satisfied identically, where $\phi_I \equiv \phi|_{y=y_I}$.

To study the 4-dimensional effective gravitational coupling, as well as the radion stability, it is found convenient to introduce the proper distance Y, defined by

$$Y = \left(\frac{5L}{6}\right)\left\{\left(\frac{y+y_0}{L}\right)^{6/5} - \left(\frac{y_0}{L}\right)^{6/5}\right\}. \tag{3.52}$$

Then, in terms of Y, the static solution (3.47) can be written as

$$ds_5^2 = e^{-2A(Y)}\eta_{\mu\nu}dx^\mu dx^\nu - dY^2, \tag{3.53}$$

with

$$\begin{aligned} A(Y) &= -\frac{1}{6}\ln\left\{\left(\frac{6}{5L}\right)(|Y|+Y_0)\right\}, & (3.54)\\ \phi(Y) &= \ln\left\{\left(\frac{6}{5L}\right)(|Y|+Y_0)\right\} + \phi_0, & (3.55)\end{aligned}$$

where $|Y|$ is defined also as that of Fig. 3.2, with

$$\begin{aligned} Y_0 &\equiv \left(\frac{5L}{6}\right)\left(\frac{y_0}{L}\right)^{6/5}, \\ Y_c &\equiv \left(\frac{5L}{6}\right)\left\{\left(\frac{y_c+y_0}{L}\right)^{6/5} - \left(\frac{y_0}{L}\right)^{6/5}\right\}, \end{aligned} \tag{3.56}$$

and $Y_2 = 0,\ Y_1 = Y_c$.

3.3.2 Radion Stability

Following [109], let us consider a massive scalar field Φ with the actions,

$$\begin{aligned} S_b &= \int d^4x \int_0^{Y_c} dY\sqrt{-g_5}\left((\nabla\Phi)^2 - M^2\Phi^2\right), \\ S_I &= -\alpha_I \int_{M_4^{(I)}} d^4x\sqrt{-g_4^{(I)}}\left(\Phi^2 - v_I^2\right)^2, \end{aligned} \tag{3.57}$$

where α_I and v_I are real constants. Then, it can be shown that, in the background of Eq. (3.53), the massive scalar field Φ satisfies the following Klein-Gordon equation

$$\Phi'' - 4A'\Phi' - M^2\Phi = \sum_{I=1}^{2} 2\alpha_I\Phi\left(\Phi^2 - v_I^2\right)\delta(Y - Y_I), \tag{3.58}$$

where a prime denotes the ordinary derivative with respect to the indicated argument, which in the present case is Y. Integrating the above equation in the neighborhood of the I-th brane, we find that

$$\left.\frac{d\Phi(Y)}{dY}\right|_{Y_I-\epsilon}^{Y_I+\epsilon} = 2\alpha_I \Phi_I \left(\Phi_I^2 - v_I^2\right), \tag{3.59}$$

where $\Phi_I \equiv \Phi(Y_I)$. Setting

$$z \equiv M(Y+Y_0), \quad \Phi = \left(\frac{z}{M}\right)^{1/6} u(z), \tag{3.60}$$

we find that, outside of the branes, Eq. (3.58) reduces,

$$\frac{d^2u}{dz^2} + \frac{1}{z}\frac{du}{dz} - \left(1+\frac{\nu^2}{z^2}\right)u = 0, \tag{3.61}$$

where $\nu \equiv 1/6$. Eq. (3.61) is the standard modified Bessel equation [129], which has the general solution

$$u(z) = aI_\nu(z) + bK_\nu(z), \tag{3.62}$$

where $I_\nu(z)$ and $K_\nu(z)$ denote the modified Bessel functions, and a and b are the integration constants, which are uniquely determined by the boundary conditions (3.59). Since

$$\begin{aligned} \lim_{Y\to Y_c^+}\frac{d\Phi(Y)}{dY} &= -\lim_{Y\to Y_c^-}\frac{d\Phi(Y)}{dY} \equiv -\Phi'\left(Y_c\right), \\ \lim_{Y\to 0^-}\frac{d\Phi(Y)}{dY} &= -\lim_{Y\to 0^+}\frac{d\Phi(Y)}{dY} \equiv -\Phi'(0), \end{aligned} \tag{3.63}$$

we find that the conditions (3.59) can be written in the forms,

$$\Phi'(Y_c) = -\alpha_1\Phi_1\left(\Phi_1^2 - v_1^2\right), \tag{3.64}$$

$$\Phi'(0) = \alpha_2\Phi_2\left(\Phi_2^2 - v_2^2\right). \tag{3.65}$$

Inserting the above solution back to the actions (3.57), and then integrating them with respect to Y, we obtain the effective potential for the radion Y_c,

$$V_\Phi\left(Y_c\right) \equiv -\int_{0+\epsilon}^{Y_c-\epsilon} dY\sqrt{-g_5}\left(\left(\nabla\Phi\right)^2 - M^2\Phi^2\right)$$

$$
\begin{aligned}
&+\sum_{I=1}^{2}\ \alpha_I \int_{Y_I-\epsilon}^{Y_I+\epsilon} dY\sqrt{-g_4^{(I)}}\left(\Phi^2 - v_I^2\right)^2 \\
&\qquad\qquad \times\delta\left(Y - Y_I\right) \\
=\;& e^{-4A(Y)}\Phi(Y)\Phi'(Y)\Big|_0^{Y_c} \\
&+\sum_{I=1}^{2}\alpha_I\left(\Phi_I^2 - v_I^2\right)^2 e^{-4A(Y_I)}. \qquad (3.66)
\end{aligned}
$$

In the limit that α_I's are very large [109], Eqs. (3.64) and (3.65) show that there are solutions only when $\Phi(0) \simeq v_2$ and $\Phi(Y_c) \simeq v_1$, that is,

$$
v_1 \;\simeq\; (Y_c + Y_0)^{\frac{1}{6}}[aI_\nu(z_c) + bK_\nu(z_c)], \qquad (3.67)
$$

$$
v_2 \;\simeq\; Y_0^{\frac{1}{6}}[aI_\nu(z_0) + b_\nu(z_0)], \qquad (3.68)
$$

where $z_0 \equiv MY_0$ and $z_c \equiv M(Y_c + Y_0)$. Eqs. (3.67) and (3.68) have the solutions,

$$
\begin{aligned}
a &= \frac{1}{\Delta}\left(K_\nu^{(0)}\bar{v_1} - k_\nu^{(c)}\bar{v_2}\right), \\
b &= \frac{1}{\Delta}\left(I_\nu^{(c)}\bar{v_2} - I_\nu^{(0)}\bar{v_1}\right), \qquad (3.69)
\end{aligned}
$$

where $K_\nu^{(I)} \equiv K_\nu(z_I)$, $I_\nu^{(I)} \equiv I_\nu(z_I)$, and

$$
\begin{aligned}
\Delta &\equiv I_\nu^{(c)}K_\nu^{(0)} - I_\nu^{(0)}K_\nu^{(c)}, \\
\bar{v_1} &= v_1\left(\frac{M}{z_c}\right)^{1/6}, \\
\bar{v_2} &= v_2\left(\frac{M}{z_0}\right)^{1/6}. \qquad (3.70)
\end{aligned}
$$

Inserting the above expressions into Eq. (3.66), we find that

$$
V_\Phi\left(Y_c\right) \simeq \left(\frac{6}{5}\right)^{2/3}\left(I\left(z_c\right) - I\left(z_0\right)\right), \qquad (3.71)
$$

where

$$
\begin{aligned}
I\left(z\right) \;\equiv\;& a^2\left(\nu + z\right)I_\nu^2(z) + 2ab\nu I_\nu(z)K_\nu(z) \\
&+b^2K_\nu^2(z). \qquad (3.72)
\end{aligned}
$$

3.3.2.1 $MY_0 \gg 1$ When $Y_0 \gg M^{-1}$, we have $z_0,\ z_c \gg 1$. Then, we find that [129],

$$\begin{aligned} I_\nu(z) &\simeq \frac{e^z}{\sqrt{2\pi z}}, \\ K_\nu(z) &\simeq \sqrt{\frac{\pi}{2z}}e^{-z}, \end{aligned} \tag{3.73}$$

for $z \gg 1$. Substituting them into Eq. (3.66), we find that

$$\begin{aligned} V_\Phi\left(Y_c\right) \simeq\ & M\left(\frac{6Y_0}{5L}\right)^{2/3}\left(\left(v_1^2+v_2^2\right)\coth\left(z_c-z_0\right)\right. \\ & \left. -\frac{2v_1v_2}{\sinh\left(z_c-z_0\right)}\right). \end{aligned} \tag{3.74}$$

Thus, we find that

$$V_\Phi\left(Y_c\right) \simeq V_\Phi^{(0)} \times \begin{cases} \frac{(v_1-v_2)^2 z_0^{2/3}}{\sinh(z_c-z_0)} \to \infty, & z_c \to z_0, \\ v_1^2 z_c^{2/3} \to \infty, & z_c \to \infty, \end{cases} \tag{3.75}$$

where $V_\Phi^{(0)} \equiv M^{1/3}\left(6/(5L)\right)^{2/3}$. Figs. 3.3 and 3.4 show the potential for $(z_0,\ v_1,\ v_2) = (10,\ 1.0,\ 0.1)$ and $(z_0,\ v_1,\ v_2) = (30,\ 200,\ 100)$, respectively, from which we can see clearly that it has a minimal. Therefore, the radion is indeed stable in our current setup.

3.3.2.2 $MY_0 \ll 1$ When $MY_0 \ll 1$ and $MY_c \ll 1$, we find that [129]

$$\begin{aligned} I_\nu(z) &\simeq \frac{z^\nu}{2^\nu\Gamma(\nu+1)}, \\ K_\nu(z) &\simeq \frac{2^{\nu-1}\Gamma(\nu)}{z^\nu}. \end{aligned} \tag{3.76}$$

Substituting them into Eq. (3.66), we obtain

$$V_\Phi\left(Y_c\right) \simeq \frac{1}{3}M^{1/3}\left(\frac{6}{5L}\right)^{2/3}\frac{\left(v_1-v_2\right)^2}{z_c^{2\nu}-z_0^{2\nu}}. \tag{3.77}$$

Clearly, in this limit the potential has no minima, and the corresponding radion is not stable. Therefore, there exists a minimal mass for the scalar field Φ, say, M_c, only when $M > M_c$ the corresponding radion is stable.

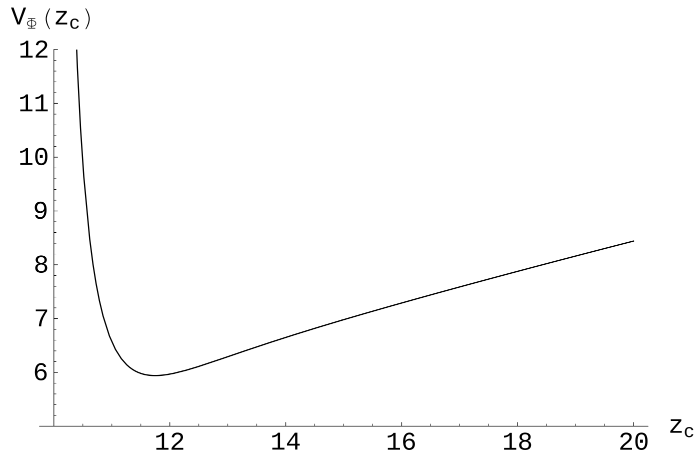

Figure 3.3: The potential defined by Eq. (3.74) in the limit of large v_I and y_0. In this particular plot, we choose (z_0, v_1, v_2)= (10, 1.0, 0.1).

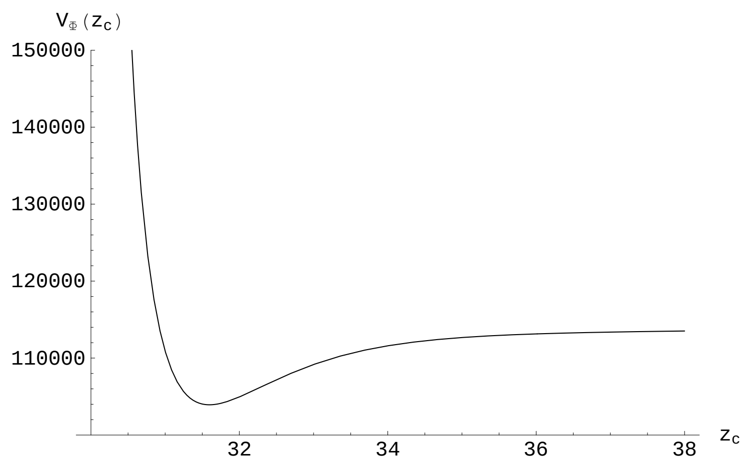

Figure 3.4: The potential defined by Eq. (3.74) in the limit of large v_I and y_0. In this particular plot, we choose (z_0, v_1, v_2)= (30, 200, 100).

It should be noted that, in the Randall-Sundrum setup [130], Y_c is required to be $Y_c \simeq 38$ in order to solve the hierarchy problem. However, in the current setup the hierarchy problem may be solved by using the ADD mechanism [105], so such a requirement is not needed here. As a result, the physical brane is not necessarily placed at $Y = Y_c$. Thus, in our current setup, we can take any of the two branes as the physical one, in which the standard matter fields are assumed to be present.

3.3.3 Radion Mass

To calculate the radion mass, we need first to find the exact relation between the radion field φ and Y_c. To this end, let us consider the linear perturbations given by [131, 132],

$$
\begin{aligned}
ds_5^2 &= e^{-2[A(Y)-F(x)]}\eta_{\mu\nu}dx^\mu dx^\nu \\
&\quad -[1+2F(x)]^2 dY^2.
\end{aligned} \tag{3.78}
$$

Then, we find

$$
\begin{aligned}
\delta R_5 &= \frac{2e^{2(A+F)}}{1+2F}\Big[(1-6F)(\nabla F)^2 \\
&\quad +(1+6F)\Box F\Big].
\end{aligned} \tag{3.79}
$$

Thus, we obtain

$$
\begin{aligned}
\delta S &= \frac{1}{\kappa_5^2}\int dY dx^4 \sqrt{g_5}\delta R_5 \\
&= \frac{2}{\kappa_5^2}\int_0^{Y_c} e^{-2A}dY \\
&\quad \times \int dx^4 e^{-2F}(\nabla F)^2(6F-3).
\end{aligned} \tag{3.80}
$$

Following [131], by defining $\varphi = \sqrt{12f}e^{-F}\sqrt{1-2F}$, we obtain

$$
\delta S = -\frac{1}{2}\int dx^4 (\nabla\varphi)^2, \tag{3.81}
$$

where

$$
f = \frac{1}{k_5^2}\int_0^{Y_c} e^{-2A}dY. \tag{3.82}
$$

Substituting Eq. (3.54) into Eq. (3.82), and in the limit $F(x) \to 0$, we can write φ as

$$
\begin{aligned}
\varphi(Y_c) &= 3\sqrt{2}\left(\frac{6}{5}\right)^{1/6} M_5^{3/2} L^{1/2} \\
&\quad \times \left\{\left(\frac{Y_c+Y_0}{L}\right)^{4/3} - \left(\frac{Y_0}{L}\right)^{4/3}\right\}^{1/2},
\end{aligned} \tag{3.83}
$$

where $M_5^3 = \kappa_5^{-2}$, as can be seen from Eqs. (3.32). When $z_0 = MY_0 \gg 1$, the potential $V(Y_c)$ given by Eq. (3.74) has a minimum at

$$MY_c = z_c - z_0 = \ln\left(\frac{v_1}{v_2}\right), \tag{3.84}$$

where, without loss of generality, we has set $v_1 > v_2$.

Combining Eq. (3.74) with Eq. (3.83), we obtain the mass of φ, which in the large MY_0 limit is given by

$$\begin{aligned} m_\varphi &= \sqrt{\frac{\partial^2 V}{2\partial\varphi^2}} \approx M^{-1/2}\frac{v_1^2}{v_2}\left(\frac{Y_0}{L}\right)^{1/6} \\ &\times \sqrt{\frac{\ln(v_1/v_2)}{\left(\left(\frac{v_1}{v_2}\right)^2 - 1\right)^3}}. \end{aligned} \tag{3.85}$$

Clearly, by properly choosing the free parameters, one can have $m_\varphi \simeq TeV$.

3.4 Localization of Gravity and 4D Effective Newtonian Potential

To study the localization of gravity and the four-dimensional effective gravitational potential, in this section let us consider small fluctuations h_{ab} of the 5-dimensional static metric with a 4-dimensional Poincaré symmetry, given by Eq. (3.47) in its conformally flat form.

3.4.1 Tensor Perturbations and the KK Towers

Since such tensor perturbations are not coupled with scalar ones [133], without loss of generality, we can set the perturbations of the scalar field ϕ to zero, i.e., $\delta\phi = 0$. We shall choose the gauge [134],

$$h_{ay} = 0, \quad h^\lambda_\lambda = 0 = \partial^\lambda h_{\mu\lambda}. \tag{3.86}$$

Then, it can be shown that [135]

$$\begin{aligned} \delta G^{(5)}_{ab} &= -\frac{1}{2}\Box_5 h_{ab} - \frac{3}{2}\left\{(\partial_c\sigma)(\partial^c h_{ab})\right. \\ &\quad \left. -2\left[\Box_5\sigma + (\partial_c\sigma)(\partial^c\sigma)\right]h_{ab}\right\}, \end{aligned}$$

$$
\begin{aligned}
\kappa_5^2 \delta T_{ab}^{(5)} &= \frac{1}{4}\left(\phi'^2 + 2e^{2\sigma}V_5\right) h_{ab}, \\
\delta T_{\mu\nu}^{(4)} &= \left(\tau_{(\phi,\psi)}^{(I)} + 2\rho_\Lambda^{(I)}\right) e^{2\sigma(y_I)} h_{\mu\nu}(x, y_I),
\end{aligned}
\tag{3.87}
$$

where $\Box_5 \equiv \eta^{ab}\partial_a\partial_b$ and $(\partial_c\sigma)(\partial^c h_{ab}) \equiv \eta^{cd}(\partial_c\sigma)(\partial_d h_{ab})$, with η^{ab} being the five-dimensional Minkowski metric. Substituting the above expressions into the Einstein field Eq. (3.7), we find that in the present case there is only one independent equation, given by

$$
\Box_5 h_{\mu\nu} + 3(\partial_c\sigma)(\partial^c h_{\mu\nu}) = 0, \tag{3.88}
$$

which can be further cast in the form,

$$
\Box_5 \tilde{h}_{\mu\nu} + \frac{3}{2}\left(\sigma'' + \frac{3}{2}\sigma'\right)\tilde{h}_{\mu\nu} = 0, \tag{3.89}
$$

where $h_{\mu\nu} \equiv e^{-3\sigma/2}\tilde{h}_{\mu\nu}$. Setting

$$
\begin{aligned}
&\tilde{h}_{\mu\nu}(x,y) = \hat{h}_{\mu\nu}(x)\psi_n(y), \\
&\Box_5 = -\left(\Box_4 + \nabla_y^2\right) = -\left(\eta^{\mu\nu}\partial_\mu\partial_\nu + \partial_y^2\right), \\
&\Box_4 \hat{h}_{\mu\nu}(x) = m_n^2 \hat{h}_{\mu\nu}(x),
\end{aligned}
\tag{3.90}
$$

we find that Eq. (3.88) takes the form of the schrödinger equation,

$$
\left(-\nabla_y^2 + V\right)\psi_n = m_n^2 \psi_n, \tag{3.91}
$$

where

$$
\begin{aligned}
V &\equiv \frac{3}{2}\left(\sigma'' + \frac{3}{2}\sigma'^2\right) \\
&= -\frac{21}{100\left(|y| + y_0\right)^2} + \frac{3\delta(y)}{5y_0} \\
&\quad -\frac{3\delta(y - y_c)}{5(y_c + y_0)}.
\end{aligned}
\tag{3.92}
$$

From the above expression we can see clearly that the potential has a delta-function well at $y = y_c$, which is responsible for the localization of the graviton on this brane.

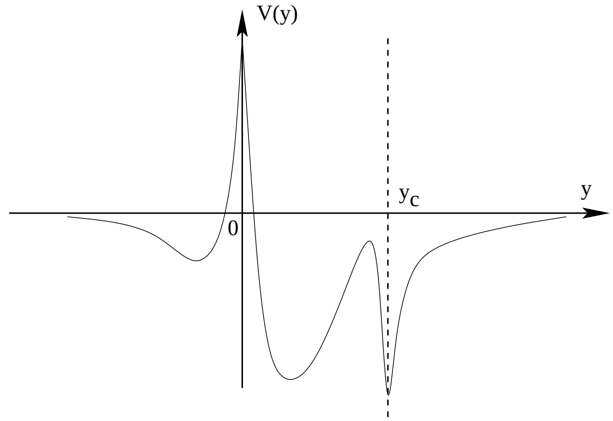

Figure 3.5: The potential defined by Eq. (3.92).

In contrast, the potential has a delta-function barrier at $y = 0$, which makes the gravity delocalized on the $y = 0$ brane. Fig. 3.5 shows the potential schematically.

Introducing the operators,

$$Q \equiv \nabla_y - \frac{3}{2}\sigma', \quad Q^\dagger \equiv -\nabla_y - \frac{3}{2}\sigma', \tag{3.93}$$

Eq. (3.91) can be written in the form of a supersymmetric quantum mechanics problem,

$$Q^\dagger \cdot Q\psi_n = m_n^2 \psi_n. \tag{3.94}$$

It should be noted that Eq. (3.94) itself does not guarantee that the operator $Q^\dagger \cdot Q$ is Hermitian, because now it is defined only on a finite interval, $y \in [0, y_c]$. To ensure its Hermiticity, in addition to writing the differential equation in the Shrödinger form, one also needs to show that it has Hermitian boundary conditions, which can be formulated as [136]

$$\begin{aligned} {\psi'}_n(0)\psi_m(0) \quad - \quad & \psi_n(0){\psi'}_m(0) = {\psi'}_n\left(y_c\right)\psi_m\left(y_c\right) \\ & -\psi_n\left(y_c\right){\psi'}_m\left(y_c\right), \end{aligned} \tag{3.95}$$

for any two solutions of Eq. (3.94). To show that in the present case this condition is indeed satisfied, let us consider the boundary conditions at $y = 0$ and $y = y_c$. Integration of Eq. (3.91) in the neighbourhood of $y = 0$ and $y = y_c$ yields, respectively, the conditions,

$$\lim_{y \to y_c^-} \psi'(y) = \frac{3}{10\,(y_c + y_0)} \lim_{y \to y_c^-} \psi(y), \tag{3.96}$$

$$\lim_{y \to 0^+} \psi'(y) = \frac{3}{10 y_0} \lim_{y \to 0^+} \psi(y). \tag{3.97}$$

Note that in writing the above equations we had used the Z_2 symmetry of the wave function ψ_n. Clearly, any solution of Eq. (3.91) that satisfies the above boundary conditions also satisfies Eq. (3.95). That is, the operator $Q^\dagger \cdot Q$ defined by Eq. (3.93) is indeed a positive definite Hermitian operator. Then, by the usual therems we can see that all eigenvalues m_n^2 are non-negative, and their corresponding wave functions $\psi_n(y)$ are orthogonal to each other and form a complete basis. Therefore, the background is gravitationally stable in our current setup.

3.4.1.1 *Zero Mode* The four-dimensional gravity is given by the existence of the normalizable zero mode, for which the corresponding wavefunction is given by

$$\psi_0(y) = N_0 \left(\frac{|y| + y_0}{L}\right)^{3/10}, \tag{3.98}$$

where N_0 is the normalization factor, defined as

$$N_0 \equiv 2 \left\{\frac{5}{2} L \left[\left(\frac{y_c + y_0}{L}\right)^{8/5} - \left(\frac{y_0}{L}\right)^{8/5}\right]\right\}^{-1/2}. \tag{3.99}$$

Eq. (3.98) shows clearly that the wavefunction is increasing as y increases from 0 to y_c. Therefore, the gravity is indeed localized near the $y = y_c$ brane.

3.4.1.2 *Non-Zero Modes* In order to have localized four-dimensional gravity, we require that the corrections to the Newtonian law from the non-zero modes, the KK modes, of Eq. (3.91), be very small, so that they will not lead to contradiction with observations. To solve Eq. (3.91) outside of the two branes, it is found convenient to introduce the quantities,

$$\psi(y) \equiv x^{1/2}\, u(x), \quad x \equiv m\,(y + y_0)\,. \tag{3.100}$$

Then, in terms of x and $u(x)$, Eq.(3.91) takes the form,

$$x^2\frac{d^2u}{dx^2} + x\frac{du}{dx} + \left(x^2 - \nu^2\right) u = 0, \tag{3.101}$$

but now with $\nu = 1/5$. Eq. (3.101) is the standard Bessel equation [129], which have two independent solutions $J_\nu(x)$ and $Y_\nu(x)$. Therefore, the general solution of Eq.(3.91) are given by

$$\psi = x^{1/2}\left(cJ_\nu(x) + dY_\nu(x)\right), \tag{3.102}$$

where c and d are the integration constants, which will be determined from the boundary conditions given by Eqs. (3.96) and (3.97). Setting

$$\begin{aligned}
\Delta_{11} &\equiv 2J_\nu\left(x_c\right) - 5x_c J_{\nu+1}\left(x_c\right), \\
\Delta_{12} &\equiv 2Y_\nu\left(x_c\right) - 5x_c Y_{\nu+1}\left(x_c\right), \\
\Delta_{21} &\equiv 2J_\nu\left(x_0\right) - 5x_0 J_{\nu+1}\left(x_0\right), \\
\Delta_{22} &\equiv 2Y_\nu\left(x_0\right) - 5x_0 Y_{\nu+1}\left(x_0\right),
\end{aligned} \tag{3.103}$$

we find that Eqs. (3.96) and (3.97) can be cast in the form,

$$\begin{pmatrix} \Delta_{11} & \Delta_{12} \\ \Delta_{21} & \Delta_{22} \end{pmatrix} \begin{pmatrix} c \\ d \end{pmatrix} = 0. \tag{3.104}$$

It has non-trivial solutions only when

$$\Delta \equiv \det\left(\Delta_{ij}\right) = 0. \tag{3.105}$$

Fig. 3.6 shows the solutions of $\Delta = 0$ for $x_0 = my_0 = 0.01,\ 1.0,\ 1000$, respectively. From this figure, two remarkable features are: (1) The spectrum of the KK towers is discrete. (2) The KK modes weakly depend on the specific values of x_0.

Table 3.1 shows the first three modes m_n $(n = 1, 2, 3)$ for $x_0 = 0.01,\ 1.0,\ 1000$, from which we can see that to find m_n it is sufficient to consider only the case where $x_0 \gg 1$.

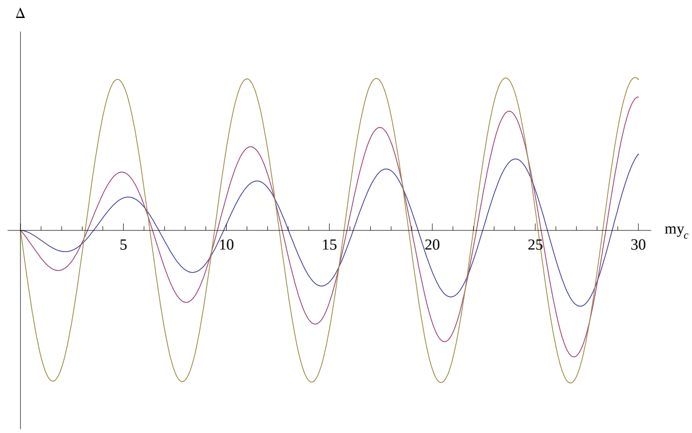

Figure 3.6: The function of Δ defined by Eq. (3.105) for $x_0 = my_0 = 0.01,\ 1.0,\ 1000,$ respectively. Note that the horizontal axis is my_c.

Table 3.1: The first three modes m_n $(n = 1, 2, 3)$ for $x_0 = 0.01,\ 1.0,\ 1000.$

x_0	$m_1 y_c$	$m_2 y_c$	$m_3 y_c$
0.01	3.55	6.72	9.87
1.0	3.25	6.41	9.56
1000	3.14	6.28	9.42

When $x_0 \gg 1$ we find that $x_c = x_0 + my_c \gg 1$, and that [129]

$$\begin{aligned} J_\nu(x) &\simeq -Y_{\nu+1}(x) \simeq \sqrt{\frac{2}{\pi x}} \cos\left(x - \frac{7}{20}\pi\right), \\ Y_\nu(x) &\simeq J_{\nu+1}(x) \simeq \sqrt{\frac{2}{\pi x}} \sin\left(x - \frac{7}{20}\pi\right). \end{aligned} \tag{3.106}$$

Inserting the above expressions into Eqs. (3.103) and (3.105), we obtain

$$\begin{aligned} \Delta &= -\sqrt{\frac{4}{\pi^2 x_0 x_c}} \left\{10\left(x_c - x_0\right)\cos\left(x_c - x_0\right)\right. \\ &\quad \left. + \left(4 + 25 x_0 x_c\right)\sin\left(x_c - x_0\right)\right\}, \end{aligned} \tag{3.107}$$

whose roots are given by

$$\tan\left(x_c - x_0\right) = -\frac{10\left(x_c - x_0\right)}{4 + 25 x_0 x_c}. \tag{3.108}$$

From this equation, we can see that m_n satisfies the bounds

$$\frac{n\pi}{y_c} < m_n < \frac{(n+1)\pi}{y_c}, \ (n = 1, 2, 3, ...). \tag{3.109}$$

Combining the above expression with Table 3.1, we find that m_n is well approximated by

$$m_n \simeq n\pi \left(\frac{l_{pl}}{y_c}\right) M_{pl}, \tag{3.110}$$

For $x_0 \gg 1$. In particular, we have

$$\begin{aligned} m_1 &\simeq 3.14 \times \left(\frac{10^{-19}\ \mathrm{m}}{y_c}\right) \mathrm{TeV} \\ &\simeq \begin{cases} 1\ \mathrm{TeV}, & y_c \simeq 10^{-19}\ \mathrm{m}, \\ 10^{-2}\ \mathrm{eV}, & y_c \simeq 10^{-5}\ \mathrm{m}, \\ 10^{-4}\ \mathrm{eV}, & y_c \simeq 10^{-3}\ \mathrm{m}. \end{cases} \end{aligned} \tag{3.111}$$

For each m_n that satisfies Eq. (3.105), the wavefunction $\psi_n(x)$ is given by

$$\begin{aligned} \psi_n(x) &= N_n x^{1/2} \left\{\Delta_{12}\left(m_n, y_c\right) J_\nu(x)\right. \\ &\quad \left. -\Delta_{11}\left(m_n, y_c\right) Y_\nu(x)\right\}, \end{aligned} \tag{3.112}$$

where $N_n \equiv N_n\left(m_n, y_c\right)$ is the normalization factor, so that

$$\int_0^{y_c} \left|\psi_n(x)\right|^2 dy = 1. \tag{3.113}$$

3.4.2 4D Newtonian Potential and Yukawa Corrections

To calculate the four-dimensional effective Newtonian potential and its corrections, let us consider two point-like sources of masses M_1 and M_2, located on the brane at $y = y_c$. Then, the discrete eigenfunction $\psi_n(x)$ of mass m_n has an Yukawa correction to the four-dimensional gravitational potential between the two particles [137, 135]

$$U(r) = G_4 \frac{M_1 M_2}{r} + \frac{M_1 M_2}{M_5^3 r} \sum_{n=1}^{\infty} e^{-m_n r} \left|\psi_n(x_c)\right|^2, \tag{3.114}$$

where $\psi_n(x_c)$ is given by Eq. (3.112). When $x_0 = m_n y_0 \gg 1$, from Eq. (3.106) we find that

$$\begin{aligned} N_n &\simeq \sqrt{\frac{\pi^2}{50 x_c y_c}}, \\ \psi_n(x_c) &\simeq \sqrt{\frac{2}{y_c}}. \end{aligned} \tag{3.115}$$

Then, it can be seen that all terms except for the first one in Eq. (3.114) are exponentially suppressed, and have negligible contributions to the 4D effective potential $U(r)$.

3.5 Cosmological Model

In this section, we shall apply the formulas developed in Section 3.2 to cosmology.

3.5.1 General Metric and Gauge Choices

The general metric for cosmology takes the form [106, 126],

$$ds_5^2 = g_{ab}dx^a dx^b = g_{MN}dx^M dx^N - e^{2\omega\left(x^M\right)}d\Sigma_k^2, \tag{3.116}$$

where $M,\ N = 0, 1$, and

$$d\Sigma_k^2 = \frac{dr^2}{1-kr^2} + r^2\left(d\theta^2 + \sin^2\theta d\varphi^2\right), \tag{3.117}$$

where the constant k represents the curvature of the 3-space, and can be positive, negative or zero. Without loss of generality, we shall choose coordinates such that $k = 0, \pm 1$. The metric (3.116) is invariant under the coordinate transformations,

$$x'^N = f^N\left(x^M\right). \tag{3.118}$$

Using these two degrees of freedom, one can choose different gauges.

3.5.1.1 *The canonical gauge* In particular, in [126] the gauge was chosen such that

$$g_{01} = 0, \quad y_I = 0,\ y_c, \tag{3.119}$$

where y_I denote the locations of the two orbifold branes, with y_c being a constant. Then, the general metric can be cast in the form,

$$ds_5^2 = N^2(t,|y|)dt^2 - B^2(t,|y|)dy^2 - B^2(t,|y|)d\Sigma_k^2, \tag{3.120}$$

where $|y|$ is defined as that given in [126] [cf. Fig. 3.2]. By using distribution theory, the field equations on the two branes were obtained explicitly in terms of the discontinuities of the metric coefficients A, B and N. For the details, we refer readers to [126]. The gauge Eq. (3.119) will be referred to as *the canonical gauge.*

3.5.1.2 *The conformal gauge* One can also choose the gauge

$$g_{00} = g_{11}, \quad g_{01} = 0, \tag{3.121}$$

so that the general five-dimensional metric takes the form,

$$ds_5^2 = e^{2\sigma(t,y)} \left(dt^2 - dy^2\right) - e^{2\omega(t,y)} d\Sigma_k^2. \tag{3.122}$$

But with this gauge, the hypersurfaces of the two branes are not fixed, and usually given by $y = y_I(t)$. We shall refer the gauge Eq. (3.121) to as *the conformal gauge.* It should be noted that in this conformal gauge, metric (3.122) still has the remaining gauge freedom,

$$t = f\left(\xi_+\right) + g\left(\xi_-\right), \quad y = f\left(\xi_+\right) - g\left(\xi_-\right) \tag{3.123}$$

where $\xi_\pm \equiv t' \pm y'$, and $f\left(\xi_+\right)$ and $g\left(\xi_-\right)$ are arbitrary functions of their indicated arguments.

It should be noted that in [138] comoving branes were considered, and it was claimed that the gauge freedom of Eq. (3.123) can always bring the two branes at rest (comoving). However, from Eq. (A5) of [138] it can be seen that this is not true (at least) at the moment of the collision, $\tilde{y}_2(t) = 0$, for which Eq. (A5) reduces to $f(t) = f(t) + 2$, which is not satisfied for any finite function $f(t)$. In addition, using Eq. (3.123), one can always bring one brane at rest, as shown in [139] (See also [138]). In this paper, we shall leave this possibility open, and choose to work with the conformal gauge, in which the branes are located on the surfaces $y = y_I(t)$.

3.5.2 Field Equations Outside the Two Branes

It can be shown that outside the two branes the field equations (3.19) for the metric (3.122) have four independent components, which can be cast in the form,

$$\begin{aligned}
&\omega_{,tt} + \omega_{,t}\left(\omega_{,t} - 2\sigma_{,t}\right) + \omega_{,yy} + \omega_{,y}\left(\omega_{,y} - 2\sigma_{,y}\right) \\
&\qquad = -\frac{1}{6}\left({\phi_{,t}}^2 + {\phi_{,y}}^2\right), \qquad (3.124) \\
&2\sigma_{,tt} + \omega_{,tt} - 3{\omega_{,t}}^2 - \left(2\sigma_{,yy} + \omega_{,yy} - 3{\omega_{,y}}^2\right) \\
&\qquad -4ke^{2(\sigma-\omega)} \\
&\qquad = -\frac{1}{2}\left({\phi_{,t}}^2 - {\phi_{,y}}^2\right), \qquad (3.125) \\
&\omega_{,ty} + \omega_{,t}\omega_{,y} - \left(\sigma_{,t}\omega_{,y} + \sigma_{,y}\omega_{,t}\right) \\
&\qquad = -\frac{1}{6}\phi_{,t}\phi_{,y}, \qquad (3.126) \\
&\omega_{,tt} + 3{\omega_{,t}}^2 - \left(\omega_{,yy} + 3{\omega_{,y}}^2\right) + 2ke^{2(\sigma-\omega)} \\
&\qquad = 2\alpha^2 e^{2(\sigma-\phi)}. \qquad (3.127)
\end{aligned}$$

On the other hand, the Klein-Gordon equation (3.20) takes the form,

$$\phi_{,tt} + 3\phi_{,t}\omega_{,t} - \left(\phi_{,yy} + 3\phi_{,y}\omega_{,y}\right) = 12\alpha^2 e^{2(\sigma-\phi)}. \qquad (3.128)$$

3.5.3 Field Equations on the Two Branes

Eqs. (3.124) - (3.128) are the field equations that are valid in between the two orbifold branes,

$$y_2(t) < y < y_1(t). \qquad (3.129)$$

The proper distance between the two branes is given by

$$\mathcal{D}(t) = \int_{y_2}^{y_1} e^{\sigma(t,y)} dy. \qquad (3.130)$$

On each of the two branes, the metric reduces to

$$ds_5^2\Big|_{M_4^{(I)}} = g_{\mu\nu}^{(I)} d\xi_{(I)}^{\mu} d\xi_{(I)}^{\nu} = d\tau_I^2 - a^2\left(\tau_I\right) d\Sigma_k^2, \qquad (3.131)$$

where $\xi^{\mu}_{(I)} \equiv \{\tau_I, r, \theta, \varphi\}$, and τ_I denotes the proper time of the I-th brane, defined by

$$
\begin{aligned}
d\tau_I &= e^{\sigma[t_I(\tau_I), y_I(\tau_I)]}\sqrt{1 - \left(\frac{\dot{y}_I}{\dot{t}_I}\right)^2}\, dt_I, \\
a\left(\tau_I\right) &\equiv e^{\omega[t_I(\tau_I), y_I(\tau_I)]},
\end{aligned}
\tag{3.132}
$$

with $\dot{y}_I \equiv dy_I/d\tau_I$, etc. For the sake of simplicity and without of causing any confusion, from now on we shall drop all the indices "I", unless some specific attention is needed. Then, the normal vector n_a and the tangential vectors $e^a_{(\mu)}$ are given, respectively, by

$$
\begin{aligned}
n_a &= e^{2\sigma}\left(-\dot{y}\delta^t_a + \dot{t}\delta^y_a\right), \\
n^a &= -\left(\dot{y}\delta^a_t + \dot{t}\delta^a_y\right), \\
e^a_{(\tau)} &= \dot{t}\delta^a_t + \dot{y}\delta^a_y, \quad e^a_{(r)} = \delta^a_r, \\
e^a_{(\theta)} &= \delta^a_\theta, \quad e^a_{(\varphi)} = \delta^a_\varphi.
\end{aligned}
\tag{3.133}
$$

Thus, we find that

$$
\begin{aligned}
\mathcal{G}^{(5)}_{\mu\nu} &= \mathcal{G}^{(5)}_{\tau}\delta^\tau_\mu\delta^\tau_\nu - \mathcal{G}^{(5)}_{\theta}\delta^m_\mu\delta^n_\nu g_{mn}, \\
E^{(5)}_{\mu\nu} &= E^{(5)}\left(3\delta^\tau_\mu\delta^\tau_\nu - \delta^m_\mu\delta^n_\nu g_{mn}\right),
\end{aligned}
\tag{3.134}
$$

where $m,\ n = r,\ \theta,\ \varphi$, and

$$
\begin{aligned}
\mathcal{G}^{(5)}_{\tau} &\equiv \frac{1}{3}e^{-2\sigma}\left({\phi_{,t}}^2 - {\phi_{,y}}^2\right) - \frac{1}{24}\left(5\left(\nabla\phi\right)^2 - 6V_5\right), \\
\mathcal{G}^{(5)}_{\theta} &\equiv \frac{1}{24}\left(8{\phi_{,n}}^2 + 5\left(\nabla\phi\right)^2 - 6V_5\right), \\
E^{(5)} &\equiv \frac{1}{6}e^{-2\sigma}\left((\sigma_{,tt} - \omega_{,tt}) - (\sigma_{,yy} - \omega_{,yy})\right. \\
&\quad \left. + ke^{2(\sigma-\omega)}\right),
\end{aligned}
\tag{3.135}
$$

with

$$
V_5 \equiv 6\alpha^2 e^{-2\phi}. \tag{3.136}
$$

Then, it can be shown that the four-dimensional field equations on each of the two branes take the form,

$$\begin{aligned} H^2 \quad &+ \quad \frac{k}{a^2} = \frac{8\pi G}{3}\left(\rho + \tau_\phi\right) + \frac{1}{3}\Lambda + \frac{1}{3}\mathcal{G}^{(5)}_\tau + E^{(5)} \\ &\quad +\frac{2\pi G}{3\rho_\Lambda}\left(\rho + \tau_\phi\right)^2, \end{aligned} \tag{3.137}$$

$$\begin{aligned} \frac{\ddot{a}}{a} \quad &= \quad -\frac{4\pi G}{3}\left(\rho + 3p - 2\tau_\phi\right) + \frac{1}{3}\Lambda \\ &\quad -E^{(5)} - \frac{1}{6}\left(\mathcal{G}^{(5)}_\tau + 3\mathcal{G}^{(5)}_\theta\right) - \frac{2\pi G}{3\rho_\Lambda}\left[\rho\left(2\rho + 3p\right)\right. \\ &\quad \left. + \left(\rho + 3p - \tau_\phi\right)\tau_\phi\right], \end{aligned} \tag{3.138}$$

where $H \equiv \dot{a}/a, ,\ \Lambda \equiv \Lambda_4$ and $G \equiv G_4$.

On the other hand, from Eqs. (3.45) and (3.46) we find that

$$\phi^{(I)}_{,n} = \epsilon_I\left(\kappa_5^2\frac{\partial V_4^{(I)}}{\partial\phi} - 6\alpha\epsilon_I e^{-\phi} + \frac{1}{2}\sigma^{(I)}_\phi\right), \tag{3.139}$$

$$\left(\dot{\rho}^{(I)} + \dot{\tau}^{(I)}_\phi\right) + 3H^{(I)}\left(\rho^{(I)} + p^{(I)}\right) = \Pi^{(I)}, \tag{3.140}$$

where $H^{(I)} \equiv \left[da\left(\tau_I\right)/d\tau_I\right]/a\left(\tau_I\right)$, and

$$\Pi^{(I)} \equiv \frac{\epsilon_I}{\kappa_5^2}\phi^{(I)}_{,\tau}\phi^{(I)}_{,n}. \tag{3.141}$$

From Eqs. (3.11) and (3.133), we also find that

$$\dot{\tau}^{(I)}_\phi = \frac{\phi^{(I)}_{,\tau}}{\kappa_5^2}\left\{\kappa_5^2\frac{\partial V_4^{(I)}}{\partial\phi} - 6\alpha\epsilon_I e^{-\phi}\right\}. \tag{3.142}$$

Then, Eqs. (3.139) and (3.140) can be written as

$$\dot{\tau}^{(I)}_\phi = \Pi^{(I)} - Q^{(I)}, \tag{3.143}$$

$$\dot{\rho}^{(I)} + 3H^{(I)}\left(\rho^{(I)} + p^{(I)}\right) = Q^{(I)}, \tag{3.144}$$

where

$$Q^{(I)} \equiv \frac{1}{2\kappa_5^2}\phi^{(I)}_{,\tau}\sigma^{(I)}_\phi. \tag{3.145}$$

When there is only gravitational interaction between the scalar field and the perfect fluid, we have $\sigma_{\phi}^{(I)} = 0$ [cf. Es.(3.18)], and then the above equations reduce to

$$\dot{\tau}_{\phi}^{(I)} = \Pi^{(I)}, \ \left(Q^{(I)} = 0\right), \tag{3.146}$$

$$\dot{\rho}^{(I)} + 3H^{(I)}\left(\rho^{(I)} + p^{(I)}\right) = 0, \ \left(Q^{(I)} = 0\right). \tag{3.147}$$

3.6 A Particular Case

In Sec. 3.3, we considered only the case where both the bulk and the branes are static. In this section, we shall generalize it in two different ways: (a) moving branes in static bulk, and (b) fixed branes in time-dependent bulk. In the following, we shall consider them separately.

3.6.1 Dynamic Branes in Static Bulk

Let us consider two orbifold branes moving along the hypersurfaces given by

$$y_I = y_I\left(\tau_I\right), \tag{3.148}$$

while the bulk are still described by the five-dimensional metric (3.47) with

$$\begin{aligned}
\sigma(y) &= \frac{1}{5}\ln\left(\frac{y+y_0}{L}\right), \\
\phi(y) &= \frac{6}{5}\ln\left(\frac{y+y_0}{L}\right) + \phi_0.
\end{aligned} \tag{3.149}$$

Then, from Eq. (3.135) we find that

$$\begin{aligned}
E^{(5)} &= 0, \quad \mathcal{G}_{\tau}^{(5)} = -\frac{3}{25L^2a^{12}}, \\
\mathcal{G}_{\theta}^{(5)} &= \frac{3}{25L^2a^{12}} + 12H^2,
\end{aligned} \tag{3.150}$$

where $H \equiv \dot{a}/a$. Inserting Eqs. (3.150) into Eqs. (3.137) and (3.138), we find

$$\begin{aligned}
H^2 &= \frac{8\pi G}{3}\left(\rho + \tau_{\phi} + \rho_{\Lambda}\right) \\
&\quad + \frac{2\pi G}{3\rho_{\Lambda}}\left(\rho + \tau_{\phi}\right)^2 - \frac{1}{25L^2a^{12}}, \qquad (3.151)\\
\frac{\ddot{a}}{a} &= -\frac{4\pi G}{3}\left(13\rho + 3p + 10\tau_{\phi} + 10\rho_{\Lambda}\right)
\end{aligned}$$

$$-\frac{2\pi G}{3\rho_\Lambda}\left[8\rho + \left(13\rho + 5\tau_\phi\right)\tau_\phi + 3p\left(\rho + \tau_\phi\right)\right]$$
$$+\frac{1}{5L^2 a^{12}}. \tag{3.152}$$

On the other hand, from Eq. (3.141) we find that

$$\Pi = -6H\left(\rho + \tau_\phi + 2\rho_\Lambda\right). \tag{3.153}$$

Note that in writing the above expression, we had used Eq. (3.151). Thus, Eqs. (3.143) and (3.144) can be cast in the form,

$$\left(\dot{\rho} + \dot{\tau}_\phi\right) + 3H\left(\rho + p\right) = -6H\left(2\rho_\Lambda + \rho + \tau_\phi\right), \tag{3.154}$$

$$\left(\dot{\rho} - \dot{\tau}_\phi\right) + 3H\left(\rho + p\right) = 2Q + 6H\left(2\rho_\Lambda + \rho + \tau_\phi\right). \tag{3.155}$$

It should be noted that Eq. (3.154) can be obtained directly from Eqs. (3.151) and (3.152), as it is expected. Therefore, among the four equations, (3.151)-(3.151) and (3.154)-(3.154), only three of them are independent, while on each of the two branes, there are five unknown functions, a, ρ, p, Q and V_4 (or equivalent, τ_ϕ). Thus, to have unique solutions, we need to impose two additional conditions. One of them will be the equation of state. To study current acceleration of the universe, we choose it to be the dust fluid, i.e.,

$$p = 0. \tag{3.156}$$

The other condition could be obtained by specifying the potnetials $V_4^{(I)}(\phi)$ on each of the two branes, or by specifying the interaction terms $Q^{(I)}$. In the following, we shall consider both possibilities separately.

Case: $Q^{(I)} \neq 0$

Let us first introduce the quantities,

$$\begin{aligned}\Omega_m &= \frac{\rho_m}{\rho_{cr}}, \quad \Omega_\phi = \frac{\tau_\phi}{\rho_{cr}}, \quad \Omega_\Lambda = \frac{\rho_\Lambda}{\rho_{cr}},\\ \Omega_a &= -\frac{1}{25H_0^2 L^2 a^{12}} = \frac{\Omega_a^{(0)}}{a^{12}},\end{aligned} \tag{3.157}$$

where $\rho_{cr} \equiv 3H_0^2/8\pi G$. Then, Eqs. (3.151) and (3.154) can be written as

$$
\begin{aligned}
E^2 &= \Omega_\Lambda + \Omega_m + \Omega_\phi + \Omega_a + \frac{(\Omega_m + \Omega_\phi)^2}{4\Omega_\Lambda}, &(3.158)\\
\Omega_t^* &= -3E\left(\Omega_m + 2\Omega_t + 4\Omega_\Lambda\right), &(3.159)
\end{aligned}
$$

where $E \equiv H/H_0$, $\Omega_t^* \equiv d\Omega_t/d(H\tau)$ and

$$
\Omega_t = \Omega_m + \Omega_\phi, \tag{3.160}
$$

with the constraint,

$$
1 = \Omega_\Lambda + \Omega_t^{(0)} + \Omega_a^{(0)} + \frac{\Omega_t^{(0)}}{4\Omega_\Lambda}, \tag{3.161}
$$

where $\Omega_N^{(0)}$'s denote their current values. On the other hand, in term of $\Omega_N^{(0)}$'s, we find

$$
\begin{aligned}
\frac{a^{**}}{a} &= -5E^2 - \frac{3}{2}\Omega_m - \frac{3\Omega_m\Omega_t}{4\Omega_\Lambda}, &(3.162)\\
\tilde{Q} &\equiv \frac{2Q}{H_0\rho_{cr}} = \Omega_m^* - \Omega_\phi^* \\
&\quad -3E\left(\Omega_m + 2\Omega_\phi + 4\Omega_\Lambda\right). &(3.163)
\end{aligned}
$$

If we choose the potential $V_4(\phi)$ on each of the two branes as that given in Eq. (3.57), we find that

$$
\tau_\phi^{(I)} = \alpha_I\left(\phi^2 - v_I^2\right)^2 + 6\epsilon_I\alpha\kappa_5^{-2}e^{-\phi}. \tag{3.164}
$$

It can be shown that the influence of the last term is negligible. So, in the following we first ignore this term, and later come back to it. Without the second term, we find that

$$
\Omega_\tau = \epsilon_I\frac{\tau_\phi}{\rho_{cr}} = \Omega_\tau^{(0,I)}\left(36\ln^2 a - v_I^2\right)^2. \tag{3.165}
$$

Then, our fitting parameters can be chosen as

$$
\left\{\Omega_\Lambda, \Omega_m^{(0)}, \Omega_a^{(0)}, v_I\right\}. \tag{3.166}
$$

To fit the above model with observational data, we use the reduced Union compilation of 307 SNe supernova data [141] and BAO measurement from the SDSS data

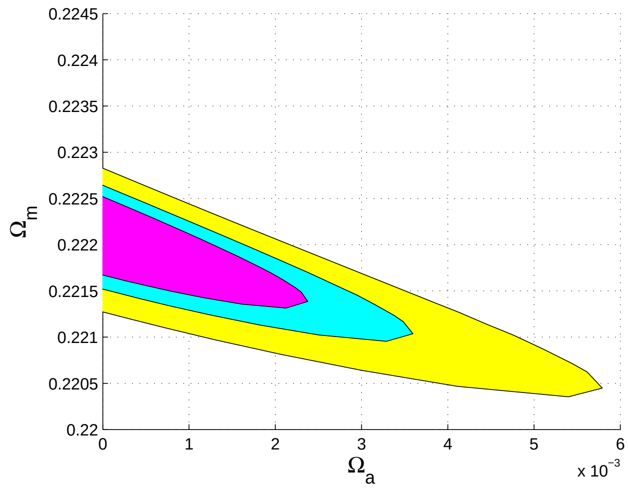

Figure 3.7: The marginalized contour of $\Omega_m - \Omega_a$ for the case where the second term in the right-hand side of Eq. (3.164) is zero.

[142, 143]. By using our numerical code, based on the publicly available MINUIT program of CERN, we find that, for $v_I = 10$, the best fitting is $\Omega_m^{(0)} = 0.22^{+0.03}_{-0.03}$, $\Omega_\Lambda = 0.003^{+0.001}_{-0.001}$, and $\Omega_a^{(0)} = -3.01^{\times}10^{-11}{}^{+0.0025}_{-0.0025}$ with $\chi^2 = 383.1$. Figs.3.7-3.8 show the marginalized contours of the $\Omega's$.

With the above best fitting values of the $\Omega's$ and v_I as initial conditions, the future evolution of the universe is shown in Figs. 3.9.

When the second term in Eq. (3.164) is not ignored, the best fitting is given by $\Omega_m^{(0)} = 0.21^{+0.01}_{-0.01}$, $\Omega_a^{(0)} = 0.06^{+0.03}_{-0.03}$, $\Omega_\Lambda = 0.003^{+0.005}_{-0.001}$, $\Omega'_\phi = -0.006^{+0.006}_{-0.003}$, and $\Omega_p^0 = -0.3218$, where $\Omega_\tau = \Omega_\phi + \Omega_p$, $\Omega_\phi = \Omega_\phi^0/a^6$, and $\Omega_p = \Omega_p^0 \left(36 \ln a^2 - v_I^2\right)^2 / v_I^4$. With these best fitting values of the $\Omega's$ as the initial conditions, the future evolution of the universe is shown in Fig.3.10, which are indistinguishable from these given by Fig. 3.9.

Case: $Q^{(I)} = 0$

When $Q = 0$, for $p = 0$ Eqs. (3.154) and (3.155) yield,

$$\Omega_t^* = -3E\left(\Omega_m + 2\Omega_t + 4\Omega_\Lambda\right), \tag{3.167}$$

$$\Omega_m = \frac{\Omega_m^{(0)}}{a^3}, \tag{3.168}$$

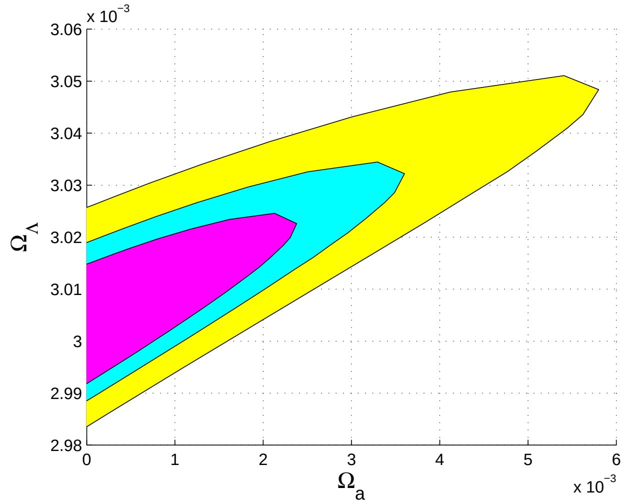

Figure 3.8: The marginalized contour of $\Omega_\Lambda - \Omega_a$ for the case where the second term in the right-hand side of Eq. (3.164) is zero.

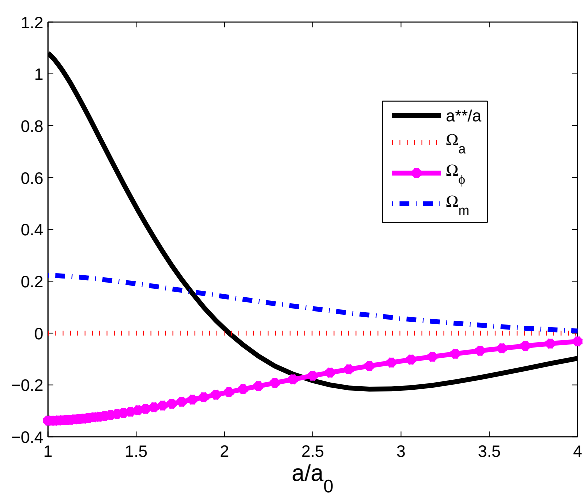

Figure 3.9: The evolution of the matter components, $\Omega' s$, and the acceleration, $a^{**}/a \equiv (d^2a/d(H_0\tau)^2)/a$ for the case where the second term in the right-hand side of Eq. (3.164) is zero.

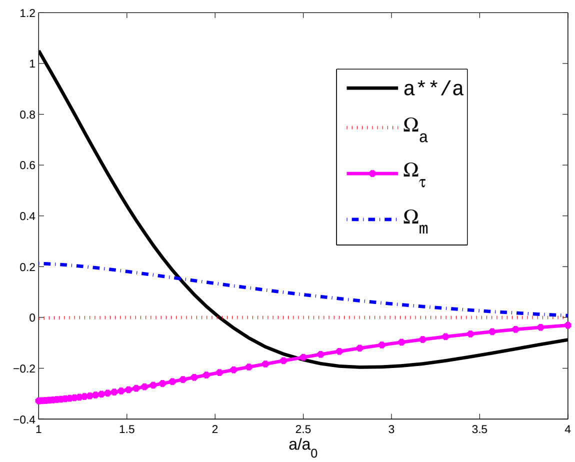

Figure 3.10: The evolution of the matter components, $\Omega' s$, and the acceleration, $a^{**}/a \equiv (d^2 a/d(H_0\tau)^2)/a$ for the case where the second term in the right-hand side of Eq. (3.164) is not zero.

while Eqs. (3.151) and (3.152) still take the same forms as these given by Eqs. (3.158) and (3.162) for the case $Q \neq 0$, i.e.,

$$E^2 = \Omega_\Lambda + \Omega_t + \Omega_a + \frac{\Omega_t^2}{4\Omega_\Lambda}, \tag{3.169}$$

$$\frac{a^{**}}{a} = -5E^2 - \frac{3}{2}\Omega_m - \frac{3\Omega_m\Omega_t}{4\Omega_\Lambda}. \tag{3.170}$$

In this case, our fitting parameters can be chosen as

$$\left\{\Omega_\Lambda, \Omega_m^{(0)}, \Omega_a^{(0)}\right\}. \tag{3.171}$$

Because the model can't fit the observations well for this case, I will not show the numerical values here in detail.

3.6.2 Fixed Branes in Time-dependent Bulk

Another way to generalize our static brane solution studied in Section IV is first to make the following coordinate transformations of the type of Eq. (3.123) [126],

$$\frac{t}{L} = f(\bar{t} + \bar{y}) + g(\bar{t} - \bar{y}),$$

$$\frac{y + y_0}{L} = f\left(\bar{t} + \bar{y}\right) - g\left(\bar{t} - \bar{y}\right), \tag{3.172}$$

where f and g are arbitrary functions of their indicated arguments. Without loss of generality, we shall assume that

$$f'g' > 0, \tag{3.173}$$

where a prime denotes the ordinary derivatives with respect to their indicated arguments. Then, in terms of $\bar{t}$ and $\bar{y}$ the five-dimensional metric (3.47) takes the form of Eq. (3.122) with $k = 0$ and

$$\begin{aligned}
\sigma(t, y) &= \frac{1}{5}\ln\left(F - G\right) + \frac{1}{2}\ln\left(4L^2 F'G'\right), \\
\omega(t, y) &= \frac{1}{5}\ln\left(F - G\right), \\
\phi(t, y) &= \frac{6}{5}\ln\left(F - G\right) + \ln\left(5\alpha L\right),
\end{aligned} \tag{3.174}$$

where $F \equiv f(t + |y|)$ and $G \equiv g(t - |y|)$, with $|y|$ being defined as that in Fig. 3.2. Note that in writing the above expressions we had first drapped the bars from $\bar{t}$ and $\bar{y}$, and then replaced y by $|y|$. Then, the normal vectors to the branes are given by

$$n_a^{(I)} = e^{\sigma(t, y_I)}\delta_a^y, \tag{3.175}$$

where $y_1 = y_c > 0$ and $y_2 = 0$. For the sake of convenience, we introduce the auxiliary function $b(t, y)$ via the relation,

$$b(t, y) \equiv \left(F + G\right)^5, \tag{3.176}$$

so that $b\left(\tau_I\right) = b\left(t\left(\tau_I\right), y_I\right)$. Then, we find that

$$\begin{aligned}
F'\left(t\left(\tau_I\right), y_I\right) &= \frac{5}{2}\left(\frac{d\tau_I}{dt}\right)\left(b^4\dot{b} + a^4\dot{a}\right), \\
G'\left(t\left(\tau_I\right), y_I\right) &= \frac{5}{2}\left(\frac{d\tau_I}{dt}\right)\left(b^4\dot{b} - a^4\dot{a}\right),
\end{aligned} \tag{3.177}$$

where $\dot{a} \equiv da/d\tau_I$, etc. Then, combining the above expressions with Eq. (3.132) we find that

$$\frac{\dot{b}^2}{a^8} - \frac{\dot{a}^2}{b^8} = \frac{1}{25L^2 a^{10} b^8}. \tag{3.178}$$

Hence, Eq. (3.135) yields

$$
\begin{aligned}
E^{(5)} &= 0, \quad \mathcal{G}_{\theta}^{(5)} = -\frac{3}{25L^2a^{12}}, \\
\mathcal{G}_{\tau}^{(5)} &= 12\left(\frac{a}{b}\right)^{10} H_b^2 - \frac{9}{25L^2a^{12}},
\end{aligned} \tag{3.179}
$$

where $H_b \equiv \dot{b}/b$. Since $\mathcal{G}_{\mu\nu}^{(5)}$ [cf. Eq. (3.22)] represents the projection of the 5D energy-mumentum tensor onto the brane through the field equations, the above expressions show clearly that such terms affect the evolution of the branes only in the early universe.

Inserting the above expresions into Eqs. (3.137)-(3.138) and Eqs. (3.143) and (3.144), we obtain the exact expressions as these given by Eqs. (3.151)-(3.152) and Eqs. (3.154)-(3.155). This remarkable feature is due to the very fact that in both cases we consider the dynamics of the most general branes in the same 5-dimensional background. Therefore, we can study brane cosmology either with the dynamical branes or with the fixed ones. The only difference is that in the case of fixed branes, an auxiliary function $b(\tau)$ nis introduced, which satisfies Eq. (3.178). Inserting Eq. (3.151) into Eq. (3.178) we obtain,

$$
H_b^2 = \frac{8\pi G}{3}\left(\frac{a}{b}\right)^{10}\left[(\rho + \rho_\Lambda + \tau_\phi) + \frac{1}{4\rho_\Lambda}(\rho + \tau_\phi)^2\right]. \tag{3.180}
$$

CHAPTER FOUR

Brany Cosmology in String Theory on S^1/Z_2

The theory of brany cosmology in Hořava-Witten heterotic M-theory on S^1/Z_2 can be applied in the framework of string theory. In this section I will give a systemic investigation of brany cosmology of string theory on S^1/Z_2 [107]

4.1 The Model

For the toroidal compactification of the Neveu-Schwarz/Neveu-Schwarz (NS-NS) sector in (5+5) dimensions, $\hat{M}_{10} = M_5 \times \mathcal{T}_5$, where $\mathcal{T}_5$ is a 5-dimensional torus, the action takes the form [153, 154],

$$\begin{aligned} \hat{S}_{10} &= -\frac{1}{2\kappa_{10}^2}\int d^{10}x\sqrt{|\hat{g}_{10}|}e^{-\hat{\Phi}}\left\{\hat{R}_{10}[\hat{g}]\right. \\ &\quad \left. +\hat{g}^{AB}\left(\hat{\nabla}_A\hat{\Phi}\right)\left(\hat{\nabla}_B\hat{\Phi}\right) - \frac{1}{12}\hat{H}^2\right\}, \end{aligned} \tag{4.1}$$

where $\hat{\nabla}_A$ denotes the covariant derivative with respect to $\hat{g}^{AB}$ with $A, B = 0, 1, ..., 9$, and $\hat{\Phi}$ is the dilaton field. The NS three-form field $\hat{H}_{ABC}$ is defined as

$$\hat{H}_{ABC} = 3\partial_{[A}\hat{B}_{BC]}, \tag{4.2}$$

where the square brackets imply total antisymmetrization over all indices. The 10-dimensional spacetimes to be considered are described by the metric,

$$\begin{aligned} d\hat{s}_{10}^2 &= \hat{g}_{AB}dx^A dx^B \\ &= \tilde{g}_{ab}\left(x^c\right)dx^a dx^b + h_{ij}\left(x^c\right)dz^i dz^j, \end{aligned} \tag{4.3}$$

where $\tilde{g}_{ab}$ is the metric on M_5, parametrized by the coordinates x^a with $a, b, c = 0, 1, ..., 4$, and h_{ij} is the metric on the compact space $\mathcal{T}_5$ with periodic coordinates z^i, where $i, j = 5, 6, ..., 9$.

By assuming that all the matter fields are functions of x^a only, it can be shown that the effective 5−dimensional action is given by,

$$\begin{aligned} S_5 &= -\frac{1}{2\kappa_5^2}\int d^5x\sqrt{|\tilde{g}_5|}e^{-\tilde{\phi}}\left\{\tilde{R}_5[\tilde{g}] + \left(\tilde{\nabla}_a\tilde{\phi}\right)\left(\tilde{\nabla}^a\tilde{\phi}\right)\right. \\ &\quad +\frac{1}{4}\left(\tilde{\nabla}_a h^{ij}\right)\left(\tilde{\nabla}^a h_{ij}\right) - \frac{1}{12}\tilde{H}_{abc}\tilde{H}^{abc} \\ &\quad \left. -\frac{1}{4}h^{ik}h^{jl}\left(\tilde{\nabla}_a B_{ij}\right)\left(\tilde{\nabla}^a B_{kl}\right)\right\}, \end{aligned} \tag{4.4}$$

where

$$\tilde{\phi} = \hat{\Phi} - \frac{1}{2}\ln|h|, \tag{4.5}$$

$$\kappa_5^2 \equiv \frac{\kappa_{10}^2}{V_0}, \tag{4.6}$$

with the 5−dimensional internal volume given by

$$V(x^a) \equiv \int d^5z\sqrt{|h|} = |h|^{1/2}V_0. \tag{4.7}$$

Note that in writing the action (4.4) we had assumed that the flux is block diagonal,

$$\left(\hat{B}_{CD}\right) = \begin{pmatrix} \tilde{B}_{ab} & 0 \\ 0 & B_{ij} \end{pmatrix}. \tag{4.8}$$

The action (4.4) is usually referred to as written in the string frame. To go to the Einstein frame, we make the following conformal transformations,

$$\begin{aligned} g_{ab} &= \Omega^2\tilde{g}_{ab}, \\ \Omega^2 &= \exp\left(-\frac{2}{3}\tilde{\phi}\right), \\ \phi &= \sqrt{\frac{2}{3}}\,\tilde{\phi}. \end{aligned} \tag{4.9}$$

Then, the action (4.4) takes the form

$$\begin{aligned} S_5^{(E)} &= -\frac{1}{2\kappa_5^2}\int d^5x\sqrt{|g_5|}\left\{R_5[g] - \frac{1}{2}(\nabla\phi)^2\right. \\ &\quad +\frac{1}{4}\left(\nabla_a h^{ij}\right)\left(\nabla^a h_{ij}\right) \\ &\quad -\frac{1}{12}e^{-\sqrt{\frac{8}{3}}\phi}H_{abc}H^{abc} \\ &\quad \left. -\frac{1}{4}h^{ik}h^{jl}\left(\nabla_a B_{ij}\right)\left(\nabla^a B_{kl}\right)\right\}, \end{aligned} \tag{4.10}$$

where ∇_a denotes the covariant derivative with respect to g_{ab}. It should be noted that, since the definition of the three-form $\hat{H}_{ABC}$ given by (4.2) is independent of the metric, it is conformally invariant. In particular, we have $H_{abc} = \tilde{H}_{abc}$ and $B_{ab} = \tilde{B}_{ab}$. However, we do have

$$\begin{aligned} H^{abc} &= g^{ad}g^{be}g^{cf}H_{def} = \Omega^{-6}\tilde{H}^{abc}, \\ H_{abc}H^{abc} &= \Omega^{-6}\tilde{H}_{abc}\tilde{H}^{abc}. \end{aligned} \tag{4.11}$$

Considering the addition of a potential term [154], in the string frame we have

$$\hat{S}^m_{10} = -\int d^{10}x\sqrt{|\hat{g}_{10}|}V^s_{10}. \tag{4.12}$$

Then, after the dimensional reduction we find

$$S_{5,m} = -V_0\int d^5x\sqrt{|\tilde{g}_5|}\;|h|^{1/2}V^s_{10}, \tag{4.13}$$

where

$$\tilde{g}_5 = \exp\left(\sqrt{\frac{50}{3}}\;\phi\right)\; g_5. \tag{4.14}$$

Changed to the Einstein frame, the action (4.13) finally takes the form,

$$S^{(E)}_{5,m} = -\frac{1}{2\kappa_5^2}\int d^5x\sqrt{|g_5|}V_5, \tag{4.15}$$

where

$$V_5 \equiv 2\kappa_5^2 V_0 V^s_{10}\exp\left(\frac{5}{\sqrt{6}}\;\phi\right)\;|h|^{1/2}. \tag{4.16}$$

If we further assume that

$$\begin{aligned} h_{ij} &= -\exp\left(\sqrt{\frac{2}{5}}\;\psi\right)\delta_{ij}, \\ h^{ij} &= -\exp\left(-\sqrt{\frac{2}{5}}\;\psi\right)\delta^{ij}, \end{aligned} \tag{4.17}$$

we find that

$$S^{(E)}_5 + S^{(E)}_{5,m} = -\frac{1}{2\kappa_5^2}\int d^5x\sqrt{|g_5|}\,\{R_5[g]$$

$$
\begin{aligned}
&-\frac{1}{2}\left((\nabla\phi)^2 + (\nabla\psi)^2 - 2V_5\right)\\
&-\frac{1}{4}e^{-\sqrt{\frac{8}{5}}\,\psi}\delta^{ik}\delta^{jl}\left(\nabla_a B_{ij}\right)\left(\nabla^a B_{kl}\right)\\
&-\frac{1}{12}e^{-\sqrt{\frac{8}{3}}\,\phi}H_{abc}H^{abc}\Big\},
\end{aligned}
\tag{4.18}
$$

where the effective 5−dimensional potential (4.14) now becomes

$$
V_5 \equiv V^0_{(5)} \exp\left(\frac{5}{\sqrt{6}}\,\phi + \sqrt{\frac{5}{2}}\,\psi\right),
\tag{4.19}
$$

where $V^0_{(5)} \equiv 2\kappa_5^2 V_0 V^s_{10}$.

To study orbifold branes, we consider the brane actions,

$$
\begin{aligned}
S^{(I)}_{4,m} \;=\; & -\int_{M_4^{(I)}} \sqrt{\left|g_4^{(I)}\right|}\left(\epsilon_I V_4^{(I)}(\phi,\psi) + g_s^{(I)}\right) d^4\xi_{(I)}\\
& + \int_{M_4^{(I)}} d^4\xi_{(I)}\sqrt{\left|g_4^{(I)}\right|}\\
& \times\mathcal{L}^{(I)}_{4,m}\left(\phi,\psi,B,\chi\right),
\end{aligned}
\tag{4.20}
$$

where $I = 1, 2$, $V_4^{(I)}(\phi,\psi)$ denotes the potential of the scalar fields ϕ and ψ, and $\xi^{\mu}_{(I)}$'s are the intrinsic coordinates of the I-th brane with $\mu,\nu = 0,1,2,3$, and $\epsilon_1 = -\epsilon_2 = 1$. χ denotes collectively the matter fields, and $g_s^{(I)}$ is a constant, which is related to the four-dimensional Newtonian constant via the relation given by Eq.(4.39) below. The variation of the total action,

$$
S_{total} = S_5^{(E)} + S^{(E)}_{5,m} + \sum_{I=1}^{2} S^{(I)}_{4,m},
\tag{4.21}
$$

with respect to the metric g_{ab} yields the field equations,

$$
\begin{aligned}
G^{(5)}_{ab} \;=\; & \kappa_5^2 T^{(5)}_{ab} + \kappa_5^2\sum_{I=1}^{2}\mathcal{T}^{(I)}_{\mu\nu}e^{(I,\,\mu)}_a e^{(I,\,\nu)}_b\\
& \times\sqrt{\left|\frac{g_4^{(I)}}{g_5}\right|}\,\delta\left(\Phi_I\right),
\end{aligned}
\tag{4.22}
$$

where $\delta(x)$ denotes the Dirac delta function normalized in the sense of [125], and the two branes are localized on the surfaces,

$$
\Phi_I\left(x^a\right) = 0.
\tag{4.23}
$$

The energy-momentum tensors $T_{ab}^{(5)}$ and $\mathcal{T}_{\mu\nu}^{(I)}$ are given by

$$
\begin{aligned}
\kappa_5^2 T_{ab}^{(5)} &\equiv \frac{1}{2}\left[(\nabla_a\phi)(\nabla_b\phi) + (\nabla_a\psi)(\nabla_b\psi)\right. \\
&\quad + \frac{1}{2} e^{-\sqrt{\frac{8}{5}}\,\psi}\left(\nabla_a B^{ij}\right)(\nabla_b B_{ij}) \\
&\quad \left. + \frac{1}{2} e^{\sqrt{\frac{8}{3}}\,\phi} H_{acd} H_b{}^{cd}\right] \\
&\quad - \frac{1}{4} g_{ab}\left[(\nabla\phi)^2 + (\nabla\psi)^2 - 2V_5\right. \\
&\quad \frac{1}{2} e^{-\sqrt{\frac{8}{5}}\,\psi}\left(\nabla_c B^{ij}\right)(\nabla^c B_{ij}) \\
&\quad \left. + \frac{1}{6} e^{\sqrt{\frac{8}{3}}\,\phi} H_{cde} H^{cde}\right], \\
\mathcal{T}_{\mu\nu}^{(I)} &\equiv \tau_{\mu\nu}^{(I)} + \left(g_s^{(I)} + \tau_{(\phi,\psi)}^{(I)}\right) g_{\mu\nu}^{(I)}, \\
\tau_{\mu\nu}^{(I)} &\equiv 2\frac{\delta \mathcal{L}_{4,m}^{(I)}}{\delta g^{(I)\,\mu\nu}} - g_{\mu\nu}^{(I)} \mathcal{L}_{4,m}^{(I)},
\end{aligned}
\tag{4.24}
$$

where $B^{ij} \equiv \delta^{ik}\delta^{jl} B_{kl}$,

$$
\begin{aligned}
\tau_{(\phi,\psi)}^{(I)} &\equiv \epsilon_I V_4^{(I)}(\phi,\psi), \\
e_{(\mu)}^{(I)\,a} &\equiv \frac{\partial x^a}{\partial \xi_{(I)}^{\mu}}, \\
e_a^{(I,\,\mu)} &\equiv g_{ab} g^{(I)\,\mu\nu} e_{(\nu)}^{(I)\,b},
\end{aligned}
\tag{4.25}
$$

and $g_{\mu\nu}^{(I)}$ is the reduced metric on the I-th brane, defined as

$$
g_{\mu\nu}^{(I)} \equiv g_{ab} e_{(\mu)}^{(I)a} e_{(\nu)}^{(I)b}\Big|_{M_4^{(I)}}. \tag{4.26}
$$

Variation of the total action Eq.(4.21) with respect to ϕ, ψ and B, respectively, yields the following equations of the matter fields,

$$
\begin{aligned}
\Box\phi &= -\frac{\partial V_5}{\partial\phi} - \frac{1}{12}\sqrt{\frac{8}{3}}\, e^{-\sqrt{\frac{8}{3}}\,\phi} H_{abc} H^{abc} \\
&\quad - 2\kappa_5^2 \sum_{I=1}^{2}\left(\epsilon_I \frac{\partial V_4^{(I)}}{\partial\phi} + \sigma_\phi^{(I)}\right) \\
&\quad \times \sqrt{\left|\frac{g_4^{(I)}}{g_5}\right|}\,\delta\left(\Phi_I\right),
\end{aligned}
\tag{4.27}
$$

$$
\begin{aligned}
\Box\psi &= -\frac{\partial V_5}{\partial\psi} - \sqrt{\frac{1}{10}} e^{-\sqrt{\frac{8}{5}}\,\psi}\left(\nabla_a B^{ij}\right)\left(\nabla^a B_{ij}\right) \\
&\quad -2\kappa_5^2 \sum_{I=1}^{2}\left(\epsilon_I \frac{\partial V_4^{(I)}}{\partial\psi} + \sigma_\psi^{(I)}\right) \\
&\quad \times\sqrt{\left|\frac{g_4^{(I)}}{g_5}\right|}\,\delta\left(\Phi_I\right), \qquad (4.28) \\
\Box B_{ij} &= \sqrt{\frac{8}{5}}\left(\nabla_a\psi\right)\left(\nabla^a B_{ij}\right) \\
&\quad -\sum_{I=1}^{2}\Psi_{ij}^{(I)}\sqrt{\left|\frac{g_4^{(I)}}{g_5}\right|}\,\delta\left(\Phi_I\right), \qquad (4.29) \\
\nabla^c H_{cab} &= \sqrt{\frac{8}{3}}\, H_{cab}\nabla^c\phi \\
&\quad -\sum_{I=1}^{2}\Phi_{ab}^{(I)}\sqrt{\left|\frac{g_4^{(I)}}{g_5}\right|}\,\delta\left(\Phi_I\right), \qquad (4.30)
\end{aligned}
$$

where $\Box \equiv g^{ab}\nabla_a\nabla_b$, and

$$
\begin{aligned}
\sigma_\phi^{(I)} &\equiv -\frac{\delta\mathcal{L}_{4,m}^{(I)}}{\delta\phi}, \\
\sigma_\psi^{(I)} &\equiv -\frac{\delta\mathcal{L}_{4,m}^{(I)}}{\delta\psi}, \\
\Psi_{ij}^{(I)} &\equiv -4\kappa_5^2 e^{\sqrt{\frac{8}{5}}\,\psi}\frac{\delta\mathcal{L}_{4,m}^{(I)}}{\delta B^{ij}}, \\
\Phi_{ab}^{(I)} &\equiv -4\kappa_5^2 e^{\sqrt{\frac{8}{3}}\,\phi}\frac{\delta\mathcal{L}_{4,m}^{(I)}}{\delta B^{ab}}. \qquad (4.31)
\end{aligned}
$$

Like we did in section 3.2.3, the 4-dimensional Einstein tensor can be represent as,

$$
G_{\mu\nu}^{(4)} = \mathcal{G}_{\mu\nu}^{(5)} + E_{\mu\nu}^{(5)} + \mathcal{F}_{\mu\nu}^{(4)}, \qquad (4.32)
$$

where

$$
\begin{aligned}
\mathcal{G}_{\mu\nu}^{(5)} &\equiv \frac{2}{3}\left\{G_{ab}^{(5)} e_{(\mu)}^a e_{(\nu)}^b \right. \\
&\qquad \left. -\left[G_{ab}n^a n^b + \frac{1}{4}G^{(5)}\right] g_{\mu\nu}\right\}, \\
E_{\mu\nu}^{(5)} &\equiv C_{abcd}^{(5)} n^a e_{(\mu)}^b n^c e_{(\nu)}^d,
\end{aligned}
$$

$$\begin{aligned}\mathcal{F}^{(4)}_{\mu\nu} &\equiv K_{\mu\lambda}K^{\lambda}_{\nu} - KK_{\mu\nu}\\ &-\frac{1}{2}g_{\mu\nu}\left(K_{\alpha\beta}K^{\alpha\beta} - K^2\right),\end{aligned} \tag{4.33}$$

where n^a denotes the normal vector to the brane, $G^{(5)} \equiv g^{ab}G^{(5)}_{ab}$, and $C^{(5)}_{abcd}$ the Weyl tensor. The extrinsic curvature $K_{\mu\nu}$ is defined as

$$K_{\mu\nu} \equiv e^{a}_{(\mu)}e^{b}_{(\nu)}\nabla_a n_b. \tag{4.34}$$

A crucial step of this approach is the Lanczos equations [156],

$$\left[K^{(I)}_{\mu\nu}\right]^- - g^{(I)}_{\mu\nu}\left[K^{(I)}\right]^- = -\kappa_5^2\mathcal{T}^{(I)}_{\mu\nu}, \tag{4.35}$$

where

$$\begin{aligned}\left[K^{(I)}_{\mu\nu}\right]^- &\equiv \lim_{\Phi_I\to 0^+}K^{(I)\,+}_{\mu\nu} - \lim_{\Phi_I\to 0^-}K^{(I)\,-}_{\mu\nu},\\ \left[K^{(I)}\right]^- &\equiv g^{(I)\,\mu\nu}\left[K^{(I)}_{\mu\nu}\right]^-.\end{aligned} \tag{4.36}$$

Assuming that the branes have Z_2 symmetry, we can express the intrinsic curvatures $K^{(I)}_{\mu\nu}$ in terms of the effective energy-momentum tensor $\mathcal{T}^{(I)}_{\mu\nu}$ through the Lanczos equations (4.35). Then, we find that $G^{(4)}_{\mu\nu}$ given by Eq.(4.32) can be cast in the form,

$$\begin{aligned}G^{(4)}_{\mu\nu} &= \mathcal{G}^{(5)}_{\mu\nu} + E^{(5)}_{\mu\nu} + \mathcal{E}^{(4)}_{\mu\nu}\\ &+\kappa_4^2\tau_{\mu\nu} + \Lambda g_{\mu\nu} + \kappa_5^4\pi_{\mu\nu},\end{aligned} \tag{4.37}$$

where

$$\begin{aligned}\pi_{\mu\nu} &\equiv \frac{1}{4}\left\{\tau_{\mu\lambda}\tau^{\lambda}_{\nu} - \frac{1}{3}\tau\tau_{\mu\nu}\right.\\ &\left.-\frac{1}{2}g_{\mu\nu}\left(\tau^{\alpha\beta}\tau_{\alpha\beta} - \frac{1}{3}\tau^2\right)\right\},\\ \mathcal{E}^{(4)}_{\mu\nu} &\equiv \frac{\kappa_5^4}{6}\tau_{(\phi,\psi)}\left[\tau_{\mu\nu} + \left(g_s + \frac{1}{2}\tau_{(\phi,\psi)}\right)g_{\mu\nu}\right],\end{aligned} \tag{4.38}$$

and

$$\begin{aligned}\kappa_4^2 &= \frac{1}{6} g_s \kappa_5^4, \\ \Lambda &= \frac{1}{12} g_s^2 \kappa_5^4. \end{aligned} \tag{4.39}$$

For a perfect fluid,

$$\tau_{\mu\nu} = (\rho + p)\, u_\mu u_\nu - p g_{\mu\nu}, \tag{4.40}$$

where u_μ is the four-velocity of the fluid, we find that

$$\pi_{\mu\nu} = \frac{\rho}{6}\left[(\rho + p)\, u_\mu u_\nu - \left(p + \frac{1}{2}\rho\right) g_{\mu\nu}\right]. \tag{4.41}$$

Note that in writing Eqs.(4.37)-(4.41), without causing any confusion, we had dropped the super indices (I).

In the rest of this part, we shall turn off the flux, i.e., $\hat{B}_{CD} = 0$, which is consistent with the field equations, provided that $\Psi_{ij}^{(I)} = 0$ and $\Phi_{ab}^{(I)} = 0$.

4.2 The General Metric of the Five-Dimensional Spacetimes

Since we shall apply such spacetimes to cosmology, let us first consider the embedding of a 3-dimensional spatial space that is homogeneous, isotropic, and independent of time. It is not difficult to show that such a space must have a constant curvature and its metric takes the form [157],

$$d\Sigma_k^2 = \frac{dr^2}{1 - kr^2} + r^2\left(d\theta^2 + \sin^2\theta d\phi^2\right), \tag{4.42}$$

where the constant k represents the curvature of the 3-space, and can be positive, negative or zero. Without loss of generality, we shall choose coordinates such that $k = 0, \pm 1$. Then, one can see that the most general metric for the five-dimensional spacetime must take the form,

$$ds_5^2 = g_{ab} dx^a dx^b = g_{MN} dx^M dx^N - e^{2\omega\left(x^N\right)} d\Sigma_k^2, \tag{4.43}$$

where $M, N = 0, 1$. Clearly, the metric (4.43) is invariant under the coordinate transformations,

$$x'^N = f^N\left(x^M\right). \tag{4.44}$$

Using these two degrees of freedom, without loss of generality, we can always set

$$g_{00} = g_{11}, \quad g_{01} = 0, \tag{4.45}$$

so that the five-dimensional metric finally takes the form,

$$ds_5^2 = e^{2\sigma(t,y)}\left(dt^2 - dy^2\right) - e^{2\omega(t,y)}d\Sigma_k^2. \tag{4.46}$$

It should be noted that metric (4.46) is still subjected to the gauge freedom,

$$t = f(t' + y') + g(t' - y'), \quad y = f(t' + y') - g(t' - y'), \tag{4.47}$$

where $f(t' + y')$ and $g(t' - y')$ are arbitrary functions of their indicated arguments.

It is also interesting to note that in [155] a different gauge was used. Instead of setting $g_{00} = g_{11}$ it was chosen that the two branes are comoving with the coordinates, so that they are located on two fixed hypersurfaces $y = 0,\ y_c$. For details, see [155].

4.3 The Field Equations Outside the Two Orbifold Branes

The non-vanishing components of the Ricci tensor outside of the two branes are given by

$$\begin{aligned}
R_{tt}^{(5)} &= \sigma_{,yy} + 3\sigma_{,y}\omega_{,y} - \left[\sigma_{,tt} + 3\omega_{,tt} + 3\omega_{,t}\left(\omega_{,t} - \sigma_{,t}\right)\right], \\
R_{ty}^{(5)} &= -3\left[\omega_{,ty} + \omega_{,t}\omega_{,y} - \left(\sigma_{,t}\omega_{,y} + \sigma_{,y}\omega_{,t}\right)\right], \\
R_{yy}^{(5)} &= \sigma_{,tt} + 3\sigma_{,t}\omega_{,t} - \left[\sigma_{,yy} + 3\omega_{,yy} + 3\omega_{,y}\left(\omega_{,y} - \sigma_{,y}\right)\right], \\
R_{mn}^{(5)} &= -e^{-2\sigma}g_{mn}\left\{\omega_{,tt} + 3\omega_{,t}{}^2 - \left(\omega_{,yy} + 3\omega_{,y}{}^2\right)\right. \\
&\quad \left. + 2ke^{2(\sigma-\omega)}\right\},
\end{aligned} \tag{4.48}$$

where now $m,\ n = r, \theta, \varphi,\quad \sigma_{,t} \equiv \partial\sigma/\partial t$ and so on. Then, it can be shown that outside of the two branes the field equations have four independent components, which can be cast into the form,

$$\begin{aligned}
&\omega_{,tt} + \omega_{,t}\left(\omega_{,t} - 2\sigma_{,t}\right) + \omega_{,yy} + \omega_{,y}\left(\omega_{,y} - 2\sigma_{,y}\right) \\
&\qquad = -\frac{1}{6}\left[\left(\phi_{,t}{}^{2} + \phi_{,y}{}^{2}\right) + \left(\psi_{,t}{}^{2} + \psi_{,y}{}^{2}\right)\right], \qquad (4.49)\\
&2\sigma_{,tt} + \omega_{,tt} - 3\omega_{,t}{}^{2} - \left(2\sigma_{,yy} + \omega_{,yy} - 3\omega_{,y}{}^{2}\right) - 4ke^{2(\sigma-\omega)} \\
&\qquad = -\frac{1}{2}\left[\left(\phi_{,t}{}^{2} - \phi_{,y}{}^{2}\right) + \left(\psi_{,t}{}^{2} - \psi_{,y}{}^{2}\right)\right], \qquad (4.50)\\
&\omega_{,ty} + \omega_{,t}\omega_{,y} - \left(\sigma_{,t}\omega_{,y} + \sigma_{,y}\omega_{,t}\right) \\
&\qquad = -\frac{1}{6}\left(\phi_{,t}\phi_{,y} + \psi_{,t}\psi_{,y}\right), \qquad (4.51)\\
&\omega_{,tt} + 3\omega_{,t}{}^{2} - \left(\omega_{,yy} + 3\omega_{,y}{}^{2}\right) + 2ke^{2(\sigma-\omega)} \\
&\qquad = \frac{1}{3}e^{2\sigma}V_5, \qquad (4.52)
\end{aligned}$$

where V_5 is given by Eq.(4.19). On the other hand, the Klein-Gordon equations (4.27) and (4.28) outside the two branes take the form,

$$\begin{aligned}
&\phi_{,tt} + 3\phi_{,t}\omega_{,t} - \left(\phi_{,yy} + 3\phi_{,y}\omega_{,y}\right) \\
&\qquad = -\frac{5}{\sqrt{6}}\, V_5 e^{2\sigma}, \qquad (4.53)\\
&\psi_{,tt} + 3\psi_{,t}\omega_{,t} - \left(\psi_{,yy} + 3\psi_{,y}\omega_{,y}\right) \\
&\qquad = -\sqrt{\frac{5}{2}}\, V_5 e^{2\sigma}. \qquad (4.54)
\end{aligned}$$

4.4 The Field Equations on the Two Orbifold Branes

Eqs.(4.48) - (4.54) are the field equations that are valid in between the two orbifold branes, $y_2(t_2) < y < y_1(t_1)$, where $y = y_I(t_I)$ denote the locations of the two branes. The proper distance between the two branes is given by,

$$\mathcal{D} \equiv \int_{y_2}^{y_1} \sqrt{-g_{yy}}\,dy. \qquad (4.55)$$

On each of the two branes, the metric reduces to

$$\left.ds_5^2\right|_{M_4^{(I)}} = g^{(I)}_{\mu\nu} d\xi^{\mu}_{(I)} d\xi^{\nu}_{(I)} = d\tau_I^2 - a^2\left(\tau_I\right) d\Sigma_k^2, \qquad (4.56)$$

where $\xi^{\mu}_{(I)} \equiv \{\tau_I, r, \theta, \varphi\}$, and τ_I denotes the proper time of the I-th brane, defined by

$$\begin{aligned}
d\tau_I &= e^{\sigma}\sqrt{1-\left(\frac{\dot{y}_I}{\dot{t}_I}\right)^2}\, dt_I, \\
a(\tau_I) &\equiv \exp\left\{\omega\left[t_I(\tau_I), y_I(\tau_I)\right]\right\},
\end{aligned} \tag{4.57}$$

with $\dot{y}_I \equiv dy_I/d\tau_I$, etc. For the sake of simplicity and without causing any confusion, from now on we shall drop all the indices "I", unless some specific attention is needed. Then, the normal vector n_a and the tangential vectors $e^a_{(\mu)}$ are given, respectively, by

$$\begin{aligned}
n_a &= \epsilon e^{2\sigma}\left(-\dot{y}\delta^t_a + \dot{t}\delta^y_a\right), \\
n^a &= -\epsilon\left(\dot{y}\delta^a_t + \dot{t}\delta^a_y\right), \\
e^a_{(\tau)} &= \dot{t}\delta^a_t + \dot{y}\delta^a_y, \quad e^a_{(r)} = \delta^a_r, \\
e^a_{(\theta)} &= \delta^a_\theta, \quad e^a_{(\varphi)} = \delta^a_\varphi,
\end{aligned} \tag{4.58}$$

where $\epsilon = \pm 1$. When $\epsilon = +1$, the normal vector n^a points toward the increasing direction of y, and when $\epsilon = -1$, it points toward the decreasing direction of y. Then, the four-dimensional field equations on each of the two branes take the form,

$$\begin{aligned}
H^2 &+ \frac{k}{a^2} = \frac{8\pi G}{3}\left(\rho + \tau_{(\phi,\psi)}\right) + \frac{1}{3}\Lambda + \frac{1}{3}\mathcal{G}^{(5)}_{\tau} + E^{(5)} \\
&+ \frac{2\pi G}{3\rho_\Lambda}\left(\rho + \tau_{(\phi,\psi)}\right)^2,
\end{aligned} \tag{4.59}$$

$$\begin{aligned}
\frac{\ddot{a}}{a} &= -\frac{4\pi G}{3}\left(\rho + 3p - 2\tau_{(\phi,\psi)}\right) + \frac{1}{3}\Lambda \\
&- E^{(5)} - \frac{1}{6}\left(\mathcal{G}^{(5)}_{\tau} + 3\mathcal{G}^{(5)}_{\theta}\right) - \frac{2\pi G}{3\rho_\Lambda}\left[\rho\left(2\rho + 3p\right)\right. \\
&\left.+ \left(\rho + 3p - \tau_{(\phi,\psi)}\right)\tau_{(\phi,\psi)}\right],
\end{aligned} \tag{4.60}$$

where $H \equiv \dot{a}/a$, $\rho_\Lambda \equiv \Lambda_4/(8\pi G_4)$, and

$$\begin{aligned}
\mathcal{G}^{(5)}_{\tau} &\equiv \frac{1}{3}e^{-2\sigma}\left[\left(\phi_{,t}{}^2 + \psi_{,t}{}^2\right) - \left(\phi_{,y}{}^2 + \psi_{,y}{}^2\right)\right] \\
&- \frac{1}{24}\left\{5\left[(\nabla\phi)^2 + (\nabla\psi)^2\right] - 6V_5\right\},
\end{aligned}$$

$$\begin{aligned}
\mathcal{G}_\theta^{(5)} &\equiv \frac{1}{24}\Big\{8\left(\phi_{,n}{}^2+\psi_{,n}{}^2\right)-6V_5 \\
&+5\left[(\nabla\phi)^2+(\nabla\psi)^2\right]\Big\}, \\
E^{(5)} &\equiv \frac{1}{6}e^{-2\sigma}\left[(\sigma_{,tt}-\omega_{,tt})-(\sigma_{,yy}-\omega_{,yy})\right. \\
&\left.+ke^{2(\sigma-\omega)}\right], \qquad (4.61)
\end{aligned}$$

with $\phi_{,n} \equiv n^a\nabla_a\phi$. If the typical size of the extra dimensions is R, then it can be shown that

$$\rho_\Lambda = \frac{\Lambda_4}{8\pi G_4} = 3\left(\frac{R}{l_{pl}}\right)^{10}\left(\frac{M_{10}}{M_{pl}}\right)^{16} M_{pl}{}^4, \qquad (4.62)$$

where M_{pl} and l_{pl} denote the Planck mass and length, respectively. If M_{10} is in the order of TeV [158], we find that, in order to have ρ_Λ be in the order of its current observations value $\rho_\Lambda \simeq 10^{-47}\ GeV^4$, the typical size of the extra dimensions should be $R \simeq 10^{-22}\ m$, which is well below the current experimental limit of the extra dimensions [159].

4.5 A Particular Case

In this section, we consider a specific solution of the five-dimensional bulk and the corresponding Friedmann equations on the orbifold branes.

4.5.1 Exact Solutions in the Bulk

It can be shown that the following solution satisfies the field equations in the bulk,

$$\begin{aligned}
\sigma(t) &= \frac{1}{9}\ \ln(t)+\frac{1}{2}\ln\left(\frac{7}{6}\right), \\
\omega(t) &= \frac{10}{9}\ \ln(t), \\
\phi(t) &= -\frac{5}{18}\sqrt{6}\ \ln(t)+\phi_0, \\
\psi(t) &= -\frac{\sqrt{10}}{6}\ \ln(t)+\psi_0, \qquad (4.63)
\end{aligned}$$

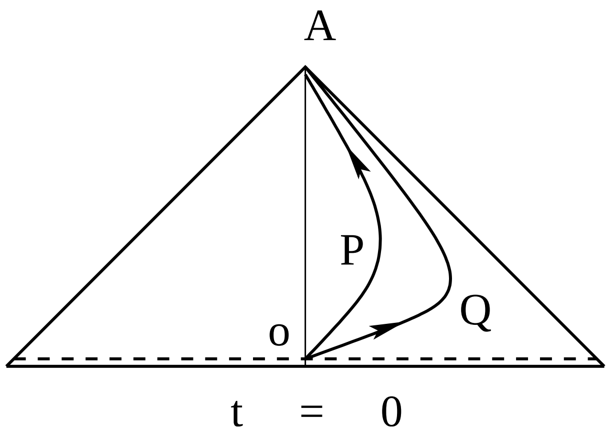

Figure 4.1: The Penrose diagram for the metric given by Eq.(4.65) in the text, where the spacetime is singular at $t = 0$. The curves OPA and OQA describes the history of the two orbifold branes located on the surfaces $y = y_I(\tau_I)$ with $I = 1, 2$. The bulk is the region between these two lines.

for $k = -1$, where

$$\phi_0 = \frac{\sqrt{6}}{5}\left\{\ln\left(\frac{2}{3V^0_{(5)}}\right) - \sqrt{\frac{5}{2}}\,\psi_0\right\}, \tag{4.64}$$

with ψ_0 being an arbitrary constant. Then, the corresponding 5-dimensional metric takes the form,

$$ds_5^2 = \left(\frac{7}{6}\right) t^{2/9}\left(dt^2 - dy^2\right) - t^{20/9} d\Sigma^2_{-1}. \tag{4.65}$$

Clearly, the spacetime is singular at $t = 0$ where all the four spatial dimensions collapse into a point singularity, a big bang like. This can be seen more clearly from the expression,

$$\psi_{,a}\psi^{,a} = \frac{3}{5}\phi_{,a}\phi^{,a} = \frac{5}{21} t^{-20/9}. \tag{4.66}$$

The corresponding Penrose diagram is given by Fig. 4.1.

Lifting the solution to the 10-dimensional superstring spacetime, we find that in the string frame the metric (4.3) takes the form,

$$\begin{aligned} d\hat{s}^2_{10} &= \hat{g}_{AB}dx^A dx^B \\ &= e^{\sqrt{\frac{2}{3}}\,\phi_0}\left\{\left(\frac{7}{6}\right) t^{-1/3}\left(dt^2 - dy^2\right) - t^{5/3} d\Sigma^2_{-1}\right\} \\ &\quad - e^{\sqrt{\frac{2}{5}}\,\psi_0} t^{-1/3}\delta_{ij}dz^i dz^j. \end{aligned} \tag{4.67}$$

The corresponding dilaton field is given by

$$\hat{\Phi} = -\frac{5}{3}\ln(t) + \hat{\Phi}_0, \tag{4.68}$$

where $\hat{\Phi}_0 \equiv \sqrt{3/2}\,\phi_0 + \sqrt{5/2}\,\psi_0$, from which we find

$$\hat{\Phi}_{,A}\hat{\Phi}^{,A} = \frac{50}{21}e^{-\sqrt{\frac{2}{3}}\,\phi_0}t^{-5/3}. \tag{4.69}$$

Clearly, it is also singular at $t = 0$, but with a weaker strength in comparing to that of the five-dimensional spacetime given by Eq.(4.19). A critical difference is that in the string frame the proper distance along the y-direction becomes decreasing as t increases, in contrast to that in the Einstein frame, as can be seen clearly from Eqs.(4.65) and (4.67).

4.5.2 Generalized Friedmann Equations on The Branes

On the other hand, from Eq.(4.61) we find that

$$\begin{aligned} E^{(5)} &= -\frac{1}{42a^2}, \quad \mathcal{G}^{(5)}_{\tau} = \frac{31}{126a^2}, \\ \mathcal{G}^{(5)}_{\theta} &= \frac{20}{81a^{9/5}}\dot{y}^2 - \frac{13}{378a^2}, \end{aligned} \tag{4.70}$$

where now $a(\tau) = t^{10/9}(\tau)$, and $\dot{y}$ is given by

$$\dot{y} = \epsilon_y a^{9/10}\left[\left(\frac{9}{10}\right)^2 H^2 - \frac{6}{7a^2}\right]^{1/2}, \tag{4.71}$$

with $\epsilon_y = \pm 1$. Inserting Eqs.(4.70) and (4.71) into Eqs.(4.59) and (4.60), we find that

$$\begin{aligned} H^2 &= \frac{8\pi G}{3}\left(\rho + \tau_{(\phi,\psi)} + \rho_\Lambda\right) + \frac{200}{189a^2} \\ &\quad + \frac{2\pi G}{3\rho_\Lambda}\left(\rho + \tau_{(\phi,\psi)}\right)^2, \end{aligned} \tag{4.72}$$

$$\begin{aligned} \frac{\ddot{a}}{a} &= \frac{4\pi G}{5}\left(3\rho_\Lambda + 3\tau_{(\phi,\psi)} - 2\rho - 5p\right) \\ &\quad - \frac{2\pi G}{3\rho_\Lambda}\left[\frac{1}{10}\left(\rho + \tau_{(\phi,\psi)}\right)^2 + \rho\left(2\rho + 3p\right)\right. \\ &\quad \left. + \left(\rho + 3p - \tau_{(\phi,\psi)}\right)\tau_{(\phi,\psi)}\right]. \end{aligned} \tag{4.73}$$

It is remarkable to note that these two equations do not depend on both ϵ defined in Eq.(4.58) and ϵ_y defined in Eq.(4.71). Combining Eqs.(4.72) and (4.73), we obtain

$$\left(\dot{\rho} + \dot{\tau}_{(\phi,\psi)}\right) + 3H\left(\rho + p\right) = -\frac{H}{20\Delta}\left[4\left(\rho + \rho_\Lambda + \tau_{(\phi,\psi)}\right) + \frac{\left(\rho + \tau_{(\phi,\psi)}\right)^2}{\rho_\Lambda}\right], \quad (4.74)$$

where

$$\Delta \equiv 1 + \frac{1}{2\rho_\Lambda}\left(\rho + \tau_{(\phi,\psi)}\right). \quad (4.75)$$

Eq.(4.74) shows clearly the interaction among the matter fields confined on the branes and the bulk. This can also be seen from Eq.(4.70).

4.5.3 Current Acceleration of the Universe

To study current acceleration of the universe, we first set

$$p = 0, \quad (4.76)$$

and then introduce the quantities,

$$\begin{aligned} \Omega_m &= \frac{\rho_m}{\rho_{cr}}, \quad \Omega_\tau = \frac{\tau_{(\phi,\psi)}}{\rho_{cr}}, \quad \Omega_\Lambda = \frac{\rho_\Lambda}{\rho_{cr}}, \\ \Omega_k &= \frac{200}{189 H_0^2 a^2} = \frac{\Omega_k^{(0)}}{a^2}, \end{aligned} \quad (4.77)$$

where $\rho_{cr} \equiv 3H_0^2/8\pi G$. It should be noted the slight difference between Ω_k defined here and the one normally used, $\Omega_k = -k/(H_0^2 a^2)$. Then, Eqs.(4.72), (4.74) and (4.71) can be written as

$$E^2 = \Omega_\Lambda + \Omega_t + \Omega_k + \frac{{\Omega_t}^2}{4\Omega_\Lambda}, \quad (4.78)$$

$$\begin{aligned} \Omega_t^* = &-\frac{E}{\Delta}\left\{\frac{1}{5}\left(\Omega_\Lambda + 16\Omega_t - 15\Omega_\tau\right)\right. \\ &\left.+\frac{\Omega_t}{20\Omega_\Lambda}\left(31\Omega_t - 30\Omega_\tau\right)\right\}, \end{aligned} \quad (4.79)$$

$$\begin{aligned} y^* = &\ \epsilon_y\left(\frac{9}{10}\right)\left(\frac{\Omega_k^{(0)}}{\Omega_k}\right)^{9/20} \\ &\times\sqrt{\Omega_\Lambda + \Omega_t + \frac{{\Omega_t}^2}{4\Omega_\Lambda}}, \end{aligned} \quad (4.80)$$

where $E \equiv H/H_0,\ y^* \equiv dy/d(H_0\tau)$, and

$$\Omega_t = \Omega_m + \Omega_\tau, \tag{4.81}$$

with the constraint,

$$1 = \Omega_k^{(0)} + \Omega_\Lambda + \Omega_t^{(0)} + \frac{{\Omega_t^{(0)}}^2}{4\Omega_\Lambda}, \tag{4.82}$$

where $\Omega_N^{(0)}$'s denote their current values. On the other hand, in terms of Ω's, we find

$$\begin{aligned} \frac{a^{**}}{a} &= \frac{3}{10}\left(3\Omega_\Lambda - 2\Omega_t + 5\Omega_\tau\right) \\ &\quad + \frac{3\Omega_t}{40\Omega_\Lambda}\left(7\Omega_t - 10\Omega_\tau\right). \end{aligned} \tag{4.83}$$

To study Eqs.(4.78)-(4.80) and (4.83) further, we need to specify Ω_τ. In the following, we shall consider two different cases.

4.5.3.1 $V_4^{(I)} = V_{(4)}^0 \exp\left\{\frac{n}{2}\left(\frac{5}{\sqrt{6}}\,\phi + \sqrt{\frac{5}{2}}\,\psi\right)\right\}$

If we choose the potential $V_4^{(I)}(\phi,\psi)$ on each of the two branes as [cf. Eq.(4.19)],

$$V_4^{(I)} = V_{(4)}^0 \exp\left\{\frac{n}{2}\left(\frac{5}{\sqrt{6}}\,\phi + \sqrt{\frac{5}{2}}\,\psi\right)\right\}, \tag{4.84}$$

where $V_{(4)}^0$ and n are arbitrary constants, we find that

$$\Omega_\tau = \epsilon_I \frac{V_{(4)}^0}{\rho_{cr}}\left(\frac{2}{3V_{(5)}^0}\right)^{n/2}\frac{1}{a^n} \equiv \frac{\Omega_\tau^{(0)}}{a^n}. \tag{4.85}$$

Then, our fitting parameters in this case can be chosen as

$$\left\{\Omega_\Lambda, \Omega_m^{(0)}, \Omega_k^{(0)}\right\}, \tag{4.86}$$

for any given n.

Fitting the above model to the 182 gold supernova Ia data [147] and the BAO parameter from SDSS [148], by using our numerical code [149], based on the publicly available MINUIT program of CERN, we find that, for $n = 1$, the best fitting is $\Omega_m = 0.24 \pm {}^{0.03}_{0.03}$, $\Omega_\Lambda = 0.76 \pm {}^{0.37}_{0.27}$, and $\Omega_k = 0.00 \pm {}^{0.05}_{0.00}$ with $\chi^2 = 172.4$. Figs. 2-4

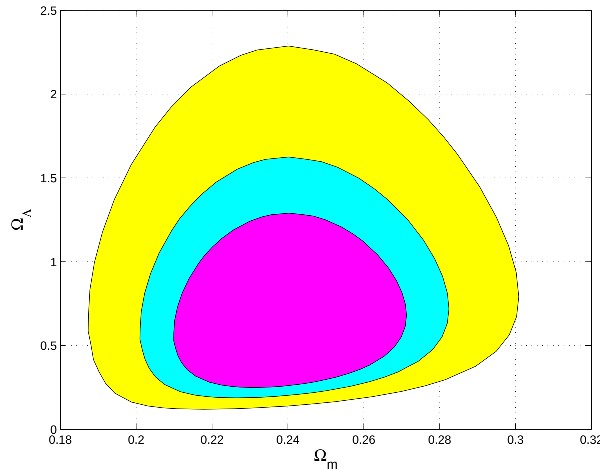

Figure 4.2: The marginalized contour of $\Omega_m - \Omega_\Lambda$ for the potential given by Eq.(4.84) with $n = 1$.

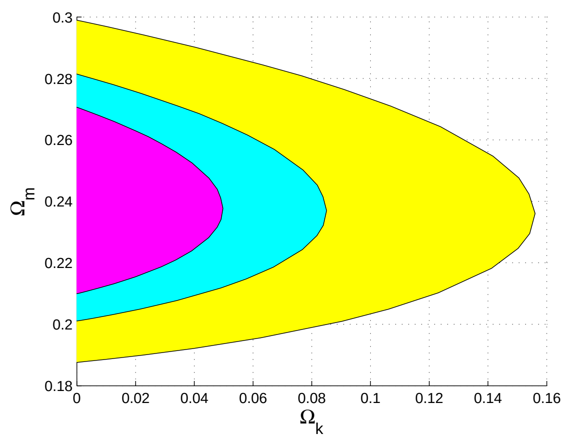

Figure 4.3: The marginalized contour of $\Omega_m - \Omega_k$ for the potential given by Eq.(4.84) with $n = 1$.

show the marginalized contours of the Ω's, from which we can see that the effect of the interaction between the bulk and the brane is negligible, and the later evolution of the universe follows more or less the same pattern as that of the ΛCDM model in the Einstein theory of gravity.

For $n = 3.5$, we find that the best fitting is $\Omega_m = 0.27 \pm^{0.03}_{0.03}$, $\Omega_\Lambda = 0.58 \pm^{0.11}_{0.12}$, and $\Omega_k = 0.00 \pm^{0.06}_{0.00}$ with $\chi^2 = 164.2$. Figs. 4.2-4.7 show the marginalized contours of the Ω's.

The above shows clearly that the case with $n = 3.5$ is observationally more

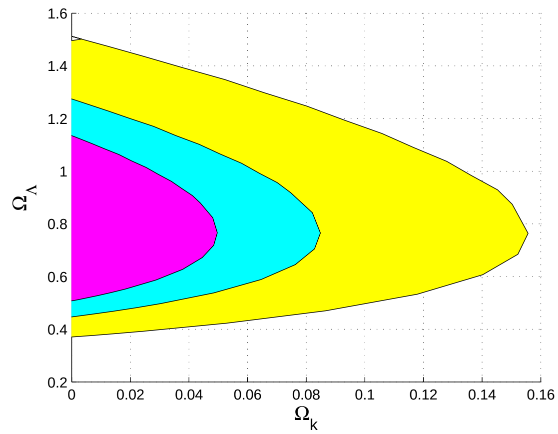

Figure 4.4: The marginalized contour of $\Omega_k - \Omega_\Lambda$ for the potential given by Eq.(4.84) with $n = 1$.

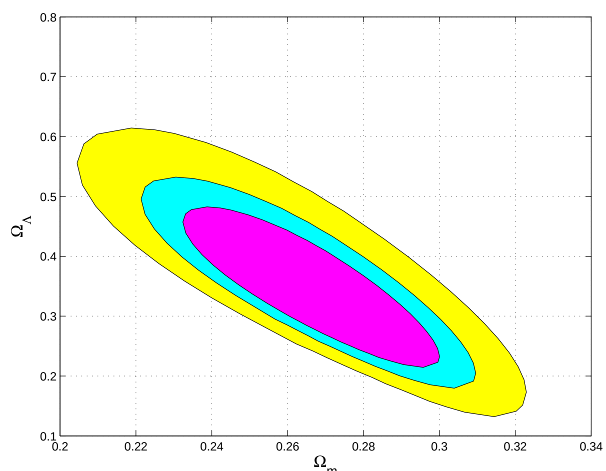

Figure 4.5: The marginalized contour of $\Omega_m - \Omega_\Lambda$ for the potential given by Eq.(4.84) with $n = 3.5$.

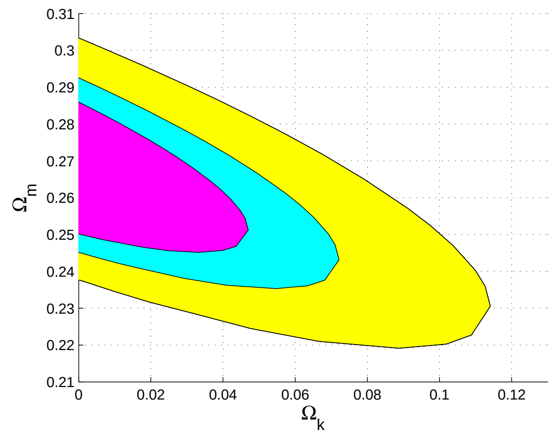

Figure 4.6: The marginalized contour of $\Omega_m - \Omega_k$ for the potential given by Eq.(4.84) with $n = 3.5$.

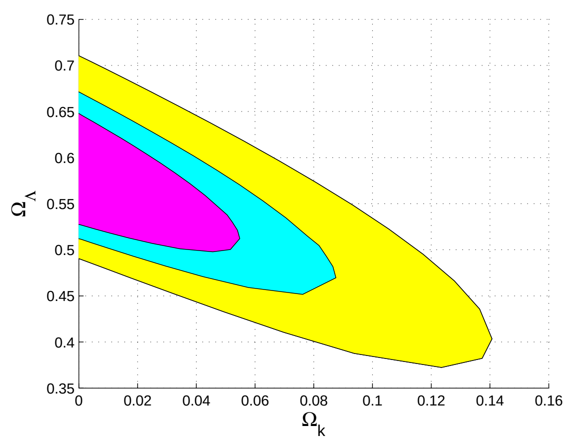

Figure 4.7: The marginalized contour of $\Omega_k - \Omega_\Lambda$ for the potential given by Eq.(4.84) with $n = 3.5$.

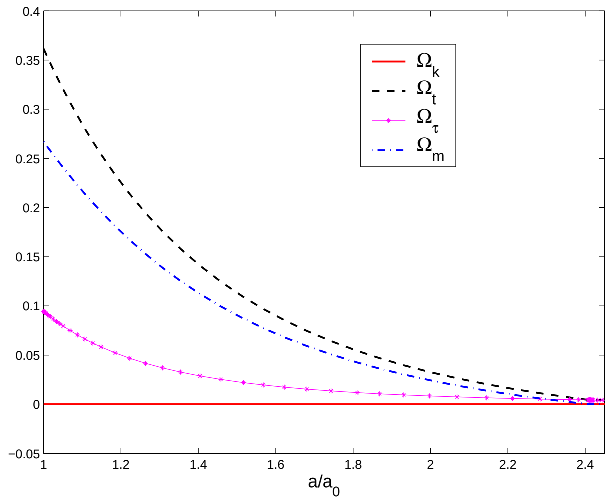

Figure 4.8: The evolution of the matter components, Ω_i's, for the potential given by Eq.(4.84) with $n = 3.5$.

favorable than that of $n = 1$. We have also fitted the data with various values of n, and found that the best fitting value of n is about $n = 3.5$.

With the above best fitting values of the Ω's and n as initial conditions, the future evolution of the universe is shown in Figs. 8 and 9, from which we can see that all of them, except for Ω_Λ, decreases rapidly, and Ω_Λ soon dominates the evolution of the universe, whereby a de Sitter universe is resulted.

From the metrics of Eqs.(4.65) and (4.67), on the other hand, one may naively conclude that the radion in the present case is not stable, as the proper distance given by Eq.(4.55) seems either to increases to infinity (in the Einstein frame, given by Eq.(4.65)) or to decreases to zero (in the string frame, given by Eq.(4.67)), as $t \rightarrow \infty$. A closer investigation shows that the problem is not as simple as it looks like. In particular, since $y_I = y_I(\tau_I)$, Eq.(4.55) makes sense only when the relation $\tau_1 = \tau_1(\tau_2)$ is known. In the present case, we transform such a dependence to the expansion factor a, and plot it out in Fig. 4.10, together with $y_I(a)$, from which we can see clearly that the distance between the two branes remains almost constant. This indicates that the radion might be stable. Certainly, before a definitive conclusion is reached, more detailed investigations are needed.

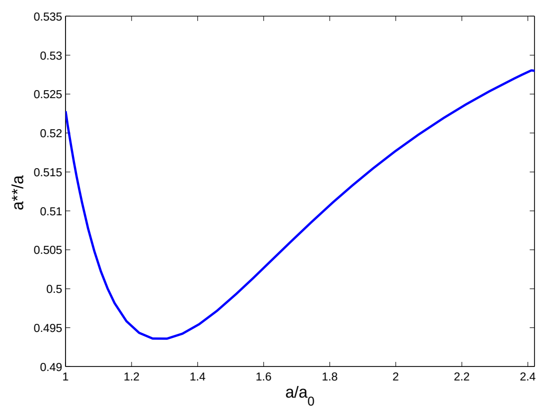

Figure 4.9: The evolution of the acceleration $a^{**}/a \equiv (d^2a/d\,(H_0\tau)^2)/a$ for the potential given by Eq.(4.84) with $n = 3.5$.

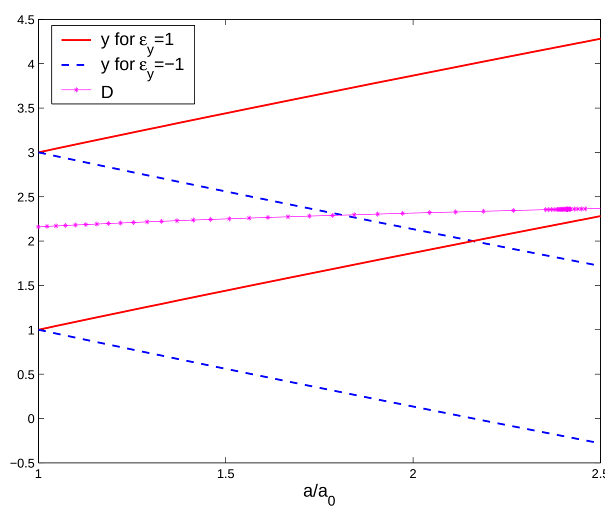

Figure 4.10: The locations of the two branes $y_I(a)$, and the proper distance $\mathcal{D}$ between the two branes for the potential given by Eq.(4.84) with $n = 3.5$. The initial conditions are chosen so that $y_1(a_0) = 3$ and $y_2(a_0) = 1$. The choice of $\epsilon_y = +1$ ($\epsilon_y = -1$) corresponds to the case where the branes move towards the increasing (decreasing) direction of y.

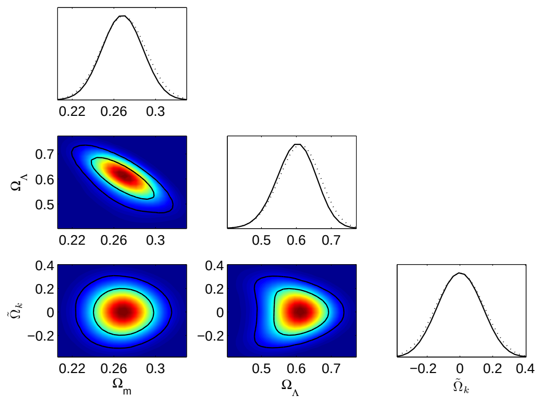

Figure 4.11: The marginalized probabilities and contours for the potential given by Eq.(4.84) with $n = 3.5$.

We also fit the above model with $n = 3.5$ by using our Monte-Carlo Markov Chain (MCMC) code [150], based on the publicly available package COSMOMC [160], and find that the best fitting is $\Omega_m = 0.27 \pm ^{0.04}_{0.03}$, $\Omega_\Lambda = 0.61 \pm ^{0.09}_{0.10}$, and $\tilde{\Omega}_k = -0.0026 \pm ^{0.2339}_{0.2396}$ with $\chi^2 = 164.10$, where

$$\Omega_k \equiv \tilde{\Omega}_k^2. \tag{4.87}$$

The corresponding marginalized probabilities and contours are given in Fig. 4.11. Clearly, these best fitting values are consistent with those obtained above by using our MINUIT code [149].

4.5.3.2 $V_4^{(I)} = \lambda_4^{(I)} \left(\psi^2 - {v_I}^2\right)^2$ To stabilize the radion, Goldberger and Wise proposed to choose the potential $V_4^{(I)}$ as [109],

$$V_4^{(I)}(\phi, \psi) = \lambda_4^{(I)} \left(\psi^2 - {v_I}^2\right)^2, \tag{4.88}$$

where $\lambda_4^{(I)}$ and ${v_I}^2$ $(I = 1, 2)$ are constants. Then, we find that

$$\Omega_\tau^{(I)} = \Omega_\tau^{(0,I)} \left(\left(\frac{3}{\sqrt{40}} \ln(a)\right)^2 - {v_I}^2\right)^2, \tag{4.89}$$

where $\Omega_\tau^{(0,I)} \equiv \epsilon_I \lambda_4^{(I)}/\rho_{cr}$. Note that in writing the above expressions, without loss

Table 4.1: The best fitting values of Ω_i for a given v_I of the potential given by Eq.(4.88).

v_I	χ^2	Ω_m	$\tilde{\Omega}_k$	Ω_Λ	$\Omega_\Lambda + \Omega_\tau$
0.1	171.28	$0.25\pm^{0.03}_{0.04}$	$-0.0009\pm^{0.21}_{0.22}$	$0.72\pm^{0.05}_{0.05}$	0.73
0.3	168.10	$0.29\pm^{0.05}_{0.05}$	$-0.0006\pm^{0.41}_{0.41}$	$1.06\pm^{0.15}_{0.17}$	0.47
0.5	157.50	$0.29\pm^{0.04}_{0.04}$	$-0.008\pm^{0.46}_{0.44}$	$1.28\pm^{0.31}_{0.28}$	0.70
1.0	156.69	$0.29\pm^{0.03}_{0.04}$	$-0.002\pm^{0.52}_{0.52}$	$1.64\pm^{0.71}_{0.48}$	0.64
3.0	156.38	$0.28\pm^{0.03}_{0.04}$	$-0.008\pm^{0.53}_{0.56}$	$1.93\pm^{1.01}_{0.73}$	0.57
10.0	166.35	$0.28\pm^{0.05}_{0.03}$	$-0.002\pm^{0.62}_{0.62}$	$1.97\pm^{2.17}_{0.74}$	0.56

of any generality, we had set $\psi_0 = 0$. Then, the fitting parameters can be taken as,

$$\left\{\Omega_\Lambda, \Omega_m^{(0)}, \Omega_k^{(0)}, v_I\right\}. \tag{4.90}$$

Fitting the above model to the 182 gold supernova Ia data [147] and the BAO parameter from SDSS [148], we first study the dependence of χ^2 on v_I. Table 4.1 shows such a dependence and the best fitting values of Ω_i's for each given v_I.

From the table we can see that χ^2 decreases until $v_I \simeq 3.0$ and then starts to increase, as v_I is continuously increasing. However, Ω_Λ and its uncertainty also increase as v_I is increasing, while Ω_m and Ω_k remain almost the same. Since Ω_τ acts as a varying cosmological constant, Table 4.1 shows that the total effective cosmological constant $\Omega_\Lambda^{eff.} \equiv \Omega_\Lambda + \Omega_\tau$ is between 0.47 and 0.73.

Fig. 4.12 shows the marginalized probabilities and contours for the potential given by Eq.(4.88) with $v_I = 0.5$, and Fig. 4.13 shows the future evolution of the corresponding acceleration of the universe. From there we can see that the acceleration increases to a maximal value and then starts to decrease. As the time is continuously increasing, it will pass the zero point and then becomes negative. Thus, in the present model, the domination of the cosmological constant is only temporary. Due to the presence of the potential term, represented by Ω_τ, the universe will be in its decelerating expansion phase again in the future, whereby all problems connected with a far future de Sitter universe are resolved [146]. The effects of Ω_τ can be seen

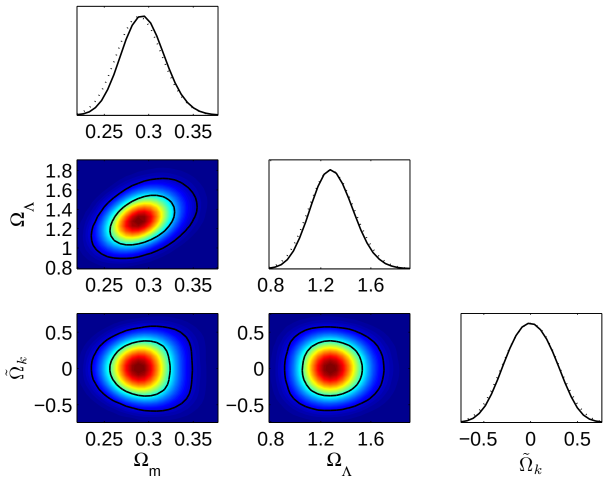

Figure 4.12: The marginalized probabilities and contours for the potential given by Eq.(4.88) with $v_I = 0.5$.

clearly from Fig. 4.14, from which we can see that both Ω_m and Ω_k decrease rapidly, and soon Ω_τ dominates the evolution of the universe.

These are the common features for any given value of v_I. Figs. 4.15, 4.16, and 4.17 show, respectively, the marginalized probabilities and contours, the future evolution of a^{**}/a and of Ω_i for $v_I = 0.1$.

In addition, we also find that the proper distance between the two orbifold branes defined by Eq.(4.55) is not sensitive to the choice of v_I, and remains almost constant during the future evolution of the universe, as shown in Fig. 4.18. This also indicates that the radion might be stable in the present case, too.

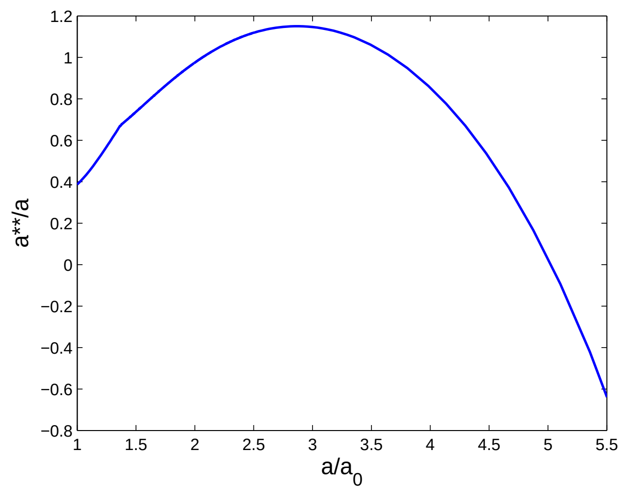

Figure 4.13: The acceleration a^{**}/a for the potential given by Eq.(4.88) with $v_I = 0.5$.

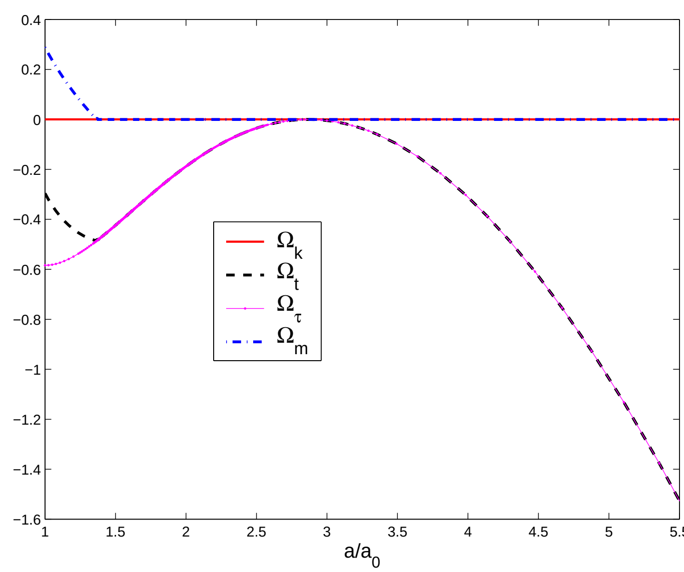

Figure 4.14: The future evolution of Ω_i for the potential given by Eq.(4.88) with $v_I = 0.5$.

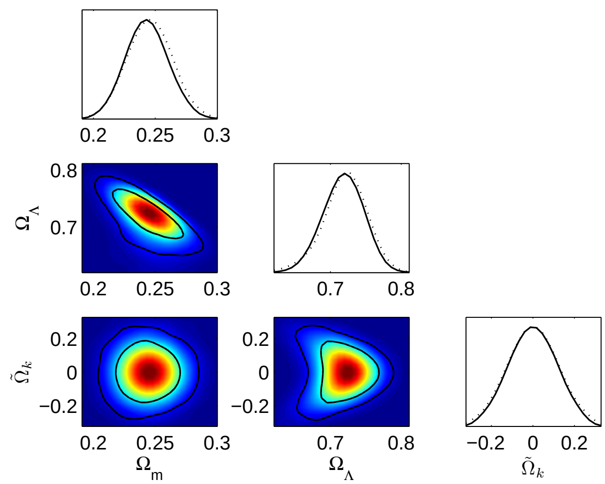

Figure 4.15: The marginalized probabilities and contours for the potential given by Eq.(4.88) with $v_I = 0.1$.

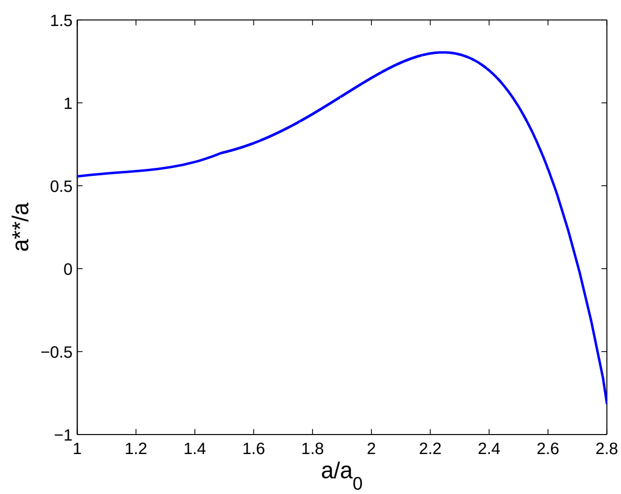

Figure 4.16: The acceleration a^{**}/a for the potential given by Eq.(4.88) with $v_I = 0.1$.

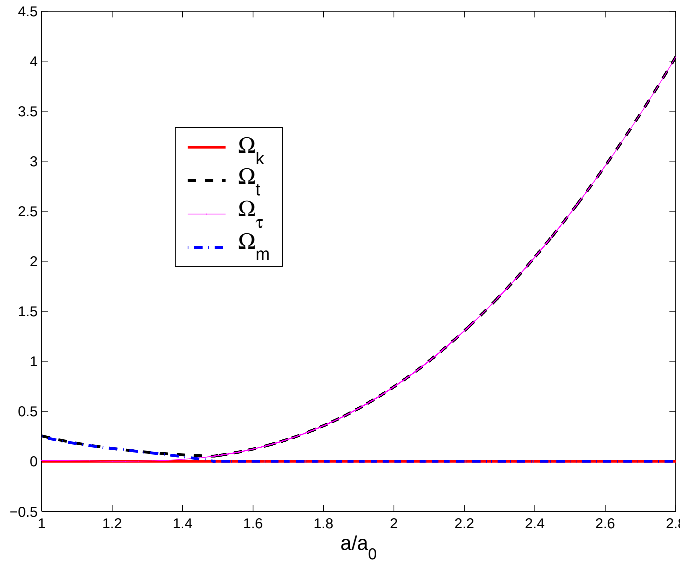

Figure 4.17: The future evolution of Ω_i for the potential given by Eq.(4.88) with $v_I = 0.1$.

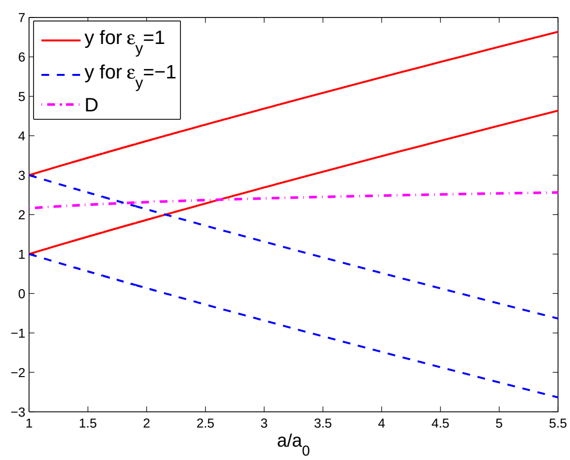

Figure 4.18: The locations of the two branes, $y_I(a)$, and the proper distance, $\mathcal{D}$, between the two branes for the potential given by Eq.(4.88) with $v_I = 0.5$. The initial conditions are chosen so that $y_1(a_0) = 3$ and $y_2(a_0) = 1$. The choice of $\epsilon_y = +1$ ($\epsilon_y = -1$) corresponds to the case where the branes move towards the increasing (decreasing) direction of y.

CHAPTER FIVE

Conclusions and Future Work

5.1 Conclusions

In this dissertation, I discussed two subjects:

- Highly effective and efficient parameter estimation algorithms and their applications to cosmology.
- The late cosmic acceleration of the universe in string/M theory on S^1/Z_2.

In Part I, I first developed two highly effective and efficient numerical codes, and then apply them to study the holographical dark energy model and the ΛCMD model with curvature. By fitting these models with the most recent observational data sets, I find various tight constraints on the cosmological parameters involved in the models.

In part II, I study the late cosmic acceleration of the universe in the framework of brane worlds with orbifold symmetry in both the Hořava-Witten heterotic M theory and the string theory on S^1/Z_2. In each of the two theories, I first develop the general formulas to describe orbifold branes, and then systematically study the two most important issues in brane worlds: (1) the radion stability and radion mass; and (2) the localization of gravity, the effective 4-dimensional Newtonian potential and its Yukawa corrections due to the high order Kaluza-Klein (KK) modes. I find that the radion is stable in both theories and its mass is in the order of GeV, which is well above the current observation constraint. The gravity is always localized on the visible (TeV) brane, and the spectra of the gravitational KK towers are discrete and have a mass gap of TeV. The contributions of high order Yukawa corrections to the Newtonian constant are negligible. Using the large extra dimensions in our setups, I also show that the cosmological constant can be lowered to its current observational value. Applying the formulas to cosmology, I study several models in both M theory and string theory on S^1/Z_2, and find that a late transient acceleration of the universe is a generic feature of our setups. This desirable feature is the result of the interaction of the bulk and the brane.

5.2 Future Work

In our work, we did consider the backreaction of the Goldberger-Wise field Φ in the radion stability. In the Randall-Sandrum model [130], it was shown that such effects do not change the main conclusions of the stability of radion [140]. It would be very interesting to show that it is also the case here. It is also very important to study constraints from other physical considerations, such as the solar system tests, the formation of large-scale structure, and the early universe.

BIBLIOGRAPHY

[1] R. d'Inverno, *Introducing Einstein's relativity,* (Oxford, UK: Clarendon 1992)

[2] S. Dodelson, *Modern Cosmology,* (Amsterdam, Netherlands: Academic Pr. 2003)

[3] P. J. E. Peebles, *Principles of physical cosmology,* (Princeton, USA: Univ. Pr. 1993)

[4] P. J. E. Peebles and B. Ratra, Rev. Mod. Phys. **75**, 559 (2003)

[5] A. G. Riess *et al.* [Supernova Search Team Collaboration], Astron. J. **116**, 1009 (1998)

[6] E. W. Kolb and M. S. Turner, Front. Phys. **69**, 1 (1990).

[7] A.G. Riess *et al.*, Astron. J. **116**, 1009 (1998);

[8] J. Dunkley *et al.*, arXiv:0811.4280 [astro-ph].

[9] Edwin Hubble, Proceedings of the National Academy of Sciences of the United States of America **15**, 168 (1929)

[10] V. Sahni and A. A. Starobinsky, Int. J. Mod. Phys. D **9**, 373 (2000)

[11] S. M. Carroll, Living Rev. Rel. **4**, 1 (2001)

[12] E. Komatsu *et al.* [WMAP Collaboration], Astrophys. J. Suppl. **180**, 330 (2009)

[13] Y. B. Zel'dovich, Sov. Phys. Usp. **11**, 381 (1968).

[14] A. A. Penzias and R. W. Wilson, Astrophys. J. **142**, 419 (1965).

[15] W. -M. Yao et al., Journal of Physics G **33**, 1 (2006).

[16] Trond Hjorteland, http://trond.hjorteland.com/thesis/hoved.html

[17] R. Fletcher, *Practical Methods of Optimization,* (Wiley, 2000)

[18] http://lcgapp.cern.ch/project/cls/work-packages/mathlibs/minuit/home.html

[19] N. Christensen, R. Meyer, L. Knox and B. Luey, Class. Quant. Grav. **18**, 2677 (2001)

[20] Q. Wu, Y. Gong, A. Wang and J. S. Alcaniz, Phys. Lett. B **659**, 34 (2008)

[21] A.G. Riess *et al.*, Astron. J. **116**, 1009 (1998);
S. Perlmutter *et al.*, Astrophy. J. **517**, 565 (1999).

[22] A.G. Riess *et al.*, astro-ph/0611572

[23] W.M. Wood-Vasey *et al.*, astro-ph/0701041;
T.M. Davis *et al.*, astro-ph/0701510.

[24] D.J. Eisenstein *et al.*, Astorphys. J. **633**, 560 (2005).

[25] Spergel, D. N. et al., Astrophys. J. Suppl. **170**, 377 (2007)

[26] B. Ratra and P.J.E. Peebles, Phys. Rev. D **37**, 3406 (1988);

[27] V. Sahni and A. A. Starobinsky, Int. J. Mod. Phys. D **9**, 373 (2000);
T. Padmanabhan, Phys. Rep. **380**, 235 (2003);
P.J.E. Peebles and B. Ratra, Rev. Mod. Phys. **75**, 559 (2003);
E.J. Copeland, M. Sami and S. Tsujikawa, Int. J. Mod. Phys. D **15**, 1753 (2006);
J.S. Alcaniz, Braz. J. Phys. **36**, 1109 (2006).

[28] A. Cohen, D. Kaplan, A. Nelson, Phys. Rev. Lett. **82**, 4971 (1999).

[29] S.D.H. Hsu, Phys. Letter. B **594**, 13 (2004).

[30] M. Li, Phys. Lett. B **603**, 1 (2004).

[31] T. Padmanabhan, Class. Quantum Grav. **22**, L107 (2005).

[32] Q.G. Huang and Y.G. Gong, J. Cosmol. Astropart. Phys. **08**, 006 (2004);
Y.G. Gong, B. Wang and Y.Z. Zhang, Phys. Rev. D **72**, 043510 (2005);
H.-C. Kao, W.-L. Lee and F.-L. Lin, Phys Rev. D **71**, 123518 (2005);
X. Zhang and F.Q. Wu, Phys. Rev. D **72**, 043524 (2005).

[33] B. Wang, Y.G. Gong and E. Abdalla, Phys. Lett. B **624**, 141 (2005).

[34] F.C. Carvalho and A. Saa, Phys. Rev. **D70**, 087302 (2004);
L. Perivolaropoulos, JCAP **0510**, 001 (2005).

[35] Y.G. Gong, Phys. Rev. D **70**, 064029 (2004);
Y.G. Gong and Y.Z. Zhang, Class. Quantum Grav. **22**, 4895(2005);
Q.G. Huang, M. Li, J. Cosmol. Astropart. Phys. **08**, 013 (2004);
B. Chen, M. Li and Y. Wang, astro-ph/0611623;
B. Wang, C.Y. Linand E. Abdalla, Phys. Lett. B **637**, 357 (2006);
S. Nojiri and S.D. Odintsov, Gen. Rel. Grav. **38**, 1285 (2006);
B. Guberina,R. Horvat and H. Nikolic, Phys. Rev. D **72**, 125011 (2005);

[36] D. Pavon and W. Zimdahl, Phys. Lett. B **628**, 206 (2005);
N. Banerjee and D. Pavon, Phys. Lett. B **647**, 477 (2007).

[37] H. Kim, H.W. Lee and Y.S. Myung, Phys. Lett. B **632**, 605 (2006).

[38] B. Wang, Y.G. Gong and R.-K. Su, Phys. Lett. B **605**, 9 (2005).

[39] R. R. Caldwell, Phys. Lett. B **545**, 23 (2002);
V. Faraoni, Int. J. Mod. Phys. **D11**, 471 (2002);
J. A. S. Lima, J. V. Cunha and J. S. Alcaniz, Phys. Rev. **D68**, 023510 (2003);
P. F. Gonzalez-Diaz, Phys. Rev. **D68**, 021303 (2003);
J. S. Alcaniz, Phys. Rev. **D69**, 083521 (2004);
S. Nesseris and L. Perivolaropoulos, Phy. Rev. **D70**, 123529 (2004);
J. Santos and J. S. Alcaniz, Phys. Lett. **B619**, 11 (2005).

[40] Y. Wang and P. Mukherjee, Astrophys. J. **650**, 1 (2006).

[41] Alam, U., Sahni, V., Saini, T.D. & Starobinsky, Mon. Not. Roy. Astron. Soc. **354**, 275 (2004)

[42] Alam, U., Sahni, V., & Starobinsky, JCAP **008**, 0406(2004).

[43] Astier, P., Phys. Lett. B **8**, 500 (2001).

[44] Cardone, V. F., Troisi, A. & Capozziello, S., Phys. Rev. D **69**, 083517 (2004).

[45] Chevallier, M. & Polarski, D., Int. J. Mod. Phys. D **10**, 213 (2001).

[46] Choudhury, T. R. & Padmanabhan, T., A&A **429**, 807 (2005).

[47] Copeland, E. J., Sami, M. & Tsujikawa, S., Int. J. Mod. Phys. D **15**, 1753 (2006).

[48] Corasaniti, P.S. & Copeland, E. J., Phys. Rev. D **67**, 063521 (2003)

[49] Efstathiou, G. Mon. Not. Roy. Astron. Soc. **310**, 842 (1999).

[50] Eisenstein, D. J. et al., Astrophys. J. **633**, 560, (2005).

[51] Elgarøy, O. & Multamäki, T. 2007, arXiv: astro-ph/0702343

[52] Freedman, W. L. et al., Astrophys. J. **553**,47 (2001).

[53] Gerke, B. F. & Efstathiou, G. Mon. Not. Roy. Astron. Soc. **335**, 33 (2002).

[54] Gong, Y. G., Int. J. Mod. Phys. D **14**, 599 (2005).

[55] Gong, Y. G., Class. Quantum Grav. **22**, 2121 (2005).

[56] Gong, Y. G. & Zhang, Y. Z., Phys. Rev. D **72**, 043518 (2005).

[57] Gong, Y. G. & Wang, A., Phys. Rev. D **73**, 083506 (2006).

[58] Gong, Y. G. & Wang, A., Phys. Rev. D **75**, 043520 (2007).

[59] Gong, Y.G. & Wang, A., Phys. Lett. B **652**, 63 (2007).

[60] Y. Gong, A. Wang, Q. Wu and Y. Z. Zhang, JCAP **0708**, 018 (2007)

[61] Huterer, D. & Turner, M. S. 2001, Phys. Rev. D **64**, 123527

[62] Huterer, D. & Cooray, A. 2005, Phys. Rev. D **71**, 023506

[63] Ichikawa, K. & Takahashi, T. 2006, Phys. Rev. D **73**, 083526

[64] H. K. Jassal, J. S. Bagla and T. Padmanabhan, Mon. Not. Roy. Astron. Soc. **356**, L11 (2005)

[65] Jönsson, J., Goobar, A., Amanullah, R. & Bergström, L., JCAP **007** 0409(2004).

[66] Lee, S., Phys. Rev. D **71**, 123528 (2005).

[67] Lewis, A. & Bridle, S., Phys. Rev. D **66**, 103511 (2002).

[68] Linder, E. V., Phys. Rev. Lett. **90**, 091301 (2002).

[69] Padmanabhan, T., Phys. Rep. **380**, 235 (2003).

[70] Peebles, P. J. E. & Ratra, B., Rev. Mod. Phys. **75**, 559 (2003).

[71] Perlmutter, S. et al., Astrophys. J. **517**, 565 (1999).

[72] Riess, A. G. et al., Astron. J. **116**, 1009 (1998).

[73] Riess, A. G. et al., 2006, arXiv: astro-ph/0611572

[74] Sahni, V. & Starobinsky, A. A., Int. J. Mod. Phys. D **9**, 373 (2000).

[75] E. Papantonopoulos, *The Physics of the Early Universe,* (Springer: New York, 2005)

[76] Wang, Y. Astrophys. J. **536**, 531 (2000)

[77] Wang, Y. & Mukherjee, P. Astrophys. J. **606**, 654 (2004)

[78] Wang, Y. & Mukherjee, P. Astrophys. J. **650**, 1 (2006)

[79] Wang, Y. & Mukherjee, P. 2007, arXiv: astro-ph/0703780

[80] Wang, Y. & Tegmark, M., Phys. Rev. Lett. **92**, 241302 (2004).

[81] Weller, J. & Albrecht, A., Phys. Rev. Lett. **86**, 1939 (2001).

[82] Weller, J. & Albrecht, A., Phys. Rev. D **65**, 103512 (2002).

[83] Wetterich, C., Phys. Lett. B **594**, 17 (2004).

[84] Zhu, Z. H., Fujimoto, M. K. & He, X. T., A&A, **417**, 833 (2004).

[85] Maurizio Gasperini, *Elements of String Cosmology,* (Cambridge University Press, 2007)

[86] E. Witten, Nucl. Phys. B **443**, 85 (1995) [arXiv:hep-th/9503124].

[87] J. E. Lidsey, D. Wands and E. J. Copeland, Phys. Rept. **337**, 343 (2000)

[88] Q. Wu and A. Wang, arXiv:0810.5377 [hep-th].

[89] A.G. Riess *et al.*, Astrophys. J. **607**, 665 (2004);
P. Astier *et al.*, Astron. and Astrophys. **447**, 31 (2006);
D.N. Spergel *et al.*, astro-ph/0603449;
W.M. Wood-Vasey *et al.*, astro-ph/0701041;
T.M. Davis *et al.*, astro-ph/0701510.

[90] S. Sullivan, A. Cooray, and D.E. Holz, arXiv:0706.3730;
A. Mantz, *et al.*, arXiv:0709.4294;
J. Dunkley, *et al.*, arXiv:0803.0586;
E. Komatsu, *et al.*, arXiv:0803.0547.

[91] W. Fischler, *et al.*, JHEP, **07**, 003 (2001);
J.M. Cline, *ibid.*, **08**, 035 (2001);
E. Halyo, *ibid.*, **10**, 025 (2001);
S. Hellerman, *ibid.*, **06**, 003 (2003).

[92] R. R. Caldwell, R. Dave and P. J. Steinhardt, Phys. Rev. Lett. **80**, 1582 (1998);
A. R. Liddle and R. J. Scherrer, Phys. Rev. D**59**, 023509 (1999);
P. J. Steinhardt, L. M. Wang and I. Zlatev, *ibid.*, **59**, 123504 (1999).

[93] G. R. Dvali, G. Gabadadze and M. Porrati, Phys. Lett. B**484**, 112 (2000);
C. Deffayet, *ibid.*, **502**, 199 (2001);
V. Sahni and Y. Shtanov, JCAP, **0311**, 014 (2003).

[94] S. Capozziello, S. Carloni, and A. Troisi, arXiv:astro-ph/0303041;
S.M. Carroll, *et al*, Phys. Rev. D **70**, 043528 (2003);
S. Nojiri and S.D. Odintsov, *ibid.*, **68**, 123512 (2003).

[95] E.J. Copeland, M. Sami and S. Tsujikawa, Int. J. Mod. Phys. D**15**, 1753 (2006);
J. Frieman, M. Turner, and D. Huterer, arXiv:0803.0982;
R. Durrer and R. Maartens, arXiv:0811.4132;

[96] L. Susskind, arXiv:hep-th/0302219.

[97] R. Bousso and J. Polchinski, JHEP, **006**, 006 (2000).

[98] P.K. Townsend and N.R. Wohlfarth, Phys. Rev. Lett. **91**, 061302 (2003).

[99] G. W.Gibbons, *Supersymmetry, Supergravity and Related Topics* (World Scientific, Sigapore, 1985).

[100] N. Ohta, Phys. Rev. Lett. **91**, 061303 (2003).

[101] N.R. Wohlfarth, Phys. Lett. B **563**, 1 (2003);

[102] J.K. Webb, *et al*, Phys. Rev. Lett. **87**, 091301 (2001);
J.M. Cline and J. Vinet, Phys. Rev. D **68**, 025015 (2003);
N. Ohta, Prog. Theor. Phys. **110**, 269 (2003);
Int. J. Mod. Phys. A **20**, 1 (2005);
C.M. Chen, *et al*, JHEP, **10**, 058 (2003);
E. Bergshoeff, Class. Quantum Grav. **21**, 1947 (2004);
Y. Gong and A. Wang, *ibid.*, **23**, 3419 (2006);
I.P. Neupane and D.L. Wiltshire, Phys. Rev. D **72**, 083509 (2005);
Phys. Lett. B **619**, 201 (2005);
K. Maeda and N. Ohta, *ibid.*, B **597**, 400 (2004);
Phys. Rev. D **71**, 063520 (2005);
K. Akune, K. Maeda and N. Ohta, *ibid.*, 103506 (2006);
V. Baukh and A. Zhuk, *ibid.*, **73**, 104016 (2006);
A. Krause, Phys. Rev. Lett. **98**, 241601 (2007);
I.P. Neupane, *ibid.*, **98**, 061301 (2007).

[103] Y.-G. Gong, A. Wang, and Q. Wu, Phys. Lett. B **663**, 147 (2008)

[104] H. Horava and E. Witten, Nucl. Phys. B**460**, 506 (1996); **475**, 94 (1996).

[105] N. Arkani-Hamed, S. Dimopoulos and G. Dvali, Phys. Lett. B**429**, 263 (1998);
I. Antoniadis, *et al.*, Phys. Lett., B**436**, 257 (1998).

[106] A. Wang and N.O. Santos, Phys. Lett. B**669**, 127 (2008)

[107] Q. Wu, N.O. Santos, P. Vo, and A. Wang, JCAP **09**, 004 (2008).

[108] A. Wang and N. O. Santos, Phys. Lett. B **669**, 127 (2008).

[109] W.D. Goldberger and M.B. Wise, Phys. Rev. Lett. **83**, 4922 (1999).

[110] A. Lukas, *et al.*, Phys. Rev. D **59**, 086001 (1999); Nucl. Phys. B **552**, 246 (1999).

[111] W. Chen, *et al*, Nucl. Phys. B **732**, 118 (2006);
J.-L. Lehners, P. McFadden, and N. Turok, Phys. Rev. D **75**, 103510 (2007).

[112] C. Csaki, J. Erlich, and C. Grojean, Gen. Relativ. Grav. **33**, 1921 (2001).

[113] N. Arkani-Hamed, *et al*, Phys. Lett. B **480**, 193 (2000);
S. Kachru, M.B. Schulz, and E. Silverstein, Phys. Rev. D **62**, 045021 (2000).

[114] V.A. Rubakov, Phys. Usp. **44**, 871 (2001);
S. Förste, Fortsch. Phys. **50**, 221 (2002);
C.P. Burgess, *et al*, JHEP, **0201**, 014 (2002);
E. Papantonopoulos, Lect. Notes Phys. **592**, 458 (2002);
R. Maartens, Living Reviews of Relativity **7** (2004);
P. Brax, C. van de Bruck and A. C. Davis, Rept. Prog. Phys. **67**, 2183 (2004);
U. Günther and A. Zhuk, arXiv:gr-qc/0410130 ;
P. Brax, C. van de Bruck, and A.C. Davis, Rept. Prog. Phys. **67**, 2183 (2004);
V. Sahni, arXiv:astro-ph/0502032;
R. Durrer, arXiv:hep-th/0507006;
D. Langlois, arXiv:hep-th/0509231 (2005);
A. Lue, Phys. Rept. **423**, 1 (2006);
D. Wands, arXiv:gr-qc/0601078;
R. Maartens, arXiv:astro-ph/0602415.

[115] Y. Aghababaie, *et al*, Nucl. Phys. B **680**, 389 (2004); JHEP, **0309**, 037 (2003);
C.P. Burgess, Ann. Phys. **313**, 283 (2004);
C.P. Burgess , J. Matias, and F. Quevedo, Nucl.Phys. B **706**, 71 (2005).

[116] S. Forste, *et al*, Phys. Lett. B **481**, 360 (2000); JHEP, **0009**, 034 (2000);
C. Csaki, *et al*, Nucl. Phys. B **604**, 312 (2001);
J.M. Cline and H. Firouzjahi, Phys. Rev. D **65**, 043501 (2002).

[117] K. Koyama, arXiv:0706.1557.

[118] C.P. Burgess, arXiv:0708.0911.

[119] K. Benakli, Int. J. Mod. Phys. D **8**, 153 (1999);
H.S. Reall, Phys. Rev. D **59**, 103506 (1999);
A. Lukas, B.A. Ovrut, and D. Waldram, *ibid.*, **60**, 086001 (1999).

[120] J. Cline, C. Grojean, and G. Servant, Phys. Rev. Lett. **83**, 4245 (1999);
C. Csaki *et al*, Phys. Lett. B **462**, 34 (1999).

[121] G.W. Gibbons and S.W. Hawking, Phys. Rev. D **12**, 2752 (1977).

[122] S.C. Davis, Phys. Rev. D **67**, 024030 (2003).

[123] D. Konikowska, M. Olechowski, and M.G. Schmidt, Phys. Rev. D **73**, 105018 (2006).

[124] W. Israel, Nuovo Cim. B **44**, 1 (1966); *ibid.*, B **48**, 463 (1967).

[125] F. Leblond, R.C. Myers, and D.J. Winters, JHEP, **07**, 031 (2001).

[126] A. Wang, R.-G. Cai, and N.O. Santos, Nucl. Phys. B **797**, 395 (2008).

[127] T. Shiromizu, K.-I. Maeda, and M. Sasaki, Phys. Rev. D **62**, 024012 (2000);
R.-G. Cai and L.-M. Cao, Nucl. Phys. B **785**, 135 (2007).

[128] A.N. Aliev and A.E. Gumrukcuoglu, Class. Quantum Grav. **21**, 5081 (2004).

[129] M. Abramowitz and I.A. Stegun, *Handbook of Mathematical Functions* (Dover Publications, INC., New York, 1972), pp.374-8.

[130] L. Randall and R. Sundrum, Phys. Rev. Lett. **83**, 3370 (1999).

[131] W.D. Goldberger and M.B. Wise, Phys. Lett. B **475**, 275 (2000).

[132] C. Charmousis, R. Gregory, and V. A. Rubakov, Phys.Rev. D **62**, 067505 (2000).

[133] J. Garriga and T. Tanaka, Phys. Rev. Lett. **84**, 2778 (2000);
T. Tanaka and X. Montes, Nucl. Phys. B **582**, 259 (2000).

[134] L. Randall and R. Sundrum, Phys. Rev. Lett. **83**, 4690 (1999).

[135] C. Csaki, J. Erlich, T. J. Hollowwood, and Y. Shirman, Nucl. Phys. B **581**, 309 (2000).

[136] C. Csaki, M.L. Graesser, and G.D. Kribs, Phys. Rev. D **63**, 065002 (2001).

[137] A. Brandhuber and K. Sfetsos, JHEP, **10**, 013 (1999).

[138] J. Martin, G.N. Felder, A.V. Frolov, M. Peloso, and L.A. Kofman, Phys. Rev. D **69**, 084017 (2004).

[139] P. Bowcock, C. Charmousis, and R. Gregory, Class. Quantum Grav. **17**, 4745 (2000).

[140] O. DeWolfe *et al*, Phys. Rev. D **62**, 046008 (2000);
L. Kofman, J. marin, and M. Peloso, *ibid.*, **70**, 085015 (2004).

[141] M.Kowalski *et al.*, arXiv: 0804.4142.

[142] D.J.Eisenstein *et al.*, Astrophys. J. **633**, 560 (2005) .

[143] E.Komatsu *et al.*, arXiv: 0803.0547.

[144] S. Weinberg, Rev. Mod. Phys. **61**, 1 (1989);
S.M. Carroll, arXiv:astro-ph/0004075;
T. Padmanabhan, Phys. Rept. **380**, 235 (2003);
S. Nobbenhuis, arXiv:gr-qc/0411093;
J. Polchinski, arXiv:hep-th/0603249;
J.M. Cline, arXiv:hep-th/0612129.

[145] A. Albrecht, *et al*, arXiv:astro-ph/0609591;
J.A. Peacock, *et al*, arXiv:astro-ph/0610906.

[146] W. Fischler, *et al.*, JHEP, **07**, 003 (2001);
J.M. Cline, *ibid.*, **08**, 035 (2001);
E. Halyo, *ibid.*, **10**, 025 (2001);
S. Hellerman, *ibid.*, **06**, 003 (2003);
L.M. Krauss and R.J. Scherrer, Gen. Relativ. Grav. **39**, 1545 (2007)

[147] A.G. Riess, *et al*, arXiv:astro-ph/0611572 (2006).

[148] D.J. Eisenstein *et al*, Astrophys. J. **633**, 560 (2005).

[149] Q. Wu, Y.-G. Gong, A. Wang, and J.S. Alcaniz, Phys. Lett. B **659**, 34 (2008);
Y.-G. Gong and A. Wang, Phys. Rev. D**75**, 043520 (2007) ; *ibid.*, D**73**, 083506 (2006).

[150] Y.-G. Gong, Q. Wu, and A. Wang, Astrophys. J. **681**, 27 (2008).

[151] V. Sahni and Y.Shtanov, JCAP **0311**, 014 (2003).

[152] G. R. Dvali, G. Gabadadze and M. Porrati, Phys. Lett. B **484**, 112 (2000);
C. Deffayet, *ibid.*, **502**, 199 (2001).

[153] J.E. Lidsey, D. Wands, and E.J. Copeland, Phys. Rept. **337**, 343 (2000);
M. Gasperini, *Elements of String Cosmology* (Cambridge University Press, Cambridge, 2007).

[154] T. Battefeld and S. Watson, Rev. Mod. Phys. **78**, 435 (2006).

[155] A. Wang, R.-G. Cai, and N.O. Santos, Nucl. Phys. B **797**, 395 (2008) .

[156] C. Lanczos, Phys. Z. **23**, 539 (1922); Ann. Phys. (Germany), **74**, 518 (1924);
W. Israel, Nuovo Cimento B **44**, 1 (1967); (Errata) B **48**, 463 (1967).

[157] J.A. Wolf, *Spaces of Constant Curvature*, Fifth Edition (Publish or Perish, Inc., Wilmington, Delaware, U.S.A., 1984).

[158] I. Antoniadis, J. Phys. Conf. Ser. **8**, 112 (2005);
V.H.S. Kumar and P.K. Suresh, arXiv:hep-th/0606194.

[159] J.C. Long *et al.*, Nature (London), **421**, 922 (2003);
D.J. Kapner, *et al.*, Phys. Rev. Lett. **98**, 021101 (2007).

[160] A. Lewis and S. Bridle, Phys. Rev. D **66**, 103511 (2002).

[161] J. Garriga and T. Tanaka, Phys. Rev. Lett. **84**, 2778 (2000);
T. Tanaka and X. Montes, Nucl. Phys. B **582**, 259 (2000);
O. DeWolfe, D.Z. freedman, S.S. Gubser, and A. Karch, Phys. Rev. D **62**, 046008 (2000);
C. Csáki, M.L. Graesser, and G.D. Kribs, *ibid.*, **63**, 065002 (2001);
J. Lesgourgues and L. Sorbo, *ibid.*, **69**, 084010 (2004);
D. Konikowska, M. Olechowski, and M.G. Schmidt, *ibid.*, **73**, 105018 (2006).